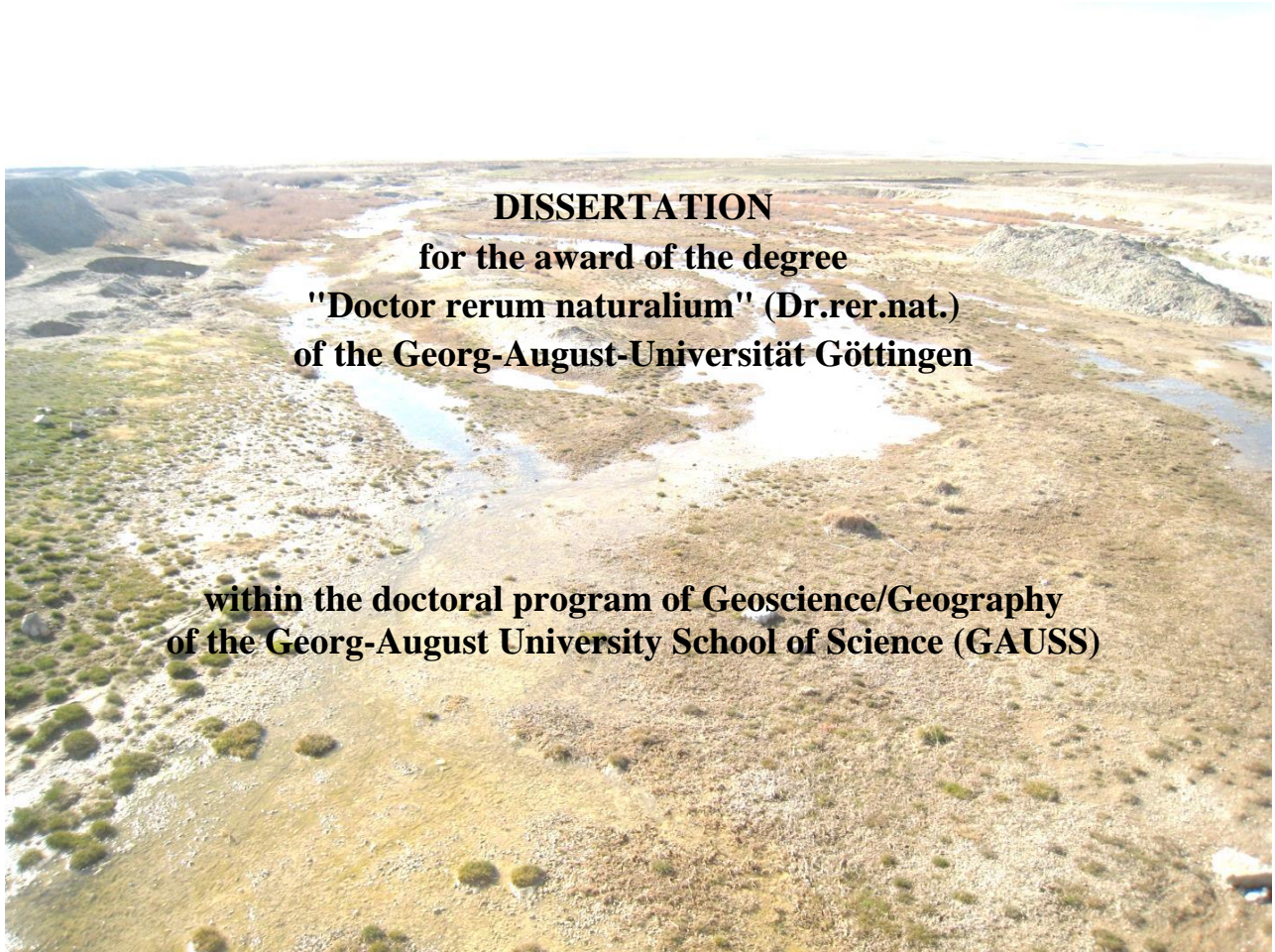


Impact of climate and land use change on water resources, crop production and land degradation in a semi-arid area (using remote sensing, GIS and hydrological modeling)



DISSERTATION
for the award of the degree
"Doctor rerum naturalium" (Dr.rer.nat.)
of the Georg-August-Universität Göttingen

within the doctoral program of Geoscience/Geography
of the Georg-August University School of Science (GAUSS)

Submitted by
Ammar Raffiei Emam

From Iran

Göttingen, February 2015

Thesis Committee

Prof. Dr. Martin Kappas, Department of Cartography, GIS and Remote Sensing, University of Göttingen

Prof. Dr. Gerhard Gerold, Department of Landscape Ecology, University of Göttingen

Members of the Examination Board

Reviewer: Prof. Dr. Martin Kappas, Department of Cartography, GIS and Remote Sensing, University of Göttingen

Second Reviewer: Prof. Dr. Gerhard Gerold, Department of Landscape Ecology, University of Göttingen

Further members of the Examination Board:

Prof. Dr. Karl-Heinz Pörtge, Institute of Geography, University of Göttingen

PD Dr. Pavel Propastin, Department of Cartography, GIS and Remote Sensing, University of Göttingen

PD Dr.-Ing. Rüdiger Schaldach, Center for Environment System Research, University of Kassel

Dr. Stefan Erasmi, Department of Cartography, GIS and Remote Sensing, University of Göttingen

Date of the oral examination: 23.02.2015

To my wife Elaheh and my parents

Preface

The present thesis “Impact of climate and land use change on water resources, crop production and land degradation in a semi-arid area (using remote sensing, GIS and hydrological modeling)” has been submitted in partial fulfillment of the requirements for the Ph.D. degree at the University of Göttingen (Germany). The main supervisor was Professor Martin Kappas and the second supervisor was Prof. Dr. Gerharld Gerold.

The thesis contains an introduction with objectives and research questions as well as a general literature review, a summary of characteristics of the study area, four manuscripts and finally a summary and conclusion.

The study was undertaken at the Department of Cartography, GIS and Remote Sensing from October 2010 to February 2015. An external research stay of one month was spent at the EAWAG, Swiss Federal Institute of Aquatic Science and Technology, Switzerland, with Dr. Karim C. Abbaspour.

Göttingen, February 2015

Ammar Rafiei Emam

Table of Content

Preface.....	IV
Table of Content.....	V
List of figures	VIII
List of tables	XII
Acknowledgments.....	XIII
Abstract.....	XV
CHAPTER 1:Introduction	1
1-1. Overview.....	1
1-2. Research objectives.....	2
1-3. Research questions.....	3
1-4.Thesis outline	3
1-5. General Literature review	6
1-5-1. Land degradation	6
1-5-2. Climate change	7
1-5-3.Water resources in Iran.....	9
1-5-4. Hydrological models.....	12
1-5-4-1. Hydrological models and climate change.....	13
1-5-4-2. SWAT hydrologic model	14
1-5-5. Remote sensing and GIS in hydrological modeling.....	15
1-6. References.....	16
CHAPTER 2:Study area.....	23
2-1. Climate data and TLAP and PLAPS calculations	23
2-2. Hydrometric stations and hydrographs of rivers	24
2-3. Geology and stratigraphy	30
2-4. References:.....	33
CHAPTER 3:Simulation of water balance components in a watershed located in central drainage basin of Iran.....	35
3-1-Introduction	35
3-2-Material and Methods	36

3-2-1- Study area.....	36
3-2-2. Land use mapping.....	40
3-2-3. Hydrological Model.....	41
3-2-4. Calibration and sensitivity analysis	43
3-3. Results and Discussion.....	45
3-3-1. Hydrological response unit	45
3-3-2. Model Calibration	50
3-3-3. Quantification of components.....	54
3-4. Conclusion	57
3-5. References.....	57
CHAPTER 4:Estimation of groundwater recharge and its relation with land degradation: Case study of a semi-arid river basin in Iran.....	61
4-1. Introduction.....	62
4-2. Materials and method.....	64
4-2-1. Study area	64
4-2-2. Groundwater recharge.....	68
4-2-3. Model input.....	69
4-2-4. Model setup	70
4-2-5. Model Calibration.....	71
4-3. Results and Discussion.....	72
4-3-1. Calibration of model for crop yield	77
4-3-2. Groundwater recharge, water level and land subsidence	78
4-4. Summary and Conclusions.....	83
4-5. References.....	84
CHAPTER 5:Assessing the impact of climate change on water resources, crop production and land degradation in a semi-arid river basin	91
5-1. Introduction.....	92
5-2. Material and methods.....	94
5-2-1. Study area	94
5-2-2. The SWAT Simulator, model setup, calibration and uncertainty analysis.....	97
5-2-3. Climate change model	99
5-2-4. Land use change (Urbanization)	101

5-3. Results and discussion	101
5-3-1. Downscaling results.....	102
5-3-2. Impact of climate change on precipitation and temperature	103
5-3-3. Impact of climate change on water balance components	106
5-3-4. Land-use change scenario.....	107
5-3-5. Impact of climate change on crop production.....	108
5-3-6. Land degradation and water table	112
5-4. Summary and conclusions	114
5-5. References.....	115
CHAPTER 6:Estimating actual evapotranspiration from MODIS time series compared to a hydrological model in a semi-arid catchment in Iran	123
6-1. Introduction.....	124
6-2. Material and Methods	125
6-2-1. Study area	125
6-2-2. Satellite and meteorological data	126
6-2-3. Mapping of Land use/land cover	127
6-2-4. Surface energy balance algorithm.....	128
6-2-5. A hydrological model for water balance assessment	131
6-3. Results.....	132
6-3-1. Reference Evapotranspiration, ETr.....	133
6-3-2. SEBAL energy fluxes	134
6-3-3. Mapping monthly actual evapotranspiration.....	135
6-4. Discussion and conclusions.....	137
6-5. References.....	139
CHAPTER 7:General Summary and Conclusion.....	146

List of figures

Figure 1-1. The population rate in Iran from 1950 to 2050 (U.S. Census Bureau)	2
Figure 1-2. The framework of the research	5
Figure 1-3. Relation between CO ₂ concentration and yield changes in some selected crops (by CCSP, 2008)	8
Figure 1-4. Per capita blue water resources distribution in the period of 1980-2002 – derived from (Abbaspour et al. 2009)	10
Figure 1-5. Comparing water usage in the world, developing and developed countries	11
Figure 1-6. Water use in different sectors in Iran, showing huge water consumption in the agriculture sector	11
Figure 1-7. Ranking of countries in irrigated agriculture, Iran has the 7 th largest amount of irrigated land in the world	11
Figure 1-8. The classification of hydrological models (after Refsgaard, 1996; represented by Alkhoury, 2011)	13
Figure 2-1. The meteorological stations in and around the basin	25
Figure 2-2. The PLAPS estimation in the study area	25
Figure 2-3. The position of hydrometric stations inside and outside the basin	26
Figure 2-4. Gharehchay River discharge at the Omarabad outlet	27
Figure 2-5. The view of Gharehchay River including the Omarabad hydrometric station	27
Figure 2-6- Zehtaran River discharge from 1977 to 2008	28
Figure 2-7- The view of Zehtaran River with the hydrometric station. The irrigation channels lead to change in the hydrological characteristics in the basin	28
Figure 2-8. Sirab-Khomigan River discharge since 1977	29
Figure 2-9. The view of Sirab-Khomigan River	29
Figure 2-10- Different hydrological characteristics in the hydrological process of the basin (e.g. Sirab-Khomigan River discharge)	30

Figure 2-11. Geology map of the Razan-Ghavand area	32
Figure 3-1. Water balance concept	36
Figure 3-2. Razan-Ghavand study area	37
Figure 3-3. Typical land use types inside the watershed: a) bare land, b) rangeland good condition in north watershed, c) rangeland poor condition in south watershed, d) agriculture (e.g. alfalfa)	41
Figure 3-4. Land use map	46
Figure 3-5- Soil map	48
Figure 3-6- Slope map	49
Figure 3-7. Calibration and validation of river discharge	53
Figure 3-8-a,b,c. Average monthly 95PPU (2003-2008) of actual evapotranspiration(AET), surface runoff(SURQ) and soil water content(SW) against with precipitation(PERCIP)	55
Figure 3-9. Average spatial distribution of yearly average of precipitation (PRECIP), actual evapotranspiration(AET), Percolation (PERC), Surface runoff (SURQ) and Soil water content (SW) for the years 2003 to 2008.	56
Figure 4-1. Location of the study area in northwestern part of central drainage basin of Iran (Razan-Ghavand watershed). The location of land subsidence, a dominate land degradation phenomenon, has been shown in west of the basin. The distribution of rain gages and temperature stations and also hydrometric stations has been shown in the map.....	66
Figure 4-2. The location of piezometric wells in the study area	67
Figure 4-3. Conceptual of SWAT model (Adapted from Neitsch et al.,2005)	69
Figure 4-4. The sensitivity analysis of CN2 parameter by decreasing 7 percent, and increasing 14 and 35 percent of CN2 value against surface runoff production	74
Figure 4-5. Result of calibration and validation in a & b: Omarabad station (No.71); c & d: Sirab khomigan (No.41) and e & f: Zehtaran (No.14)	76
Figure 4-6-a,b. Statistical results of dominate and non-dominate HRU in SWAT model	77
Figure 4-7-a,b. Calibration (left graph) and validation (right graph) results of annual average (2003–2008 for calibration and 1998–2002 for validation) crop yield for rainfed and irrigated	

wheat in study region. The green point is observation, and the gray band expresses the 95% prediction uncertainty (95PPU)	78
Figure 4-8. Relation between mean annual groundwater recharge and groundwater level from 1998 to 2008	79
Figure 4-9. Average yearly of groundwater recharge and precipitation distributions in each sub basin in the watershed	81
Figure 4-10. Mean annual precipitation in Razan-Ghahavand study area, showing drought cycles from 1999 to 2008. An increase precipitation in 2002 and 2003 may have significantly increased on groundwater recharge in 2003	81
Figure 4-11. Depth to groundwater at different locations in the study area. Bores No.1, 2, and 3 are located in North of area. Bore No. 4 in East, and bores No. 5 and 6 are located in West of area	82
Figure 4-12. Trend of groundwater recharge and groundwater level in west of the watershed, where land subsidences has been occurred	82
Figure 5-1. Region of Razan-Ghahavand watershed showing the hypsometric map, distribution of river and streams, hydrometric and climatic stations (e.g. rain gage and synoptic)	96
Figure 5-2. Some features of land degradation in the area (e.g. soil salinization in arable lands, rangeland degradation, and land subsidence)	97
Figure 5-3. Results of SWAT calibration–validation for one selected hydrometric station	102
Figure 5-4.a,b. Comparison of the observed and generated mean and standard deviation of monthly rainfall and minimum temperatures at the Ghahavand station (1983-2009). bs: base line, gen: generated, sd: standard deviation	102
Figure 5-5. Mean monthly precipitation in baseline (1997-2008), and future (2046-2065) in three different emission scenarios according to the ensemble multi models	103
Figure 5-6. Spatial pattern of average annual precipitation (a), maximum temperature (e) and actual evapotranspiration(i) for the historic period (1998-2008). Percent difference calculated of precipitation based on future and historic data (b-d),% difference maximum temperature (f-h) and the pattern of percent difference calculated of ET based on future and historic data (j-l)	105

Figure 5-7. The absolute surface temperature changes ($^{\circ}\text{C}$) in north of study area in GCM period with respect to the baseline period for three different emission scenarios, according to the CCSM3 model	106
Figure 5-8. Spatial pattern of deep aquifer recharge, surface runoff, and soil water content in historical (1998-2008) and future (2046-2065) periods. The pattern of deep aquifer recharge (a) and % difference calculated of DARCH based on future and historic data (b-d). The distribution of average annual surface runoff (e) and % difference calculated of SURQ based on future and historic data (f-h). The spatial patter of soil water content (i) and % difference calculated of SW based on future and historic data(j-l)	109
Figure 5-9. Anomaly graph of irrigated and rain-fed wheat yield in the GCMs scenarios	110
Figure 5-10. Temperature stress during growing season for rain-fed and irrigated lands	110
Figure 5-11. Water stress uncertainty analysis in different scenarios both for irrigated and rain-fed areas	111
Figure 5-12. Means monthly water stress in irrigated and rain-fed lands	111
Figure 5-13. a: The hydrographs of Razan-Ghahavand Aquifer, b: the hydrograph of degraded area in particular	113
Figure 5-14. The hydrograph of Razan-Ghahavand Aquifer in 2046-2065 predicted by ARIMA model	113
Figure 6-1. Map of study area, including streams, hydrometric, temperature and rain gages ...	126
Figure 6-2. Flowchart of process of surface energy balance technique to estimating actual evapotranspiration (ETa)	131
Figure 6-3. The calibration and validation of the crop yield in the RGB.....	133
Figure 6-4. ETa in April, a: based on surface energy balance technique, b: surface water balance model	136
Figure 6-5. Anomaly graph of monthly average of ETa. The gray box shows the 95PPU band simulated by 500 iterations; M95PPU means the median of iterations. The star sign shows the Eta value simulated by SEBAL..	136

List of tables

Table 2-1. Climate stations include mean annual precipitation and temperature	22
Table 2-2. The area covered by each hydrometric station including the number of sub-basins...	26
Table 2-3 -Geological units in the study area	31
Table 3-1. Overview of weather data availability	38
Table 3-2. Soil characteristics in different land types	39
Table 3-3. Statistical results of land use classes	47
Table 3-4. Information of soil map	47
Table 3-5. Information of Slope map	49
Table 3-6. Parameters for river discharge calibration and their initial and final ranges	51
Table 3-7. The most Sensitive parameters including their t-value and p-value	52
Table 3-8. Statistical result of calibration and validation	53
Table 4-1. The most sensitive parameters and their initial and final ranges	73
Table 5-1. Sub basins affected to flow in each station including the rate of discharge	95
Table 5-2. The rate of groundwater recharge in HRUs 515, 571 (in the west of basin) and whole basin in base line and percent difference calculated of GWR based on the future (2046-2065) and historic (1998-2008) data	113
Table 6-1. Specification of MODIS products used in ET modeling	127
Table 6-2. Overpass date and time of terra sensor.....	127
Table 6-3. ETr calculated at the time of satellite image based on Hargreaves method	134
Table 6-4. Surface energy fluxes at Hot and Cold pixels on 13th April 2008	134

Acknowledgments

This research was made possible with the support and contribution of many individuals and organizations. I would like to take this opportunity here to express my thanks to them all.

First of all, I would like to express my grateful thanks to my supervisor, Prof. Dr. Martin Kappas, who has helped me in every step of my research. His brilliant guidance enabled me to plan my PhD research correctly and his valuable comments and feedback helped me to progress in my study objectives. I would also like to thank my second supervisor Prof. Dr. Gerharld Gerold.

My very special thanks go to Dr. Karim Abbaspour, at the EAWAG institute, Switzerland, who supported and helped me, especially during my stay at EAWAG in Dübendorf, Switzerland.

Many thanks to Dr. Samira Akhavan at Boali-Sina University, Hamedan, Iran, for providing a part of the data for this study, and for her guidance to calibrate my model, especially during my stay in Hamedan. I would also like to thank Mr. Daryoush Sarhadi and Mr. Mohamadreza Sadeghi Manesh, who helped me during my field trip and field study in the Razan-Ghahavand area in Hamedan, Iran.

Thanks also go to all of my colleagues at the department of cartography, GIS and remote sensing, especially Dr. Stefan Erasmi, Dr. Jan Dregner, Dr. Seyed Zaynalabadi Hosseini and Mr. Hong Quang Nguyen for their help and guidance and for the challenging discussions during this study. Many thanks go to my friends Mr. Hamidreza Abbasi and Dr. Enayatollah Ranjineh Khojasteh for their support throughout the research process.

I am also grateful to the Ministry of Science, Research, and Technology (MSRT) in Iran for supporting me to undertake my PhD study in Germany. I would like to thank the Iran Meteorological Organization (WSIMO), the Iran Water Resources Management Company (IWRMC), the Hamedan Regional Water Co. (HMRW), the National Cartographic Center of Iran (NCC), the Forests, Range and Watershed Management Organization (FRWO), the Research Institute of Forests and Rangelands (RIFR) in Iran for their collaboration by making literature and data available.

Last but not least, I am deeply indebted to my lovely wife Elaheh. I would not have been able to accomplish my academic studies and My PhD without her patience, tolerance, inspiration and her emotional support. Thanks for everything Elaheh. Finally, I would like to express my gratitude to my parents who have supported and encouraged me throughout all the stages of my life.

Abstract

Water resources have become scarcer in semi-arid regions of Iran due to increasing water use and recurrent drought. Any change to the hydrological cycle may have significant effects on the fragile ecosystems of Iran's arid and semi-arid regions. Moreover, it can lead to land degradation. Therefore, water resources should be considered quantitatively for better planning and management.

The main goal of this research was the impact assessment of climate and land use change on water resources (e.g. groundwater recharge, surface runoff, soil water content, actual evapotranspiration), and crop production in the Razan-Ghahavand Basin (RGB) in the central drainage basin of Iran. To attain this goal the objectives were: to model the availability of water resources components in temporal and spatial aspects, to estimate groundwater recharge (as groundwater is the main source of the water supply in RGB), to model crop yields in irrigated and rain-fed lands, to assess the relationship between water balance fluxes and land degradation. And, finally, to compare the results of actual evapotranspiration estimated by a remotely sensed process and a hydrological model.

The first step of the research was a detailed quantification of the water balance components (e.g. percolation, evapotranspiration, soil water) of the RGB by means of hydrological modeling. To do this, a SWAT (Soil and Water Assessment Tools) physically based and spatially distributed, and an eco-hydrological model was conducted. The model was calibrated by SUFI-2 algorithm in two steps: Firstly, the model was calibrated based on the monthly river discharge. Then the calibrated model was recalibrated again by annual crop yield. The calibration of crop yield leads to estimate the evapotranspiration term better, which consequently increased our knowledge of estimating other water fluxes such as aquifer recharge.

The sensitive and uncertainty analyses were also applied to assess the model's performance. The calibration period was from 1998 to 2001 and the validation period was from 2002-2008, both for river discharge and crop yield. The results were satisfactory for river basins and wheat yield in both calibration and validation periods. All water balance components were quantified at the sub basin level in monthly time intervals.

As groundwater is the main water resource in the RGB, the groundwater recharge specifically was estimated and the relationship between groundwater recharge, water level, and land degradation was evaluated. The results showed that there was not any significant change in groundwater recharge during the period 1998-2008. Therefore, a net withdrawal of groundwater, especially for the purpose of irrigation, leads to land degradation (e.g. land subsidence) in the area.

In the next step, an ensemble of four Global Circulation Models (GCMs) under a fourth assessment report (AR4) by the Intergovernmental Panel on Climate Change (IPCC) in three emission scenarios (e.g. A1B, A2, B1) for the period 2046-2065, were developed. The data was downscaled by the LARS-WG model in all rain gages and synoptic stations. All data were fed into the calibrated hydrological model to analyze the future effects of climate on water resources, and wheat yield in the RGB. Finally, we interpreted the relationship between climate change and land degradation across the RGB. The results showed a substantial reduction in groundwater recharge and surface runoff, while in the basin surface runoff increased. Furthermore, the results showed that urbanization increasingly leads to surface runoff and flooding in the area.

Assessing the wheat yield both in irrigated and rain-fed lands, a reduction of yield could be shown in rain-fed land due to decreasing soil moisture and rainfall leading to increasing water stress. The results also revealed that the risk of drought in the south and flooding in the north is high. The results highlighted the risk of land degradation by groundwater deterioration, soil salinization, and land subsidence in the basin.

Finally, the estimation of the remotely sensed process of evapotranspiration (i.e. surface energy balance method) was done by the SEBAL (Surface Energy Balance Algorithms for Land) method. The estimation of ETa by remote sensing is comparable to the estimation of ETa by the hydrological model. The idea behind this part of research was that, if the ETa estimated by the surface energy balance method (i.e. remote sensing process) was the same as estimated by the hydrological model, remotely sensed data could further be used to calibrate the hydrological models, especially in the area with low data availability. The results of this part showed the good relevance between monthly ETa estimated by remote sensing and ETa estimated by the hydrological model.

Introduction

1-1. Overview

Although climate change occurs naturally, the growth of the human population and associated land use conversion (e.g. urbanization) have substantially accelerated the increase of greenhouse gases (Wu et al. 2012). The increase in urban, industrial and agricultural water demand will further increase the pressure on water resources. As surface water is limited in the arid and semi-arid regions, groundwater plays a dominant role in water supply in this area. However, quantification of water components, especially groundwater recharge, is therefore essential for using and managing water resources efficiently. Furthermore, changes in climate and land use can significantly affect water resources and hydrological cycle.

In Iran, a semi-arid country, the shortage of water is the main issue for the policy makers. The population of the country increased rapidly from 1950, reaching about 75 million by 2011. The population growth rate will continue to reach above 100 million by 2050 (U.S. Census Bureau: <http://www.census.gov/population/international/data/idb>) (Figure 1-1).

Despite the water scarcity, agriculture is the largest water user in Iran. More than 90 % of the total water withdrawal is used in this sector. About 12% of the total area of Iran (i.e. 19 million ha) is agricultural land. In most of the area in central Iran, water demand exceeds the internal renewable water availability. Therefore, huge volume of water is extracted from groundwater resources to meet the water demand (Faramarzi, 2010), which led to depletion of aquifers and land degradation in most of the area in central Iran. Hence, one of the biggest concerns for Iran's water-based resources is the sustainability of the current and even future water resource allocation. As water becomes scarcer, the importance of how it is managed grows vastly. Finding a balance between what is needed by humans and animals and what is needed in the environment is an important step in the sustainability of water resources. Therefore, prediction of water balance components is useful for water resources analysis and management of watersheds such as enhancing food security, prevention of land degradation, estimation of water availability for irrigation or the calculation of the sustainable amount of groundwater withdrawal.

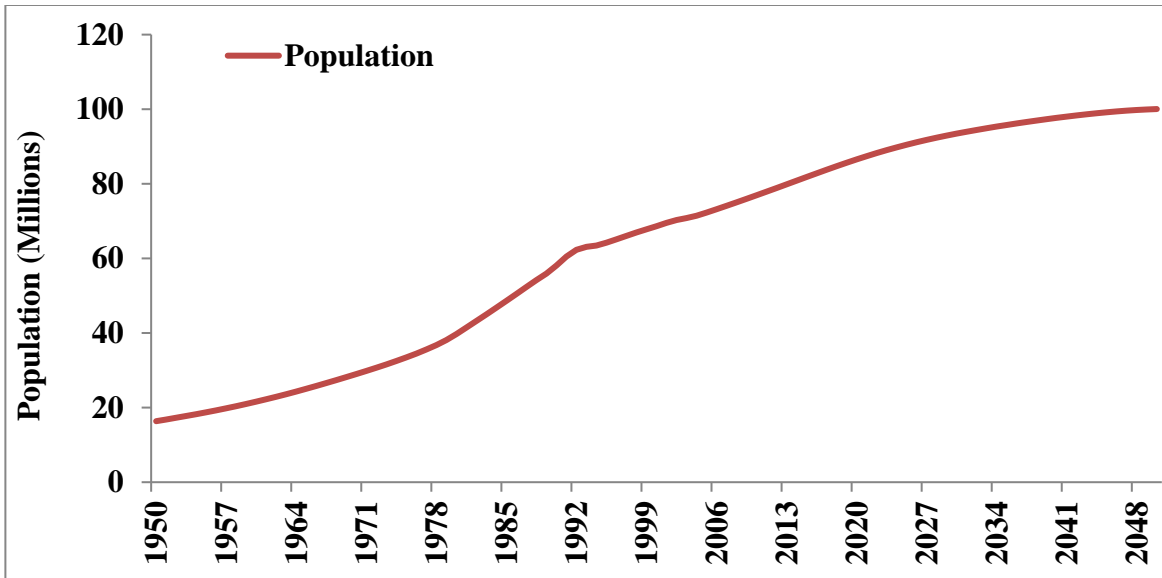


Figure 1-1. The population rate in Iran from 1950 to 2050 (U.S. Census Bureau)

In this chapter, after research objectives and research questions, some general overview about land degradation, and climate change is explained. Then, the status of water resources in Iran have been described briefly. In addition, the roles of hydrological models, remote sensing and GIS in this research have been described.

1-2. Research objectives

The main goal of this research is to investigate the impact of climate and land use change on water resources and crop production in the semi-arid Razan-Ghahavand river basin (RGB) through hydrological modeling, remote sensing and GIS techniques, and to assess the relationship between changes of water components quantities, land use and land degradation in the area.

To attain the main goal we specified the following objectives:

- To analyze the SWAT (Soil and Water Assessment Tools) eco-hydrological model in order to quantify the hydrological conditions and climate change assessments in semi-arid regions like the RGB of Iran.

- To calibrate, validate and analyze uncertainty of the SWAT model based on the river discharges and crop yields;
- To estimate water balance components (e.g. evapotranspiration, surface runoff, percolation, etc.) in spatial and temporal scales;
- To estimate deep aquifer recharge and its relationship with the groundwater level in aquifer in general and particularly in subsidence areas.
- To predict the water balance components and crop yields by single GCMs models and ensemble model, respectively during 2045-2065.
- To estimate the actual evapotranspiration by the remotely sensed process, and compare the results with ETa estimated by the hydrological model.

1-3. Research questions

The research has tried to answer the following main questions:

- What is the current and future condition of water resources in the RGB? Will the RGB be drier or wetter than in the historical period in the mid-21st century?
- What will the crop yield be both in irrigated and rain-fed lands in the RGB in the future?
- What is the effect of climate change on water resources and crop production?
- Whether remote sensing data can further be used to calibrate the hydrological models?

1-4. Thesis outline

This dissertation consists of seven chapters. The connection among research chapters can be described in the simplified flowchart (Figure 1-2).

In **chapter 1** general overview, objectives and research questions are mentioned followed by a general literature review of land degradation, climate change, water resources, the hydrological model and the role of remote sensing and GIS on the hydrological models.

In **chapter 2** the study area is explained in terms of climatology, hydrological conditions and geology.

Chapters 3 to 6 have been written in the scientific manuscript structures which have either been published or are under review in international peer-review journals or book chapters.

Chapter 3 investigates the setup of the SWAT hydrologic model for the Razan-Ghahavand semi-arid region. Preparation of suitable data to feed into the SWAT model is presented in detail. Firstly, a land use map was created by remotely sensed data and supervised classification. A soil map was spatially mapped in the ArcGIS by soil profile data in each land types. In addition, a slope map was created based on digital elevation model (DEM). Then the calibration analysis from river discharge data and the uncertainty analysis of parameters are discussed respectively. Finally, the water components like soil moisture, surface runoff, and actual evapotranspiration are presented.

Chapter 4 evaluates the estimation of deep groundwater recharge by SWAT. Then the relationship between groundwater recharge and groundwater fluctuation is discussed. To precisely estimate groundwater recharge, calibration was improved based on crop yield data. The process of crop yield calibration and uncertainty analysis is discussed in detail.

Chapter 5 focuses on the Global Circulation Model (GCM) and its impact not only on water resources but also on crop production. Furthermore, land degradation affected by climate change is discussed. Four GCMs models with three CO₂ emission scenarios have been included and analyzed. Then the ensemble model was developed from 2046-2065, because we would like to know the water availability in the mid of 21 century. On the other hand, data near to the historical period have lower uncertainty than the end of century. The method of downscaling, and its performance is also discussed.

Chapter 6 investigates the remotely sensed method to estimate actual evapotranspiration (ET_a). In this method ET_a is a residual of surface energy balance model. SEBAL (surface energy balance techniques) (Bastiaansen et al., 1998) was selected to estimate ET_a. In addition, some equations from the METRIC model, a variant of SEBAL, were selected in order to improve the performance of the SEBAL model in mountainous areas. The idea behind this part of the research was that if ET_a estimated by SEBAL was the same as the hydrologic model, the remotely sensed method could be used to further calibrate the hydrological models, especially in the area with low data availability. The method of ET_a estimation by surface energy balance is discussed in detail. Finally, the average monthly temporal ET_a estimated by SEBAL is compared to 95PPU band of ET_a estimated by the SWAT hydrologic model.

Finally, in **chapter 7**, the summarized results and a discussion about all the results are presented. Additionally, some suggestions for future researches are given.

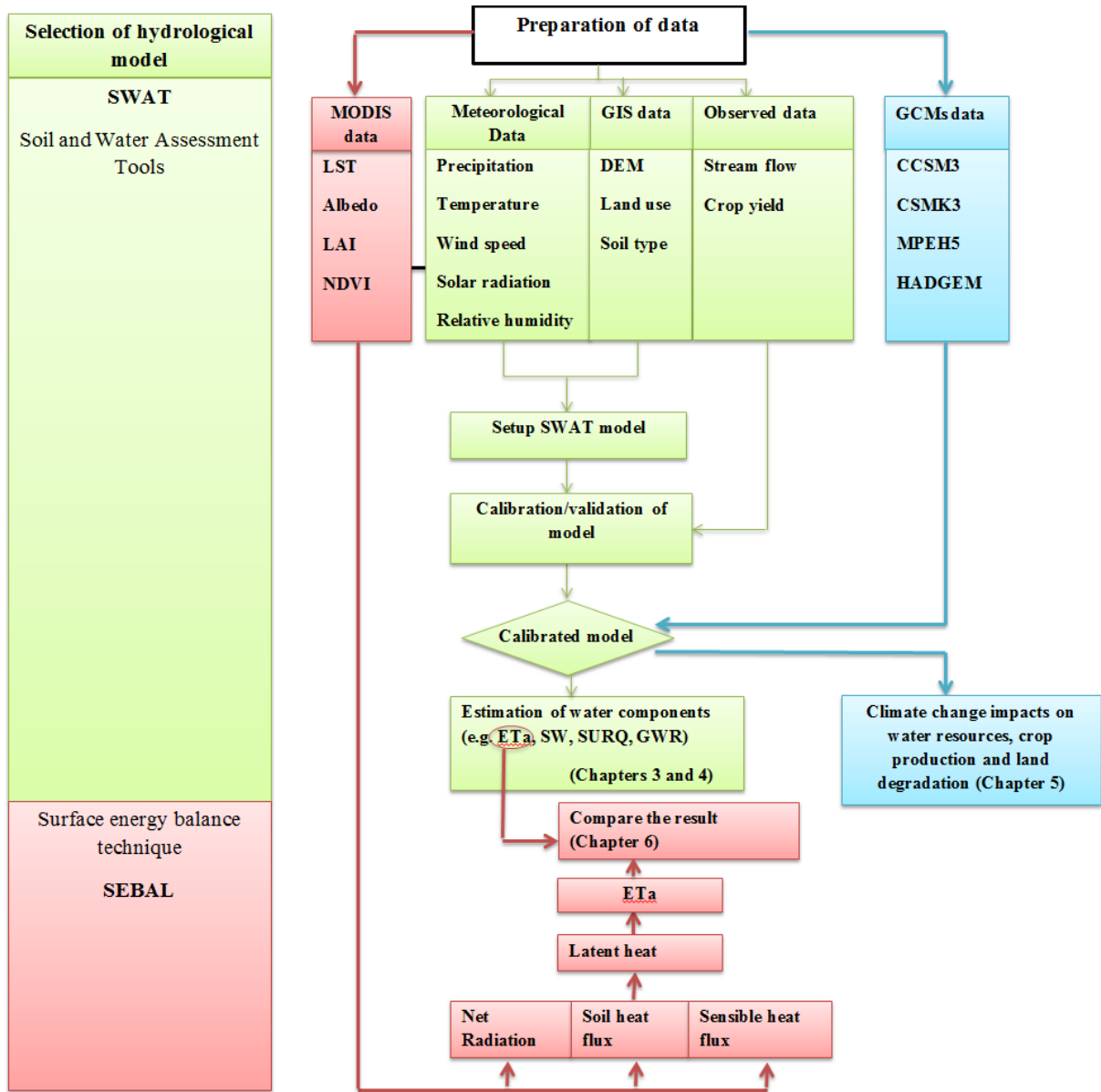


Figure 1-2. The framework of the research

1-5. General Literature review

1-5-1. Land degradation

Land degradation is defined as any decrease in the capacity of biological or economic productivity of the land caused by human activities and/or natural processes and exacerbated by climate change effects (UNCCD, 2013). Land degradation includes soil erosion by water and wind, physical (e.g. compacting, crusting) and chemical soil deterioration (e.g. salinization), biological degradation (e.g. biomass and vegetation cover decline) and water degradation (e.g. aridification) (Schwilch, 2012). Arid and semi-arid regions are very prone to land degradation and characterized by low rainfall, resulting in water scarcity, and periodic drought. The FAO mentioned that land degradation in arid, semi-arid and dry sub-humid areas is called desertification.

According to the UNCCD (2013), degraded lands have noticeably increased from 15 % in 1991 to 25 % by 2011. The FAO (2011) mentioned that 24 billion tons of fertile soil was eroded in the world's croplands, and global food production may decrease by as much as 12 % with the current scenarios of land degradation over the next 25 years. This at a time when demand for food, energy and water will be increased by at least 50 %, 45% and 30 % respectively, due to population growth and changing consumption patterns.

The surface area of Iran is about 1.648.000 km², and two thirds of the country is located in arid and semi-arid zones. Land degradation in Iran has accelerated during recent decades usually due to the rapid growth of the population over the last 30 years (urbanization), land use/cover change (especially the conversion of forest and rangelands into cultivated land), denuded soil by over- grazing of rangelands by livestock, or overutilization of wood and plants as a fuel source (exposing areas to wind erosion), overuse of water resources, and the traditional methods of agriculture and irrigation systems.

In recent years, remote sensing has played a positive role in environmental monitoring such as for ecosystem variations and land degradation, especially in dry lands. Climate variations can significantly affect ecosystem variations and land degradation. Additionally, there are anthropogenic factors, ecosystem disparities and land degradation affected by climate variations such as drought and desiccation (Lambin & Ehrlich, 1996), oscillation of rainfall (Anymba et al., 2001; Olsson et al., 2006) and rising of temperature (Xiao & Moody, 2004).

1-5-2. Climate change

Climate change refers to any significant change in a climate variable (e.g. temperature, precipitation, or wind) for a decade or longer (IPCC, 2001). It might proceed from natural factors or human activities. The term “global warming” is often used interchangeably with the term “climate change”. Global warming refers to the increasing average temperature which can contribute to global climate pattern variation. However, increasing temperatures are just one aspect of climate change.

Human activities are adding to the concentration of greenhouse gases. The carbon dioxide (CO₂) level has increased since the 1950s. Climate change due to temperature increases can have pernicious effects on the hydrological cycle through precipitation, evapotranspiration, and soil moisture. IPCC reports that the global mean surface temperature has raised 0.6 ± 0.2 °C since 1861, and estimates an increase of 2 to 4 °C over the next 100 years. Global sea levels have increased between 10 and 25 cm since the late 19th century (Singh & Kumar, 2010).

Climate change can affect water resources, crop production and the natural ecosystem. Most regions of the world are expected to experience a negative impact of climate change on water resources. However, the intensity and characteristics of the impact is different from region to region.

Changes in precipitation, temperature, and CO₂ concentration could have a significant impact on crop yields. In general, the yield of crops will increase with higher CO₂ levels (Figure 1-3). In some crops like wheat or soybeans, the yield could increase by 30 % from the doubling of CO₂ concentration. For other crops like corn, the increased yield is much smaller (CCSP, 2008). However, some factors may counteract these potential increases in yield. For instance, if the temperature increases to more than the crop’s optimal level, or if water and nutrients are not sufficient, then the yield increase trend may be reversed.

Abbaspour et al. (2009) investigated the effect of climate change on crop yield in Iran on a large scale. The results showed small increases in the winter wheat yield in some areas of Iran probably due to soil moisture, temperature, and above all air CO₂ concentration. Vaghefi et al. (2014) assessed the impact of climate change on wheat yield in Karkhe, a semi-arid river basin

of Iran. They found that the average irrigated wheat yield increased in the south of Karkhe basin up to 21%.

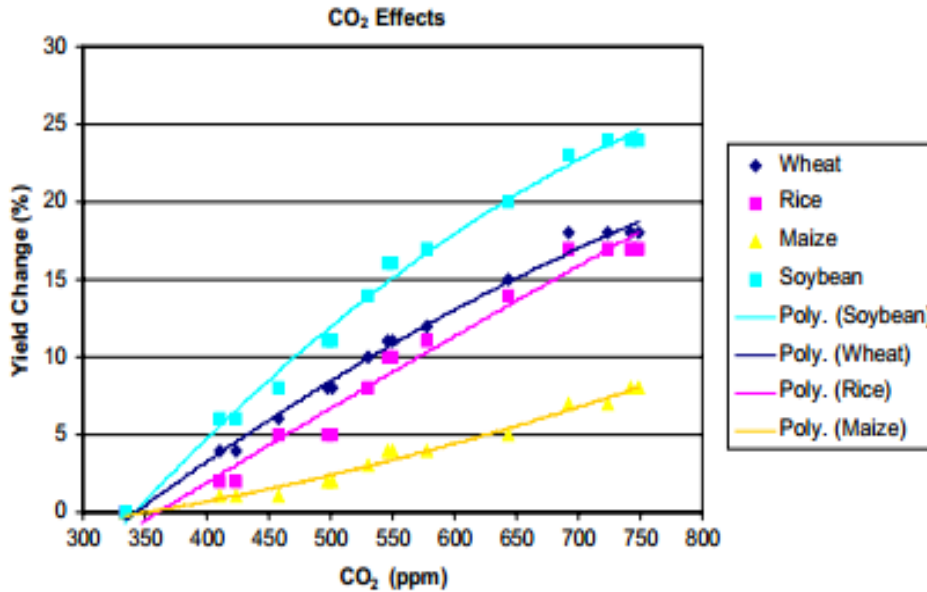


Figure 1-3. Relation between CO₂ concentration and yield changes in some selected crops (by CCSP, 2008)

Various researchers have tried to assess the impact of climate change on water resources. Faramarzi et al. (2013) mentioned the impact of climate change on water resources in Africa. They found an increase of a maximum temperature of between 1° and 3 °C on whole continent. The maximum temperature in South Africa increased more than in Central and West Africa. Abbaspour et al. (2009) revealed an increase of precipitation in the northern and western parts of Iran in the period 2013-2039 by different GCM scenarios. However, the southern part of the country could experience a decrease in precipitation. They also mentioned a decrease of blue water resources from the north to the south and from the west to the east. Actual evapotranspiration slightly decreased in the north and west of Iran owing to the assumption that land use/cover will not change in the future. Vaghefi et al. (2014) assessed the impact of GCMs model in three CO₂ emission scenarios on water resources and wheat yield in the Karkhe river basin in south west Iran. They found that in the northern part of the basin the fresh water availability will increase but in the southern part it will decrease by 44 % for the period 2020-2040. Wu et al. (2012) assess the impact of greenhouse gas emission on the terrestrial hydrologic cycle and water quality in the semi-arid James River Basin (JRB) in

the mid-western United States. They mentioned that the substantial declining of precipitation and rising air temperature by the mid-21st century could lead to a significant reduction in the water yield, soil water content and groundwater recharge.

Hydrological response to climate change has been analyzed by Lirong and Jianyun (2012) in the subtropical monsoon area, Beijiang River Basin, by the SWAT model. They fed 15 set of climate change scenarios into the calibrated hydrological model. Results revealed that when the temperature keeps the same and rainfall increases, ET and water yield will increase. However, when rainfall stays the same and the temperature increases, ET will increase while water yield decreases. The consideration of the potential impact of climate change and global warming is very important for water resource managers, which could put further stress on water availability for human use, the environment or even livestock use on a large scale (Qi et al., 2009).

1-5-3. Water resources in Iran

Iran is located between 25° and 40° north latitude and 44°-63° east longitude. The altitude which varies from -40m in the north to 5,670m in the Alborz ranges in the center of Iran, has a pronounced influence on the climate diversity ranging from a wet to a hyper arid climate. However, Iran has been known as a semi-arid country, and more than 85 percent of territory is located in arid and semi-arid regions. Annual precipitation varies from less than 50 mm in the central desert, in the center of Iran, to more than 2,000 mm in the northern part of country. Nevertheless, the country's annual precipitation is about 250 mm per year, one third of the global average. The fresh water availability for the country is estimated around 2000 m³ per capita per year (Yang et al., 2003), and it may go below 1500 m³ per capita per year by 2030 because of population growth.

Most of the territory suffers from the shortage of water resources. Figure 1-4 shows the distribution of blue water resources (the sum of the river discharge and the deep groundwater recharge) in the period 1980-2002 based on the population of 2005 (Faramarzi et al. 2009). Taking 1700 m³ per capita as the threshold of water scarcity, about 46 million people living on about 59 % of the regions were subjected to water scarcity.

The average water use in the agriculture sector of the world is 70 %, and in developing countries it is 82% (Figure 1-5), but in Iran more than 90 % of the water is used in the agricultural sector in terms of irrigation (Figure 1-6). However, due to the traditional method of irrigation and water conveyer systems, the water use efficiency is less than 35 %, which shows an average efficiency even lower than developing countries (45%), therefore a large amount of water is lost (Abbaspour et al., 2009; Panahi et al., 2009). Nevertheless, Iran has the seventh largest amount of irrigated land in the world (Figure 1-7), and although the irrigated land increased about 17 % from 2003 to 2008, the amount of water is constant. Therefore, more attention on water use efficiency is important and it should be noted for any future planning of the region.

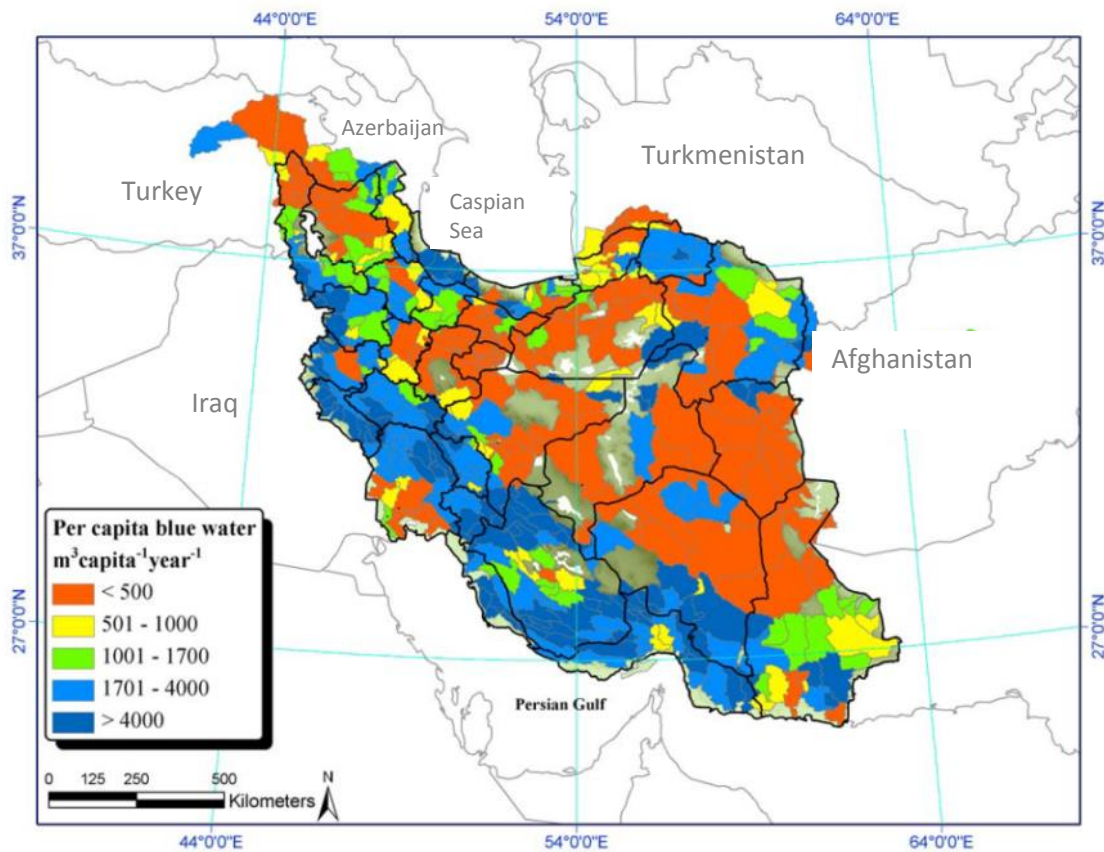


Figure 1-4. Per capita blue water resources distribution in the period of 1980-2002 – derived from (Abbaspour et al. 2009)

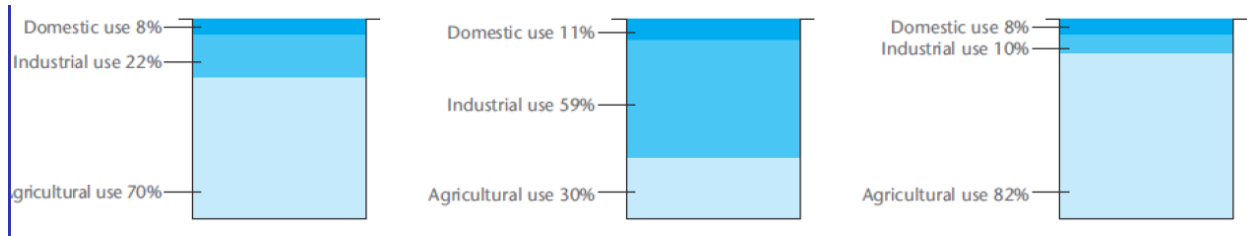


Figure 1-5. Comparing water usage in the world, developing and developed countries (UNESCO, 2003)

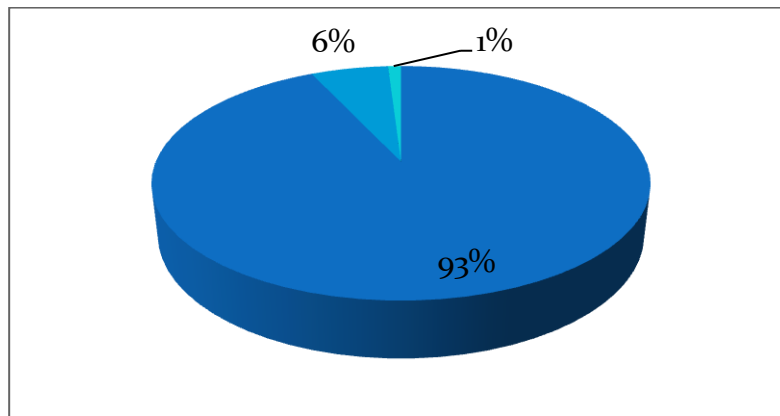


Figure 1-6. Water use in different sectors in Iran, showing huge water consumption in the agriculture sector

#	COUNTRY	AMOUNT	DATE	GRAPH
1	India	663,340 sq km	2008	
2	China	641,410 sq km	2008	
3	United States	230,000 sq km	2008	
4	Pakistan	199,900 sq km	2008	
5	Philippines	152,500 sq km	2008	
6	European Union	131,250 sq km	2003	
7	Iran	87,000 sq km	2009	
8	Indonesia	67,220 sq km	2008	
9	Mexico	64,600 sq km	2009	
10	Thailand	64,150 sq km	2008	

Figure 1-7. Ranking of countries in irrigated agriculture, Iran has the 7th largest amount of irrigated land in the world (<http://www.nationmaster.com>)

1-5-4. Hydrological models

Hydrological models are valuable tools of study in this kind of research (e.g. climate change, water resources). Many studies show the ability of hydrological models to estimate water balance components and climate change assessment (e.g. Stonefelt et al., 2000; Abbaspour et al., 2007; Schuol et al., 2008).

Hydrological models can be classified into deterministic and stochastic approaches. In the deterministic approach, a hydrologic model can be divided into empirical (black box), conceptual (grey box) or physical (white box) based. It can also be grouped into lumped or distributed based models. Stochastic approaches are derived from a time series analysis. Figure 1-8 shows the summary of hydrological classifications.

Empirical models are based on mathematical equations. Constrained Linear Systems (CLS) models (Todini & Wallis, 1977) and the Antecedent Precipitation Index (API) model (WMO, 1994) are examples of empirical models. In Lumped models, for the whole modeled area, the parameters are spatially averaged to one value. The Stanford modeling system (Crawford & Linsley, 1966) and HEC-HMS (U.S. Army Corps of Engineers) are lumped models for instance.

In a distributed model, the parameters vary spatially. MIKE-SHE model (Refsgaard & Storm, 1995), Precipitation runoff modeling system (PRMS) model (Leavesley et al., 1983), and soil and water assessment tools (SWAT) (Arnold et al., 1998) are some examples of these models.

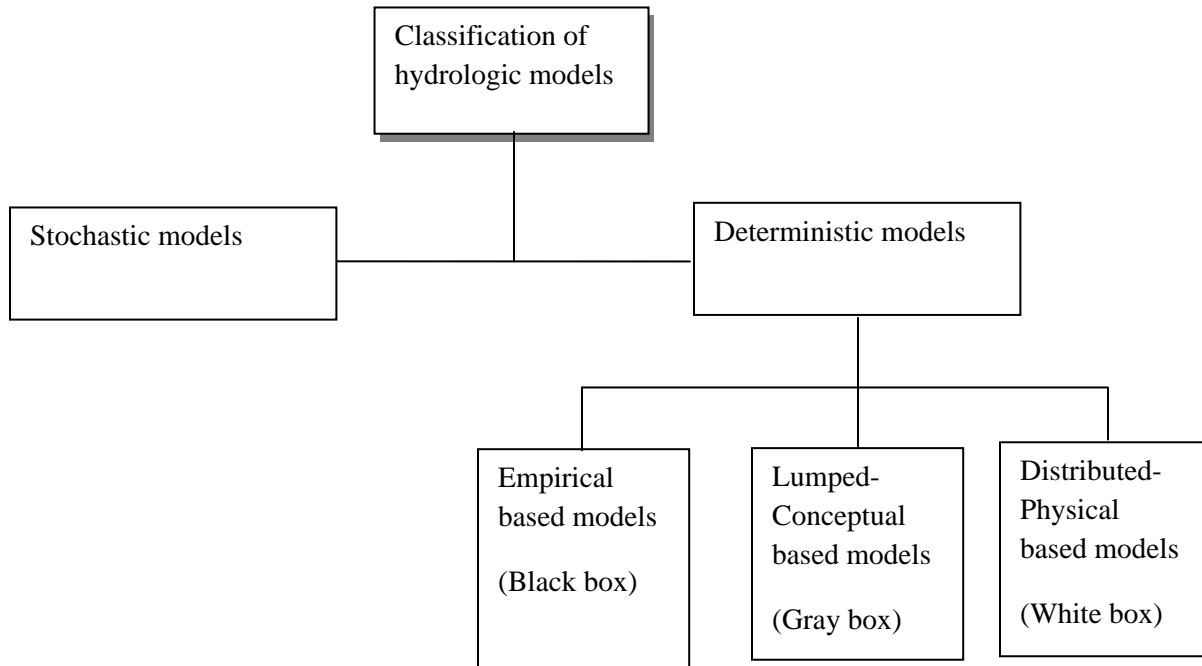


Figure 1-8. The classification of hydrological models (after Refsgaard, 1996; represented by Alkhoury, 2011)

1-5-4-1. Hydrological models and climate change

Various hydrological modeling systems have been widely used in climate change assessment. For instance, HSAMI (Fortin, 2000), a lumped rainfall-runoff model used in a research study in Lawrence, Canada, revealed higher winter discharge under climate change, which may induce modification of hydrology and the geomorphological process to riparian ecosystem (Boyer et al., 2010). The Hydrological Modeling System (HEC-HMS) was applied to the Siruana watershed, Spain and showed that local soil moisture conditions dramatically affect climate change impact on water resources (Candela et al., 2012). The hydrological Simulation Program-Fortan (HSPF) conducted in Western Turkey revealed that seasonal variations of precipitation and temperature are very important in predicting the future response of watersheds (Göncü & Albek, 2010).

Faramarzi et al. (2013) used a soil and water assessment tools (SWAT) model in order to assess the impact of climate change on fresh water availability in Africa and used five GCMs models. The results showed that the mean total quantity of water resources in Africa is likely to increase.

Surfleet et al. (2012) assessed three hydrological models for climate change assessment. They used the VIC model as a large scale approach, the PRMS model as a basin scale approach, and the GSFLOW model as a site-specific approach in different basins in USA. The results showed that appropriate parameterization of a model, estimates of uncertainty and understating the limitation of a model can change the interpretation of climate changes projections.

Bae et al. (2011) used three different hydrological models (PRMS, SLURP and SWAT) for comparing differences of PET response to climate change in the Chungju Dam basin, Korea. In this research, 13 GCM models with three emission scenarios were put into the models. The result showed that during the historical calibration, all hydrological models had a similar performance of runoff simulation, but when future GCM outputs were put into the models different results were obtained. Recently Soil and Water Assessment Tools (SWAT), have been widely used in the assessing of climate change on water resources, stream flow, and water quality (Abbaspour et al. 2009; Kim et al. 2013; Lirong and Jianyun 2012; Luo et al. 2013). In this study, SWAT is selected as a base model to represent the climate change effects on hydrology.

1-5-4-2. SWAT hydrologic model

SWAT is an eco-hydrological model developed by Arnold et al. (1998) to assess the quality and quantity of surface and groundwater and to predict the impact of land use, land management practice and climate change on the environment. It is a physically-based, semi-distributed and a continuous time scale model. One of the advantages of SWAT is that in addition to the hydrological assessment, it can simulate crop growth and production by using an incorporated EPIC model (Sharpley and Williams, 1990) in it. “EPIC (Erosion-Productivity Impact Calculator) was originally developed to simulate the impact of erosion on crop productivity and has now evolved into a comprehensive agricultural management, field scale, nonpoint source loading model” (Neitsch et al., 2009). The various components inside the SWAT model consist of hydrology, sediment, crop growth, agricultural management nutrient, and pesticides. In SWAT, a watershed is divided into sub-basins, which are then further subdivided into hydrological response units (HRUs) with homogenous land use, soil and management characteristics. In each HRU, soil water balance is considered. It contains four storage volumes: snow, the soil profile, the shallow aquifer and the deep aquifer. The soil profile can include

several layers. The soil water process contains infiltration, percolation, evaporation, plant uptake and lateral flow (Neitsch et al., 2009).

The hydrological process simulates surface runoff using SCS curve number or Green-Ampt infiltration equation (see Neitsch et al., 2009 for more information). Percolation simulates with a layered storage routing technique combined with a crack flow model. Potential evapotranspiration can be estimated by the Hargreaves, Priestley-Taylor or Penman-Monteith methods. The SWAT model can also simulate erosion from the watershed using Modified Universal Soil Loss Equation (MUSLE) (Arnold et al., 1998).

1-5-5. Remote sensing and GIS in hydrological modeling

Nowadays, remote sensing has been used as an important source of data and information for hydrological modeling (Engman & Gurney, 1991). Remote sensing has a potential to estimate or to spatially measure precipitation, snow cover, evapotranspiration, runoff, soil moisture, and water quality. Furthermore, satellite images can provide information about watershed properties (e.g. topography, stream network properties).

Precipitation is a key variable in the hydrological cycle and remote sensing has the potential to provide precipitation estimation where rain gage observations are limited. There are numerous remotely sensed methods to estimate the precipitation (e.g. Microwave-link methods). Nevertheless, remote sensing can contribute to estimate evapotranspiration. MODIS long-term data is useful data to estimate evapotranspiration temporally. Surface energy balance techniques have already been used to estimate actual evapotranspiration by the remote sensing process. Bastiaansen et al. (1998) developed SEBAL model (Surface energy balance algorithm for land) to estimate actual evapotranspiration. In SEBAL all satellite images with thermal band (e.g. MODIS, ASTER, LANDSAT), can be used. The accuracy of ET_a estimated by SEBAL is compared with lysimeter data, which shows a high accuracy of estimated ET_a by satellite images. The SEBAL model was used in different areas (Bandara, 2006; Alexandridis, 2003; Tasumi et al., 2000). Allen et al. (2007) developed a METRIC model as a variant of SEBAL in Idaho.

Furthermore, the geographical information system (GIS) is widely used with remote sensing. GIS can analyze different sorts of data with the same geographic situation. Remote sensing can provide required data for GIS, and then all analyses can be done in the GIS. Nowadays, many hydrological models have interfaced with GIS in order to analyze the data more easily. ArcSWAT is a SWAT interface with ArcGIS and provides more facilities for a hydrologist to deal with the hydrological problems. For example, spatial data such as DEM, soil and land use can feed into the interface model through the GIS.

1-6. References

- Abbaspour KC, Faramarzi M, Ghasemi SS, Yang H (2009) Assessing the impact of climate change on water resources in Iran. *Water Resources Research* 45.
- Abbaspour KC, Yang J, Maximov I, Siber R, Bogner K, Mieleitner J, Zobrist J, Srinivasan R (2007) Modelling hydrology and water quality in the pre-alpine/alpine Thur watershed using SWAT, *Journal of Hydrology* 333: 413– 430.
- Alexandridis T (2003) Scale effect on determination of hydrological and vegetation parameters using remote sensing techniques and GIS. PhD Thesis. Aristotle University of Thessalonikh, Greece
- Alkhoury W (2011) Hydrological modeling in the meso scale semiarid region of Wadi Kafrein / Jordan. A PhD thesis. University of Goettingen, Germany.
- Allen R, Tasumi M, Trezza R (2007) Satellite-Based Energy Balance for Mapping Evapotranspiration with Internalized Calibration (METRIC)—Model. *Journal of Irrigation and drainage engineering* 133 (4):15. doi: 10.1061//asce/0733-9437/2007/133:4/380.
- Anyamba A, Tucker CJ, Eastman JR (2001) NDVI anomaly patterns over Africa during the 1997/98 ENSO warm event. *International Journal of Remote Sensing* 22: 1847-1859.

- Arnold JG, Srinivasan R, Muttiah RS, Williams JR (1998) Large area hydrologic modeling and assessment—Part 1: model development. *Journal of American Water Resources Association* 34:73–89
- Bae D-H, Jung I-W, Lettenmaier DP (2011) Hydrologic uncertainties in climate change from IPCC AR4 GCM simulations of the Chungju Basin, Korea. *Journal of Hydrology* 401: 90-105
- Bandara KMPS (2006) Assessing irrigation performance by using remote sensing / Doctoral thesis, Wageningen University, Wageningen, The Netherlands
- Bastiaanssen WGM, Menenti M, Feddes RA, Holtslag AAM (1998) A remote sensing surface energy balance algorithm for land (SEBAL). 1. Formulation. *Journal of Hydrology* 212-213:198–212.
- Boyer C, Chaumont D, Chartier I, Roy AG (2010) Impact of climate change on the hydrology of St. Lawrence tributaries. *Journal of Hydrology* 384(1–2):65–83.
- Candela L, Tamoh K, Olivares G, Gomez M (2012) Modelling impacts of climate change on water resources in un-gauged and data-scarce watersheds, Application to the Siurana catchment (NE Spain). *Science of the Total Environment* 440:253–60.
- CCSP (2008) *The Effects of Climate Change on Agriculture, Land Resources, Water Resources, and Biodiversity in the United States*. A Report by the U.S. Climate Change Science Program and the Subcommittee on Global Change Research.
- Crawford N, Linsley R (1966) Digital simulation in hydrology, Stanford watershed model IV. Technical report 39. Department of Civil Engineering, Stanford University.
- Engman ET, Gurney RJ (1991) *Remote sensing in hydrology*. Chapman and Hall.
- FAO (2011) *The state of the world's land and water resources for food and agriculture (SOLAW)-Managing systems at risk*. Rome:Food and Agriculture Organization of the United Nation, London:Earthscan.

- Faramarzi M (2010) Assessment of regional water endowments, crop water productivity, and implications for intra-country virtual water trade in Iran. A PhD thesis. ETH University, Switzerland.
- Faramarzi M, Abbaspour KC, Schulin R, Yang H (2009) Modelling blue and green water resources availability in Iran. *Hydrological Processes* 23: 486-501.
- Faramarzi M, Abbaspour KC, Ashraf Vaghefi S, Farzaneh MR, Zehnder AJB, Srinivasan R, Yang H (2013) Modeling impacts of climate change on freshwater availability in Africa. *Journal of Hydrology* 480: 85-101.
- Fortin V (2000) Le modèle météo-apport HSAMI: historique, théorie et application. Institut de recherche d'Hydro-Québec, Varennes, Canada, 68p.
- Göncü S, Albek E (2010) Modeling climate change effects on streams and reservoirs with HSPF. *Water Resources Management* 24(4):707–26.
- IPCC (2001) In: Houghton JT, Ding Y, Griggs DJ, Noguer M, van der Linden P J, Dai X, Maskell K, Johnson CA (Eds.), *Climate Change 2001: The Scientific Basis, Contributions of Working Group 1 to the Third Assessment Report of the Intergovernmental Panel on Climate Change*, Cambridge University Press, Cambridge, UK
- Kim J, Choi J, Choi C, Park S (2013) Impacts of changes in climate and land use/land cover under IPCC RCP scenarios on streamflow in the Hoeya River Basin, Korea. *Science of the Total Environment* 452-453: 181-195.
- Lambin EF, Ehrlich D (1996) The Surface Temperature-Vegetation Index Space for Land Cover and Land-Cover Change Analysis. *International Journal of Remote Sensing* 17: 465-487.
- Leavesley GH, Lichty RW, Troutman BM, Saindon LG (1983) *Precipitation-runoff modeling system-User's manual*: U.S. Geological Survey Water-Resources Investigations Report 83-4238, 207 p. http://wwwbrr.cr.usgs.gov/projects/SW_MoWS/PRMS.htm.

- Lirong S, Jianyun Z (2012) Hydrological Response to Climate Change in Beijiang River Basin Based on the SWAT Model. *Procedia Engineering* 28: 241-245
- Luo Y, Ficklin DL, Liu X, Zhang M (2013) Assessment of climate change impacts on hydrology and water quality with a watershed modeling approach. *Science of the Total Environment* 450-451: 72-82
- Neitsch SL, Arnold JG, Kiniry JR, Williams JR, King KW (2009) Soil and water assessment tool. Theoretical documentation. TWRI TR-191. College Station, Texas: Texas Water Resources Institute.
- Olsson L, Eklundh L, Ardo J (2006) A recent greening of the Sahel trends, patterns and potential causes. *Journal of Arid Environment* 63: 556-566.
- Panahi F, Malekmohammadim I, Chizari M, Samani JMV (2009) The Role of Optimizing Agricultural Water Resource Management to livelihood Poverty abolition in Rural Iran. *Australian Journal of Basic and Applied Sciences* 3(4): 3841-3849.
- Qi S, Sun G, Wang Y, McNulty SG, Moore Myers JA (2009) Streamflow response to climate and landuse changes in a coastal watershed in North Carolina. *Transactions ASABE*, 52
- Refsgaard JC (1996) Terminology, modelling protocol and classification of hydrological model codes. In (Eds.): M.B. Abbot and J.C. Refsgaard: *Distributed Hydrological Modelling*, pp. 17-39. Kluwer Academic Publishing. The Netherlands.
- Refsgaard JC, Storm B (1995) MIKE SHE. In (Ed.): Singh VP: *Computer Models of Watershed Hydrology*, Water Resources Publications, Colorado, USA, pp. 809–846.
- Schuol J, Abbaspour KC, Srinivasan R, Yang H (2008) Estimation of freshwater availability in the West African sub-continent using the SWAT hydrologic Model. *Journal of Hydrology* 352: 30– 49.
- Schwilch G (2012) A process for effective desertification mitigation. PhD thesis. Wageningen University.p.178.

- Sharpley AN, and Williams JR (1990) EPIC-Erosion Productivity Impact Calculator, 1. model documentation. U.S. Department of Agriculture, Agricultural Research Service, Tech. Bull. 1768.
- Singh RD, Kumar CP (2010) Impact of climate change on groundwater resources. 332-350. 2nd National Ground Water Congress. http://www.angelfire.com/nh/cpkumar/publication/CC_RDS.pdf
- Stonefelt MD, Fontaine TA, Hotchkiss TH (2000) Impacts of climate change on water yield in the Upper Wind river basin. *Journal of American Water Resources Assessment* 36: 321– 336.
- Surfleet CG, Tullos D, Chang H, Jung I-W (2012) Selection of hydrologic modeling approaches for climate change assessment: A comparison of model scale and structures. *Journal of Hydrology* 464-465: 233-248.
- Tasumi M, Bastiaanssen WGM, Allen RG (2000) Application of the SEBAL methodology for estimating consumptive use of water and stream flow depletion in the Bear River Basin of Idaho through Remote Sensing. EOSDIS Project Report, Raytheon Systems Company and the University of Idaho, USA.
- Todini E, Wallis J (1977) Using CLS for daily or longer period rainfall-runoff modelling. In (Eds): T. Ciriani, U. Maione and J. Wallis: *Mathematical Models for Surface Water Hydrology*. John Wiley & Sons. New York.
- U.S. Census Bureau: <http://www.census.gov/population/international/data/idb>
- UNCCD (2013) A Stronger UNCCD for a Land-Degradation Neutral World, Issue Brief, Bonn, Germany.
- UNESCO (2003) Water for people, water for life. United Nations World Water Development Report. www.unesdoc.unesco.org

- Vaghefi S, Abbaspour K, Mousavi SJ, Srinivasan R, Yang H (2014) Analyses of the impact of climate change on water resources components, drought and wheat yield in the semi-arid Karkheh River Basin in Iran. *Hydrological process* 28(4): 2018-2032.
- WMO (1994) *Guide to Hydrological Practices: Data Acquisition and Processing, Analysis, Forecasting and Other Applications*, WMO-No. 168, Fifth edition.
- Wu Y, Liu S, Gallant AL (2012). Predicting impacts of increased CO₂ and climate change on the water cycle and water quality in the semiarid James River Basin of the Midwestern USA. *Sciences of the Total Environment* 430: 150-160
- Xiao J, Moody A (2004) Trends in vegetation activity and their climatic correlates: chin 1982 to 1998. *International Journal of Remote Sensing* 20: 5669-5689.
- Yang H, Reichert P, Abbaspour KC, Zehnder AJB (2003) A water resources threshold and its implications for food security. *Environmental Science and Technology* 37: 3048-3054.

Study area

As characteristics in some parts of the study area were not well defined and the future chapters are based on the paper publications, I have tried here to describe them in more detail.

2-1. Climate data and TLAP and PLAPS calculations

To use the weather data in the hydrological model, we selected 25 rain gages, synoptic and climatology stations. Among all, SWAT just used 9 rain gage, synoptic and climatology stations based on the nearest distance of centroid of sub-basins to the stations (Figure 2-1). The mean annual precipitation and temperature including altitude of stations is summarized in Table 2-1.

Table 2-1. Climate stations include mean annual precipitation and temperature

Station	Latitude	Longitude	Elevation(m)	Mean annual Precipitation(mm)	Mean annual Temperature(°C)
Sarab-khomigan	35.371111°N	49.021394°E	1868	280	-
Zehtaran	35.257219°N	49.134166°E	1770	257	-
Khanabad	35.236944°N	49.51°E	1836	332	-
Famenin	35.099998°N	48.9666659°E	1660	262	-
Omarabad	35.090001°N	49.241662°E	1620	248	-
Ghahavand	34.861668°N	49.003335°E	1625	232	-
Damagh	35.433327°N	48.816662°E	1790	311	-
Hamedan	34.849992°N	48.533331°E	1749	308	11.7
Nozheh	35.199998°N	48.683327°E	1679	327	11.2
Dargazin	35.349999°N	49.066661°E	1870	360	11.4

One of the important parameters in the SWAT model is the interval rate for temperature [$^{\circ}\text{C}/\text{km}$] (TLAPS) and precipitation [$\text{mm H}_2\text{O}/\text{km}$] (PLAPS) which can have a significant affect on precipitation and temperature in a mountainous area. As the Razan-Ghahavand basin is surrounded by mountains, especially in the northern basin, we wanted to understand the rate of change of precipitation and temperature with the rise in elevation of this area.

Generally, the temperature can decrease 6 °C per kilometer related to vertical movement and increase in altitude. Owing to paucity of temperature stations in the study area, we used TLAP equal to 6 °C. This value was also used in the surface energy balance model in order to estimate actual evapotranspiration in the mountainous area based on the METRIC equations presented by Allen et al. (2007). However, PLAPS was created by rain gage data (10 stations). Generally, with the increase of altitude, the precipitation also increases with optimum elevation, which is about 2,850 m in the study area (Mahdavi, 2011).

The relation between precipitation and altitude shows an increase in precipitation. According to the equation, the PLAPS is equal to 283 mm (Figure 2-2). This rate was used in the SWAT model in order to precisely estimate precipitation in the mountainous parts of the basin.

2-2. Hydrometric stations and hydrographs of rivers

There are three hydrometric stations inside the basin, namely Omarabad, Sirab-Khomigan and Zehtaran. Therefore, the basin is delineated into three parts based on the area covered by hydrometric stations. Each hydrometric station controls a specific area. Table 2-2 shows the area that drains into each hydrometric station. Also, there is one hydrometric station outside the basin (Koshk-abad), which can be used to estimate the rate of discharge into the basin (Figure 2-3). Koshk-Abad station is used as an inlet in the SWAT model. The mean annual discharge at the Koshk-Abad hydrometric station is $2.25 \text{ m}^3\text{s}^{-1}$ based on a period of 30 years.

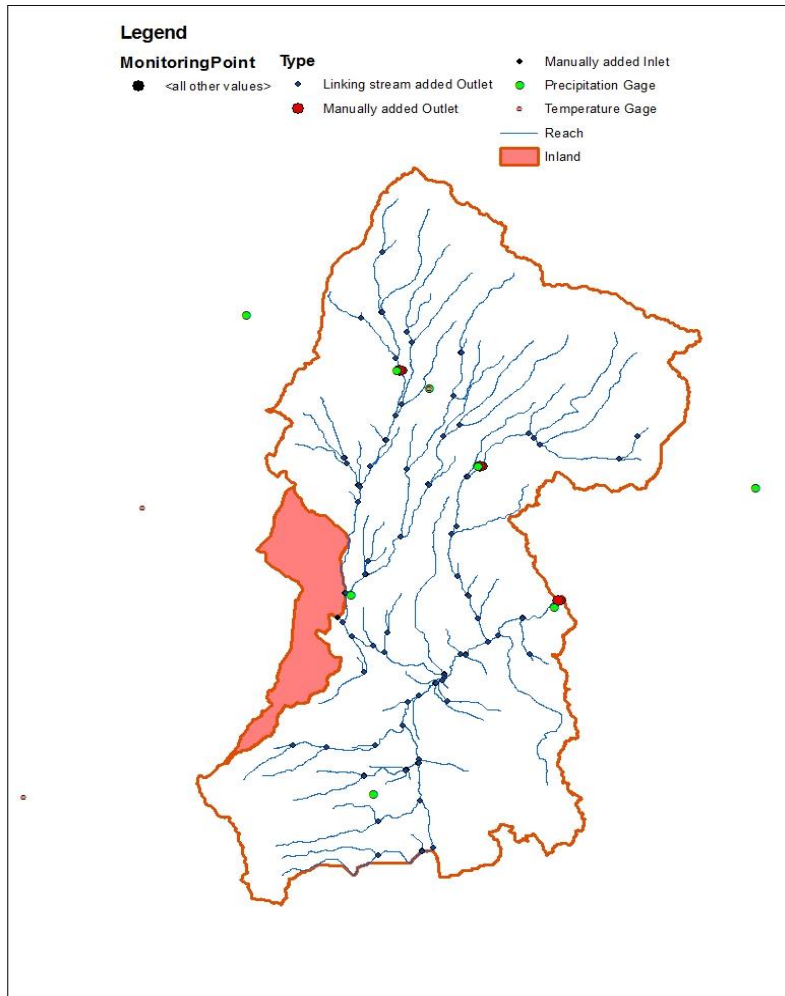


Figure 2-1. The meteorological stations in and around the basin

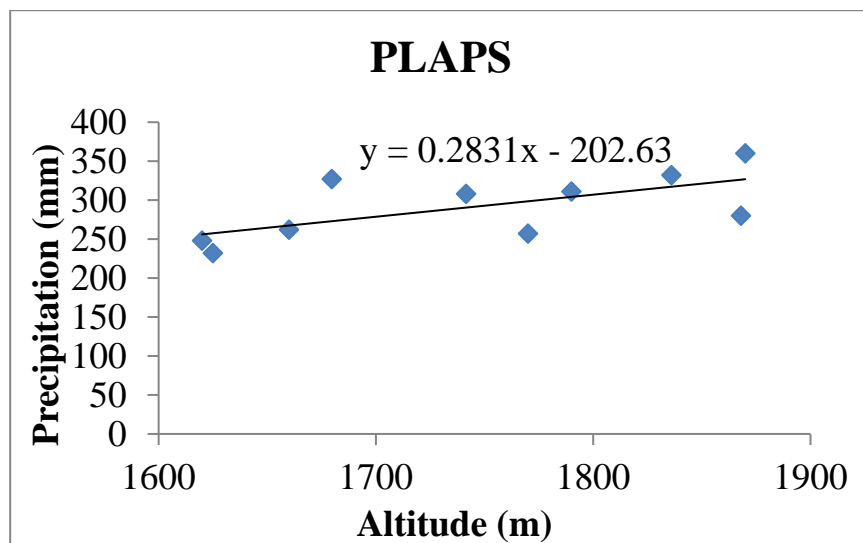


Figure 2-2. The PLAPS estimation in the study area

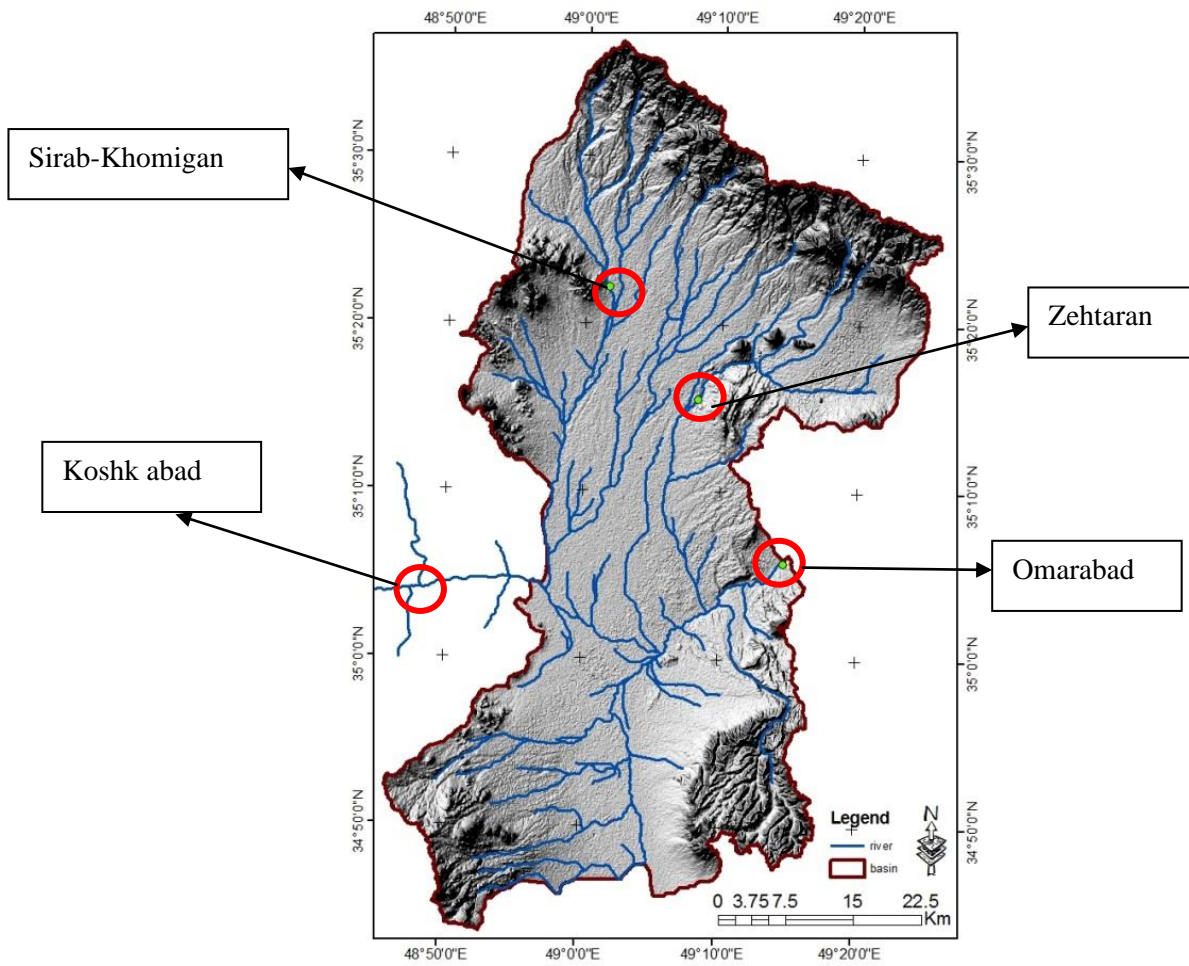


Figure 2-3. The position of hydrometric stations inside and outside the basin

Table 2-2. The area covered by each hydrometric station including the numbers of sub-basins

Stations	Sub basins*	Area(km ²)
14	1,2,3,4,5,6,12,13,14	255
41	23,26, 27,28,29,32, 33, 34, 37,38,41	420
71	The rest subbasins	2425

*The whole basin is delineated into 138 subbasins.

- Omarabad hydrometric station:

This station is located at the outlet of the basin on the Gharehchay River. The geographical position is $35^{\circ} 5' 46''$ latitude and $49^{\circ} 14' 31''$ longitude. The altitude of the station is 1,590 m. This station controls the whole hydrological process in the basin. Gharehchay River is the main river in the basin with a $6.68 \text{ m}^3\text{s}^{-1}$ mean annual discharge at this outlet. Figure 2-4 shows the hydrograph of the river at this station. The figure shows some flood events, which reveal a peak flow of more than $40 \text{ m}^3\text{s}^{-1}$. The highest peak flow was in 1980 with $80 \text{ m}^3\text{s}^{-1}$. The events in recent years (after 1997) seems lower than in previous years. However, snowmelts runoff are the most common type of flooding, which occurs through early spring in the basin. Figure 2-5 shows some photos of Gharehchay River and include the hydrometric station.

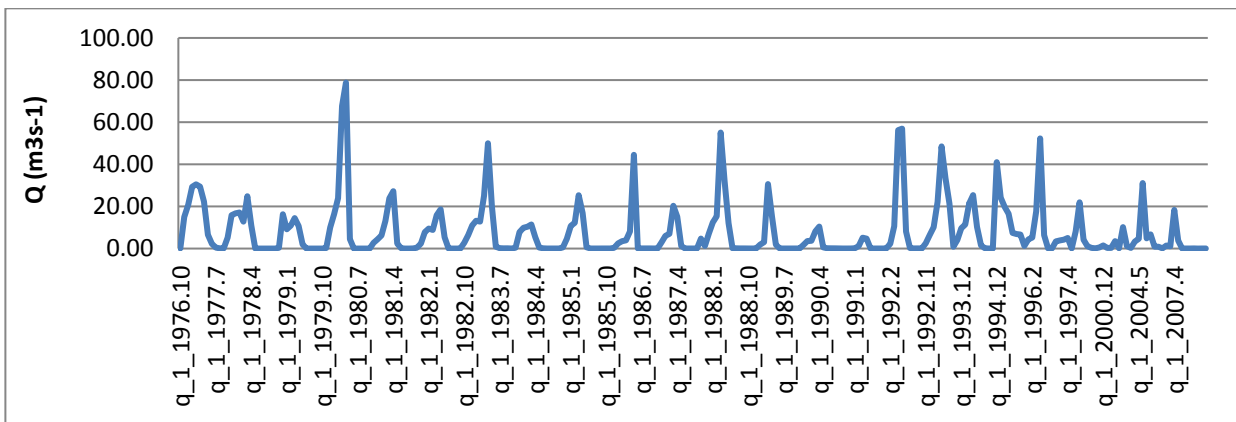


Figure 2-4. Gharehchay River discharge at the Omarabad outlet



Figure 2-5. The view of Gharehchay River including the Omarabad hydrometric station

- Zehtaran hydrometric station:

Zehtaran hydrometric station is located at the Zehtaran River in the east of the basin. The geographical position is $35^{\circ} 15' 35''$ latitude and $49^{\circ} 08' 06''$ longitude. The altitude of the station is 1,760 m. This station roughly controls 420 km^2 of the area in the east of the basin. The mean annual discharge at this outlet is $0.66 \text{ m}^3\text{s}^{-1}$. Figure 2-6 shows the hydrograph of Zehtaran River at the outlet of Zehtaran from 1977 to 2008. The highest peak flow during this time is no more than $3 \text{ m}^3\text{s}^{-1}$. Same as with the Omarabad station, the hydrological characteristics of this river after 1997 also changed, probably due to anthropogenic factors. Figure 2-7 shows some photos of Zehtaran River and include the relevant hydrometric station.

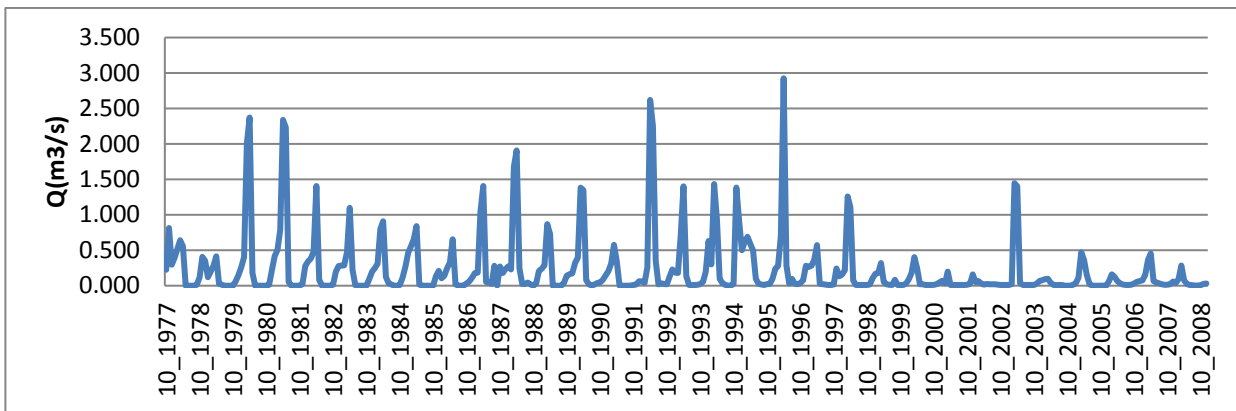


Figure 2-6. Zehtaran River discharge from 1977 to 2008



Figure 2-7. The view of Zehtaran River with the hydrometric station. The irrigation channels could change the hydrological characteristics in the basin.

- Sirab-Khomigan hydrometric station:

Sirab-Khomigan hydrometric station is located at the Sirab-Khomigan River in the west of the basin. The geographical position is $35^{\circ} 22' 13''$ latitude and $49^{\circ} 01' 41''$ longitude. The altitude of the station is 1,860 m. This station controls approximately 255 km^2 of area in the west of the basin. The mean annual discharge at this outlet is $0.33 \text{ m}^3 \text{ s}^{-1}$. Figure 2-8 shows the hydrograph of Sirab-Khomiagan River at the outlet from 1977 to 2008. The highest peak flow during this time is lower than $4 \text{ m}^3 \text{ s}^{-1}$. As with the two previous stations, the hydrological characteristics of this river changed after 1997. Figure 2-9 shows some landscape of the Sirab-Khomigan River.

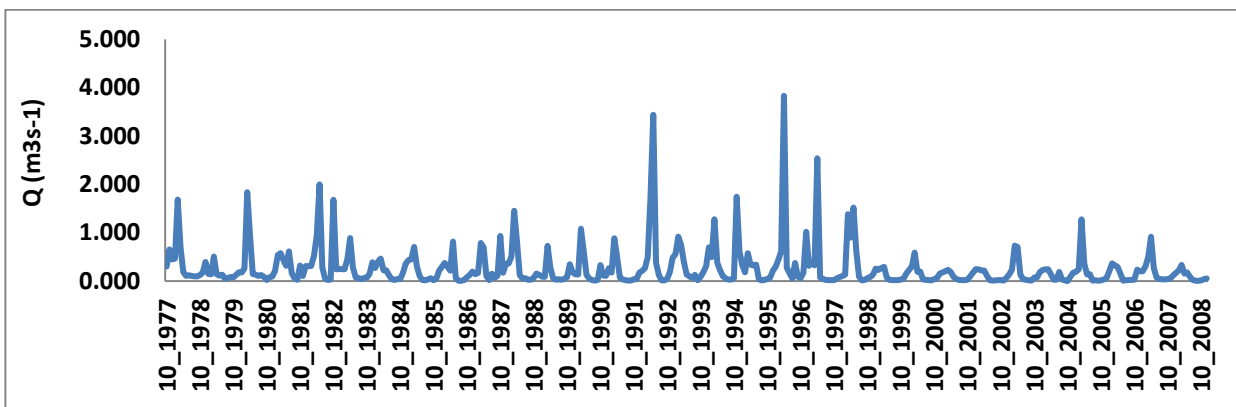


Figure 2-8. Sirab-Khomigan River discharge since 1977



Figure 2-9. The view of Sirab-Khomigan River

- Select of the calibration and validation periods

To choose the duration of calibration and validation, the characteristics of hydrographs in the basin was assessed. Figure 2-10, Sirab-khomigan's discharge, revealed two different

hydrological conditions, part I and II , from 1977 to 2008. The reason for this variation is probably due to some anthropogenic activities like irrigation channels to convey surace runoff, and also due to the decrease in precipitation and drought in recent years. As the characteristics of calibration and validation periods should have the same hydrological condition, the duration from 1997 to 2008 was selected as a whole for the temporal assessment period.

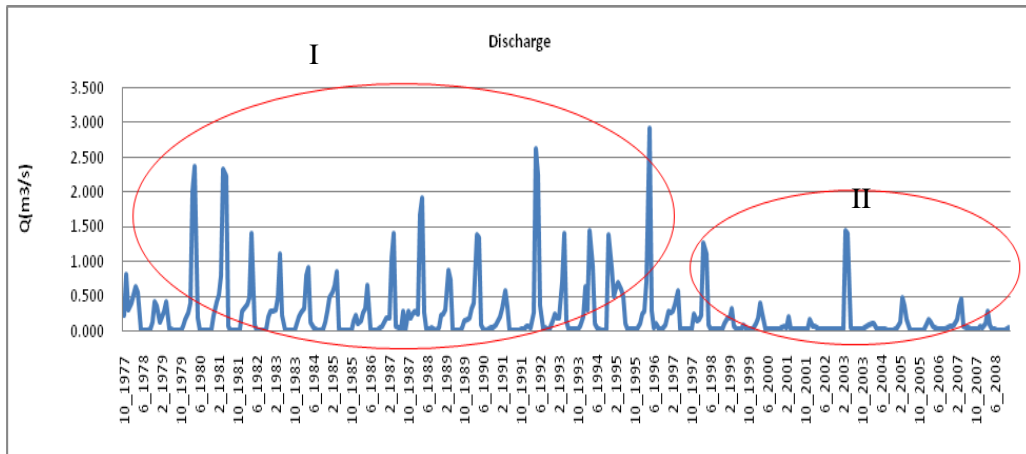


Figure 2-10. Different hydrological charachteristics in the hydrological process of the basin (e.g. Sirab-Khomigan River discharge)

2-3. Geology and stratigraphy

Razan-Ghahavand is located in the Zagros geological zone. Razan-Ghahavand has specific conditions of bedrock which are the main cause of karst development. The thickness of alluvial fan in this area varies from 20 m to 120 m. The first layer of alluvial fan is clay and silt, after that sand and silt are deposited respectively. The lime bedrock with a thin layer of marly and high $CaCO_3$ is apparent at the end of the alluvial fan in the west of the area, the place with sinkhole and land subsidence phenomena which belongs to the Eligomiosen duration.

Figure 2-11 and Table 2-3 show the geological map and related information, respectively. Geologically, the plain can be divided into two parts, north and south. The northern part of the plain consists of young alluvial trace deposits and the southern part includes old alluvial trace deposits. The northern area consists of sandstone and shale and in some parts dactic and andestic volcanics are apparent. In the south west of the area there is bedded reefal limestone, while in the south east sandstone is evident. The west of the area is comprised of limestone.

Table 2-3 -Geological units in the study area

Symbol	Geological description
EK	Well bedded , green tuff and tuffaceous shale (KARAJ FM)
Etvav	Dacitic tuff
Evai	Dacitic and andesitic volcanic
JSS	Sandstone
K1aml	Grey , thick - bedded to massive orbitolina limestone
K1c	Sandstone and conglomerate
K1dz	Marl, shale, sandstone and limestone (Darreh - Zanjir Fm .)
K1l	Thick-bedded to massive, white to pinkish, orbitolina bearing limestone (TIZKUH FM.)
L1m	Limestone , argillaceous limestone ; tile red sandstone and gypsiferous marl
OMI	Massive to thick - bedded reefal limestone
OMml	Limestone
OMviv	Andestic volcanic
Oiiv	Durite
Phh	Phyllite, slate and meta-sandstone (Hamadan Phyllites)
Qt1	High level piedmont fan and valley terraces deposits
Qt2	Low level piedmont fan and valley terraces deposits

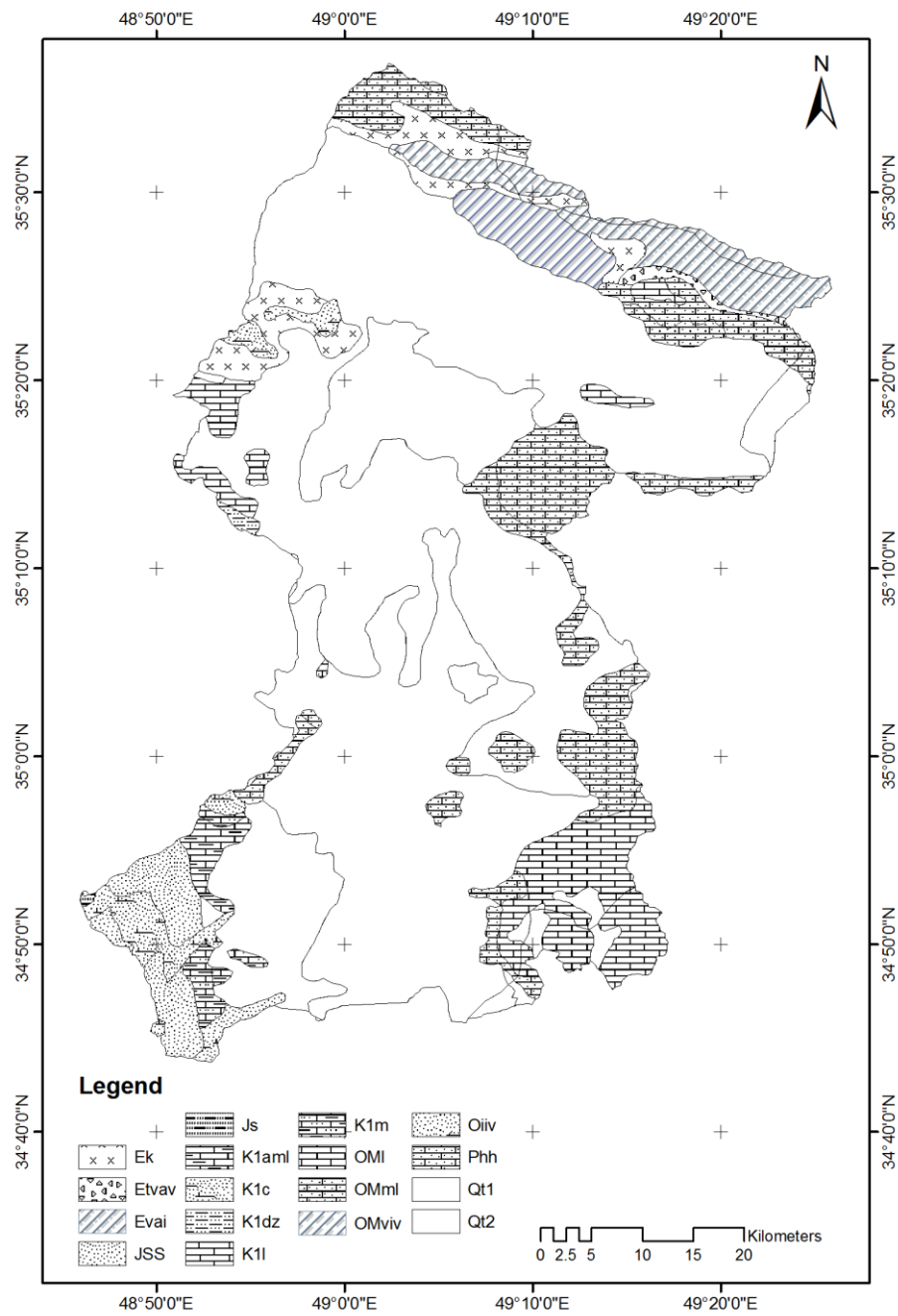


Figure 2-11. Geology map of the Razan-Ghavand area

2-4. References:

- Allen RG, Tasumi M, Trezza R (2007) Satellite-Based Energy Balance for Mapping Evapotranspiration with Internalized Calibration (METRIC)—Model. *Journal of Irrigation and drainage engineering* 133 (4):15.
- Geological Survey of Iran Organization (GSI), Geological data
- Hamedan Regional Water Co. (HMRW), Hydrological data
- Iran Water Resources Management Company (IWRMC), River discharge data
- Meteorological Organization (WSIMO), Meteorological data
- Mahdavi M 2011 *Applied hydrology*. 9th edition, Tehran University Press.
- National Cartographic Center of Iran (NCC), Topographical data

Simulation of water balance components in a watershed located in central drainage basin of Iran¹

3-1-Introduction

Water scarcity is one of the main problems in arid and semiarid regions. In Iran as a semiarid country, water resources have experienced raising pressures due to increasing demand and recurrent droughts. Considering climate change as projected by IPCC (IPCC, 2013) Iran faces severe water shortages in the next decades. Furthermore, the fresh water of the Razan-Ghahavand watershed is exploited by Iran in ever-increasing demand for sanitation, drinking, manufacturing and agriculture. Successful management of any resources requires accurate knowledge of the resource available, the uses to which it may be put, the competing demands for the resource. Therefore, estimation of water balance is critical for water management and development planning in watersheds. Understanding of the water balance in the basin is necessary to achieve sustainable water management.

The water balance is defined as “the balance between incoming water from precipitation and snowmelt and outgoing water by evapotranspiration, groundwater recharge and stream flow” (Dunne, 1978). Figure 3-1 shows the water balance concept.

The main objective of this research is to assess the temporal and spatial variation of water resources in the semiarid river Razan-Ghahavand watershed based on hydrologic modeling. The second objective is to calibrate, validate, uncertainty and sensitivity analysis of SWAT hydrologic model of Razan-Ghahavand basin based on river discharge. Finally, the calibrated hydrologic model is used for climate change and land use change assessment.

¹ This paper is published as a chapter book in “Remote Sensing of the Terrestrial Water Cycle” (V. Lakshmi, ed.). American Geophysical Union (AGU). Wiley & Sons, Inc.

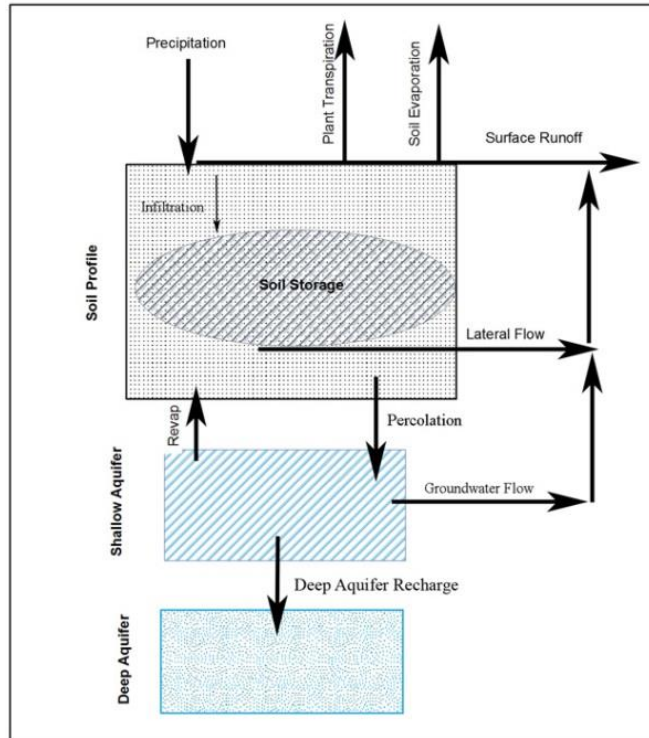


Figure 3-1. Water balance concept

3-2-Material and Methods

3-2-1- Study area

The study area is a watershed called Razan-Ghahavand with a surface area about 3100 km² which is located in a central drainage basin of Iran (Figure 3-2). The difference between minimum and maximum elevation is 1265 meter with a maximum altitude of 2842 m and a minimum altitude of 1577 m. The watershed of Razan-Ghahavand can be seen as a representative case study in comparison to other watersheds in the central drainage basin of Iran. The watershed is not located at the headwater of the basin. The main river called Gharehchay, enters the watershed from an eastward direction and exits the watershed in a westward direction. Simultaneously, two branches (Sirab Khomigan and Zehtaran) of reach drain water enter the main river from north. The climate in this area is semiarid with an average annual precipitation about 290 mm and a mean annual temperature about 11 C. Most of the area is allocated by rangelands with different animal stocking capacity. Arable land (e.g. wheat, alfalfa, etc.) is located in the center of basin and covers 30% of the watershed. Groundwater is the main source

of irrigation in this part of watershed. According to the Soil Taxonomic classification (Soil Survey Staff, 2010), Aridisols and Entisols with typical Haplocalcids and lithic Xerorthents are the most frequent soils in the watershed. The soil moisture regimes inside the area vary from weak aridic to xeric, whereat the soil temperature regime of the area is mesic. Figure 3-2 shows the rain gages, synoptic and hydrometric stations in the basin. Table 3-1 shows the characteristics of weather stations. Characteristics of soil's properties are shown in Table 3-2.

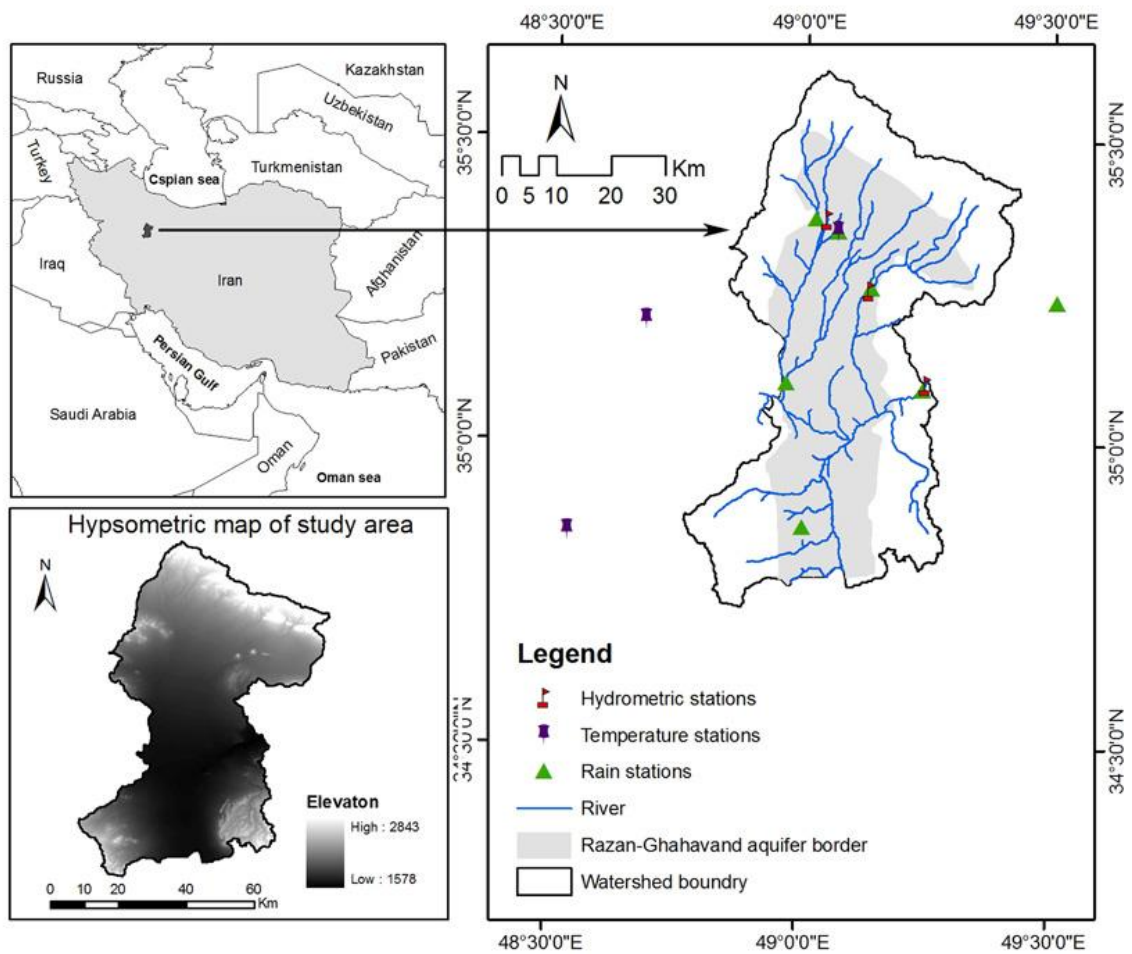


Figure 3-2. Razan-Ghahavand study area

Table 3-1. Overview of weather data availability

No.	Type	Name	Range of data availability	Time scale
1	Rain gage station	Sarab-khomigan	1976-2008	Daily
2	Rain gage	Zehtaran	1982-2008	Daily
3	Rain gage	Khanabad	1983-2008	Daily
4	Rain gage	Famenin	1991-2007	Daily
5	Rain gage	Omarabad	1984-2008	Daily
6	Rain gage	Ghahavand	1982-2008	Daily
7	Rain gage	Damagh	1990-2008	Daily
8	Synoptic station	Hamedan	1979-2008	Daily
9	Synoptic station	Nozheh	1976-2008	Daily
10	Climatology station	Dargazin	1976-2008	Daily

Table 3-2. Soil characteristics in different land types ^a

ID	Soil Class	HYD GRP	Soil depth (mm)	Texture ^b	Layer 1			Layer 2			Layer 3			Layer 4			Layer 5		
					Depth	SOL_BD	SOL_K	Depth	SOL_BD	SOL_K	Depth	SOL_BD	SOL_K	Depth	SOL_BD	SOL_K	Depth	SOL_BD	SOL_K
1	I	B	100	SaL	0-100	1.45	9.5												
2	II	B	500	SiL-L	0-15	1.37	10.7	15-50	1.43	10.9									
3	III	A	1300	L-SiCL-SiCL_SiC	0-19	1.34	5.9	19-39	1.3	4.2	39-84	1.27	2.9	84-130	1.23	2.8			
4	IV	A	1100	L-SaCL-CL-L	0-10	1.42	7.3	10-26	1.38	4.1	26-46	1.32	2.7	46-110	1.35	5.2			
5	V	B	1000	SiCL-SiCL-L	0-13	1.28	4.7	13-40	1.27	3.1	40-100	1.38	5.7						
6	VI	C	1200	SiCL-SiC-SiC-	0-18	1.27	5.2	18-68	1.22	2.9	68-120	1.21	2.8						
7	VII	C	1000	SiCL-SiC-SiC-SiC-	0-13	1.26	4.2	13-36	1.23	3	36-66	1.21	2.7	66-100	1.24	3.1			
8	VIII	D	1450	L-CL-C-SiCL-C	0-11	1.35	5.1	11-30	1.31	2.9	30-60	1.24	2.1	60-117	1.27	3.3	117-145	1.2	2.2
9	IX	C	840	CL-CL-CL-CL-	0-10	1.34	4.9	10-25	1.29	2.6	25-54	1.29	2.5	54-84	1.31	2.4			
10	X	D	1500	CL-C-C-C-C	0-10	1.36	4	10-30	1.29	1.7	30-60	1.25	2.1	60-120	1.28	1.6	120-150	1.23	2.2
11	XI	C	1200	SiCL-SiC-C-SiL	0-10	1.27	5.3	10-22	1.19	2.8	22-77	1.18	2.9	77-120	1.26	2.7			
12	XII	D	1420	SaL-C-C-SiC	0-20	1.47	10.7	20-34	1.24	1.8	34-83	1.21	2.1	83-142	1.26	3.2			
13	XIII	B	650	SiCL-C-CL-	0-15	1.31	5.9	15-37	1.23	2.4	37-65	1.32	2.6						

^aHYDGRP: Soil hydrologic group ; Depth: Depth of soil layer (cm); SOL_BD: Soil bulk density (g/cm³); SOL_K : Saturated hydraulic conductivity (mm/hr) ;

^bTexture: Sa: Sandy; L:Loamy; Si: Silty, C: Clay (e.g. SiCL: silty clay loam)

3-2-2. Land use mapping

Land use is one of the most important layers in hydrologic models and for the creation of hydrologic response units (HRU). To model surface runoff with the SCS-CN method, which is explained in the section 3-3-3. , land use information is directly needed. Remotely sensed data from Landsat TM (year 2009; source: <http://earthexplorer.usgs.gov/>) are used to derive land use/land cover (LULC) information. Preprocessing is performed with auxiliary data including topographic map information at scale of 1 : 25.000 and ground control points (GCP's) collected by GPS based field studies.

After preprocessing of the remote sensing data such as georeferencing with GCP's and fieldwork to check the various land cover/use in the landscape, a supervised land use classification is created. Figure 3-3 shows photos of typical areas with their dominant land use/cover.

Seven land use/cover classes are defined for supervised classification of the remote sensing data: Agriculture, dry farming, rangeland in good, moderate or poor condition, bare lands and urban areas. Supervised classification using different algorithms is used in order to create the LU-map with highest accuracy. The maximum likelihood classification (MLC) is preferred, which produces a minimum error in classification under the assumption that in each class the spectral data are normally distributed. Generally more spectral confusion is found between various classes: usually there are similar classes with various spectral and different classes with the same spectral content. The capability of MLC in comparison to other algorithms is reported by (Mengistu & Salami, 2007; Reis, 2008; Diallo et al., 2009).

The LU accuracy assessment will be thoroughly implemented by means of the error matrix and Kappa statistics. This is commonly accepted as a standard approach in remote sensing. Error matrices as cross tabulation of the mapped class versus the reference class is used to assess the classification accuracy. Randomly selected points are chosen as a reference class for the accuracy assessment. Overall accuracy, user's and producer's accuracies as well as the Kappa statistics is then derived from the error matrices (Congalton, 2004)

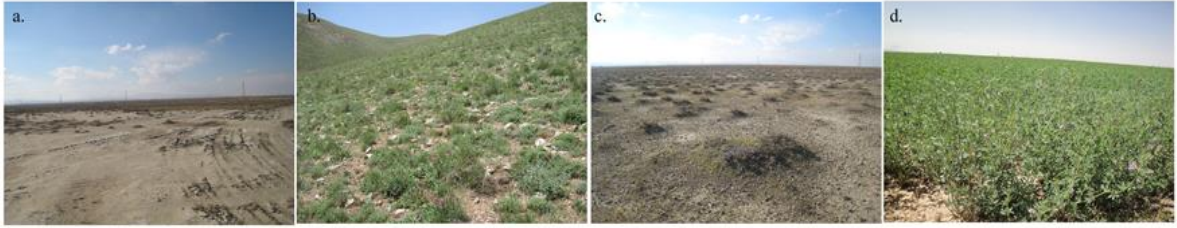


Figure 3-3. Typical land use types inside the watershed: a) bare land, b) rangeland good condition in north watershed, c) rangeland poor condition in south watershed, d) agriculture (e.g. alfalfa)

3-2-3. Hydrological Model

In this study the physical based hydrologic model SWAT (Soil Water Assessment Tool, Arnold et al., 1998) is used. SWAT can be applied in watersheds which vary from small surface areas to bigger surface areas. Many studies show the capability of this model in hydrological assessments (Schmalz et al., 2008; Rostamian et al., 2008; Schmalz & Fohrer, 2009; Srinivasan et al., 2010, Betrie et al., 2011). SWAT uses daily data as an input and delivers daily, monthly or yearly output. The local water balance represented in SWAT is based on four storage volumes: snow, soil profile (0–2 m), shallow aquifer (2–20 m), and deep aquifer (>20 m). The core for hydrological modeling builds the water balance equation:

$$SW_t = SW_0 + \sum_{i=1}^t (R_{day} - Q_{surf} - E_a - W_{seep} - Q_{gw})$$

Where: SW_t is the final soil water content, SW_0 is the initial soil water content, R_{day} is the amount of precipitation on day, Q_{surf} is the amount of surface runoff, W_{seep} is the amount of percolation and bypass flow exiting the soil profile bottom on day, E_a is the amount of evapotranspiration on day, and Q_{gw} is the amount of return flow on day.

The water balance is calculated based on hydrological response units (HRU's), which are created by integration of land use, soil type and slope class in terms of homogenous landscape units. All hydrological assessments are calculated on these HRU's. In this research various water balance components such as surface runoff, evapotranspiration, and percolation are estimated.

Surface runoff is simulated by modification of the SCS curve number (CN) method from daily rainfall and based on land use, soil hydrological group and antecedent soil moisture (USDA soil conservation service, 1972). The SCS curve number which is a watershed specific coefficient represents the runoff potential of particular land cover and soil. The SCS-CN method is based on the following relationship between rainfall and runoff (USDA-SCS, 1972):

$$Q = \frac{(R - 0.2 S)^2}{R + 0.8 S} \quad R > 0.2 S$$

$$Q=0 \quad R \leq 0.2 S$$

Where Q is the daily surface runoff (mm), R is the daily rainfall (mm), S is the retention parameter. The retention parameter (S) is related to curve number and this CN was calculated according to soil and land use condition by following equation:

$$S = 254 \left(\frac{100}{CN} - 1 \right)$$

The value of curve number is ranging from 0 to 100. A table of initial curve number (CN) is developed by SCS as a function of the soil type, land use and antecedent moisture condition (AMC). The soil condition was classified in four different categories, ranked A to D according to the potential of soils on runoff production. The difference of soil groups on surface runoff was discussed by Melesse & Shih (2002). Soil class A mostly consist of deep soil with well-drained sands and gravels, high infiltration, low runoff potential and high water transmission rates (greater than 0.30 in./hr.). Class B consist mostly of moderately deep to deep soil, moderately well to well drained soils with moderately fine to moderately coarse textures, the rate of water transmission is moderate (0.15 to 0.30 in./hr.). Soil class C has moderately fine to fine texture, with low infiltration and slow water transmission rate (0.05 to 0.15 in./hr.). Class D consists of clay soils with very slow infiltration rates and high runoff potential. They have a very low water transmission rate (0.00 to 0.05 in./hr.).

The curve number is defined in three antecedent moisture conditions by USDA. AMC-I is the lower limit of moisture representing a dry condition, AMC-II is the average moisture condition, and AMC-III is the upper limit of moisture representing a wet condition. Usually AMC-II is used

for curve number value estimation. In this study the AMC-II class of soil moisture is applied to each land use pattern.

Potential evapotranspiration (PET) is estimated using the Hargreaves method which requires daily precipitation, and minimum and maximum temperature (Hargreaves & Samani, 1985). After simulation of PET, actual evapotranspiration (AET) was estimated based on Ritchie (1972) methodology, according to leaf area index (LAI) simulated by crop-growth component inside SWAT. The Hargreaves equation is:

$$\lambda E_0 = 0.0023 \cdot H_0 \cdot (T_{mx} - T_{mn})^{0.5} \cdot (\bar{T}_{av} + 17.8)$$

Where λ is the latent heat of vaporization (MJkg^{-1}), E_0 is the potential evapotranspiration (mm d^{-1}), H_0 is the extraterrestrial radiation ($\text{MJm}^{-2} \text{d}^{-1}$), T_{mx} is the maximum air temperature for a given day ($^{\circ}\text{C}$), T_{mn} is the minimum air temperature for a given day ($^{\circ}\text{C}$), \bar{T}_{av} is the mean air temperature for a given date ($^{\circ}\text{C}$).

Percolation is derived from a storage routing technique combined with a crack-flow model to predict flow through each soil layer in the profile (Neitsch et al., 2009). The crack-flow model allows percolation of infiltrated rainfall. The storage routing technique is based on the following equation:

$$W_i = SW_{oi} \left(1 - \exp \left[\frac{-\Delta t}{TT_{perc}} \right] \right)$$

Where W_i is water percolation (mm), SW_{oi} is drainable water (mm), Δt is the length of time step (h), and TT_{perc} is the travel time for percolation through the layer (h).

3-2-4. Calibration and sensitivity analysis

The SUFI-2 algorithm (Abbaspour, 2011) is used for calibration, validation and uncertainty analysis. In this algorithm all uncertainties such as uncertainty in parameter, conceptual model and input data are depicted into the parameter ranges, and the process tries to capture most of the measured data within the 95% prediction uncertainty (95PPU) band. To calibrate the model monthly river discharge at three hydrometric stations is used. Further the model is calibrated

from 2001 – 2008 including 2 years as a warm up period and validated for 1997 – 2000. Figure 3-2 shows the position of hydrometric stations in the basin used for the calibration and sensitivity analysis.

The uncertainty of the output is quantified by 95PPU which is calculated at the 2.5% and 97.5% levels of cumulative distribution of an output variable. To assess the goodness of calibration and uncertainty performance two indices are used: the P-factor and R-factor. P-factor is the percentage of measured data bracketed by the 95PPU and R-factor is 95PPU divided by the standard deviation of measured data. P-factors around one, bracket most of data within the band, and R-factors near zero, narrowest band, are ideal. Nash–Sutcliffe model efficiency (NS) and coefficient of determination (R^2) were used to assess the SWAT model. The equation of NS is given as follows:

$$NS = 1 - \frac{\sum_{i=1}^n (Q_{obs} - Q_{sim})^2}{\sum_{i=1}^n (Q_{obs} - \text{mean}(Q_{obs}))^2}$$

Where Q_{obs} and Q_{sim} are the measured and simulated data, respectively, and n is the total number of data records. NS varies between minus infinity to 1. Usually when NS is more than 0.5 the accuracy of the model is very good and negative values show the model is not suitable (Zhi et al., 2009). The coefficient of determination, R^2 , is calculated as follows:

$$R^2 = \frac{[\sum (Q_{obs,i} - \overline{Q_{obs}})(Q_{sim,i} - \overline{Q_{sim}})]^2}{\sum (Q_{obs,i} - \overline{Q_{obs}})^2 \sum (Q_{sim,i} - \overline{Q_{sim}})^2}$$

Where $\overline{Q_{obs}}$ and $\overline{Q_{sim}}$ are the mean measured and simulated data, respectively.

A weighted version of Nash-Sutcliffe coefficient (g) was used as an objective function to compare the monthly measured and simulated discharges in multiple discharge stations:

$$g = \sum_i^n w_i NS_i$$

Many studies show the capability of SUFI-2 for calibration and uncertainty analysis (Abbaspour et al., 2007; Schuol, et al., 2008; Faramarzi et al., 2009; Yang et al., 2008).

3-3. Results and Discussion

3-3-1. Hydrological response unit

The integration of land use, soil type and slope layers derive 831 HRU's spread over 138 sub-basins. At the following details of these single information layers (land use, soil, and slope information) for hydrologic modeling are discussed:

Land use is obtained by remotely sensed data (Landsat ETM) and field studies (GPS based land use mapping, soil samples and soil mapping). In case of land use mapping, the result shows an overall accuracy for the supervised classification of 71.4 % and Kappa Coefficient of 0.66 which represents a reliable classification. Figure 3-4 shows the results of remotely sensed analysis to produce a land use map and table 3-3 presents the statistical results of each land use class.

The second information layer is build up by soil mapping (deriving a soil map). The soil map is generated using soil profile information in each land type up to 5 layers. The soil map includes 13 soil types (Figure 3-5 and Table 3-4).

The last information layer needed for hydrologic modeling contents information about slope angle distribution (Figure 3-6). It is created by DEM analysis (DEM resolution: 15 m scale) inside ArcGIS (Vers. 9.3, Spatial Data Analyst) with an output of 3 classes. Slope values less than 2 percent are predominant in the basin (Table 3-5). These land parcels (slope < 2%) are mostly farmlands in the center of the watershed. The south of the watershed is marked by lowlands with degraded soils.

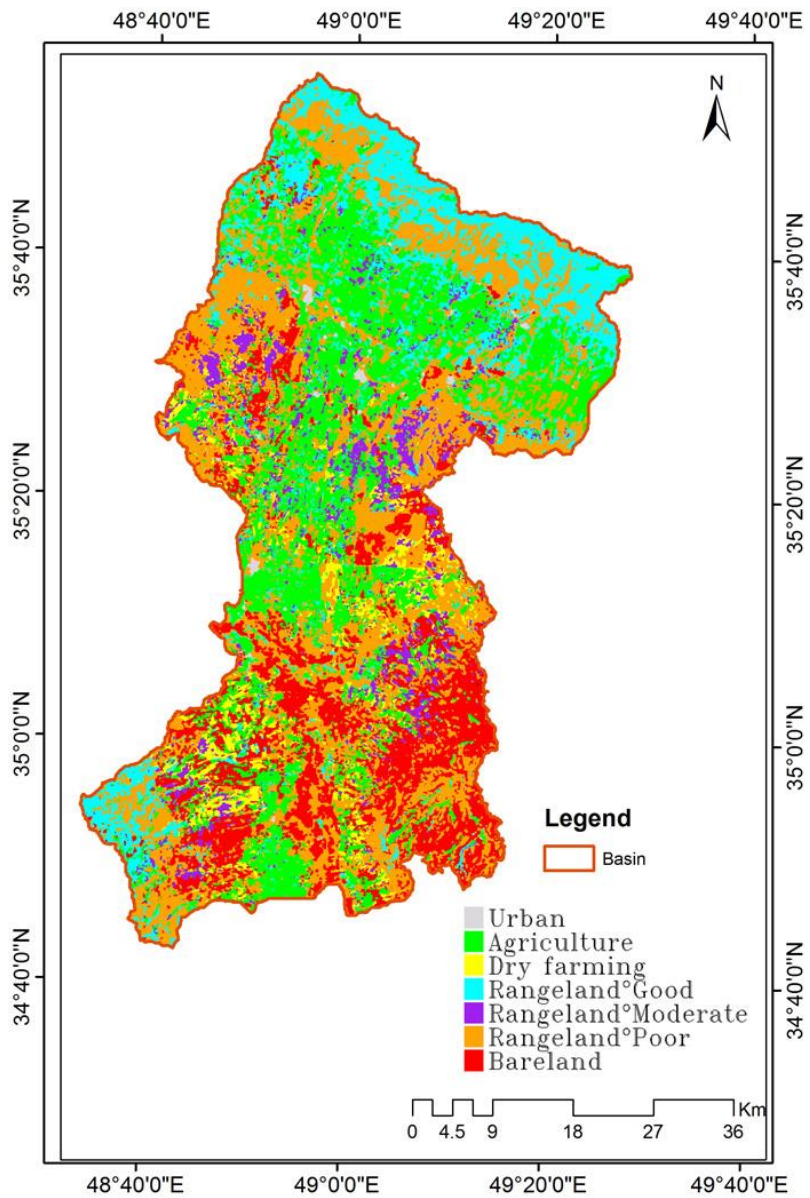


Figure 3-4. Land use map

Table 3-3. Statistical results of land use classes

	Agg.	Land Use*	Area%	Area(km²)
1	URBN	Urban	0.6	19
2	AGR	Agriculture	26	814
3	HAY	Dry farming	5.0	156
4	PAST	Rangeland_G	14.6	456
5	RNGB	Rangeland_M	5.7	177
6	SWRN	Rangeland_P	30.8	964
7	BRLD	bareland_erosion	17.3	542
			100.0	3128

* G: Good, M:Moderate, P:Poor

Table 3-4. Information of soil map

Soil class	Soil depth(mm)	No. of layers
I	100	1
II	500	2
III	1300	4
IV	1100	4
V	1000	3
VI	1200	3
VII	1000	4
VIII	1450	5
IX	840	4
X	1500	5
XI	1200	4
XII	1420	4
XIII	650	3
URBAN	-	-

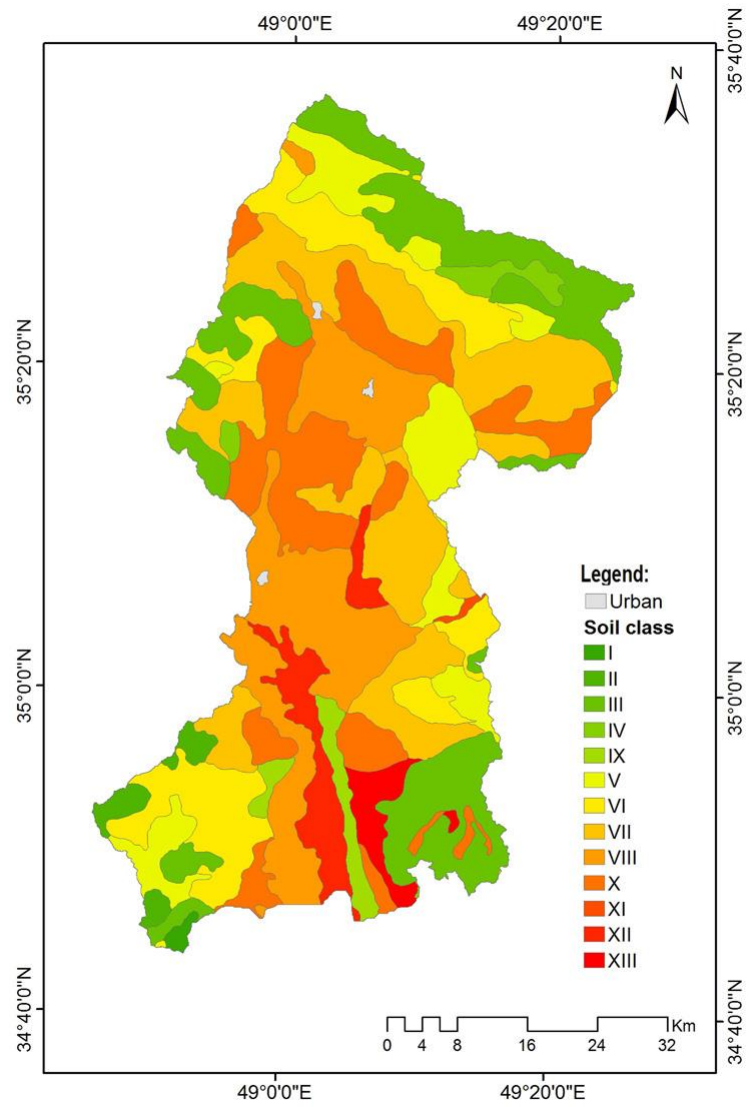


Figure 3-5- Soil map

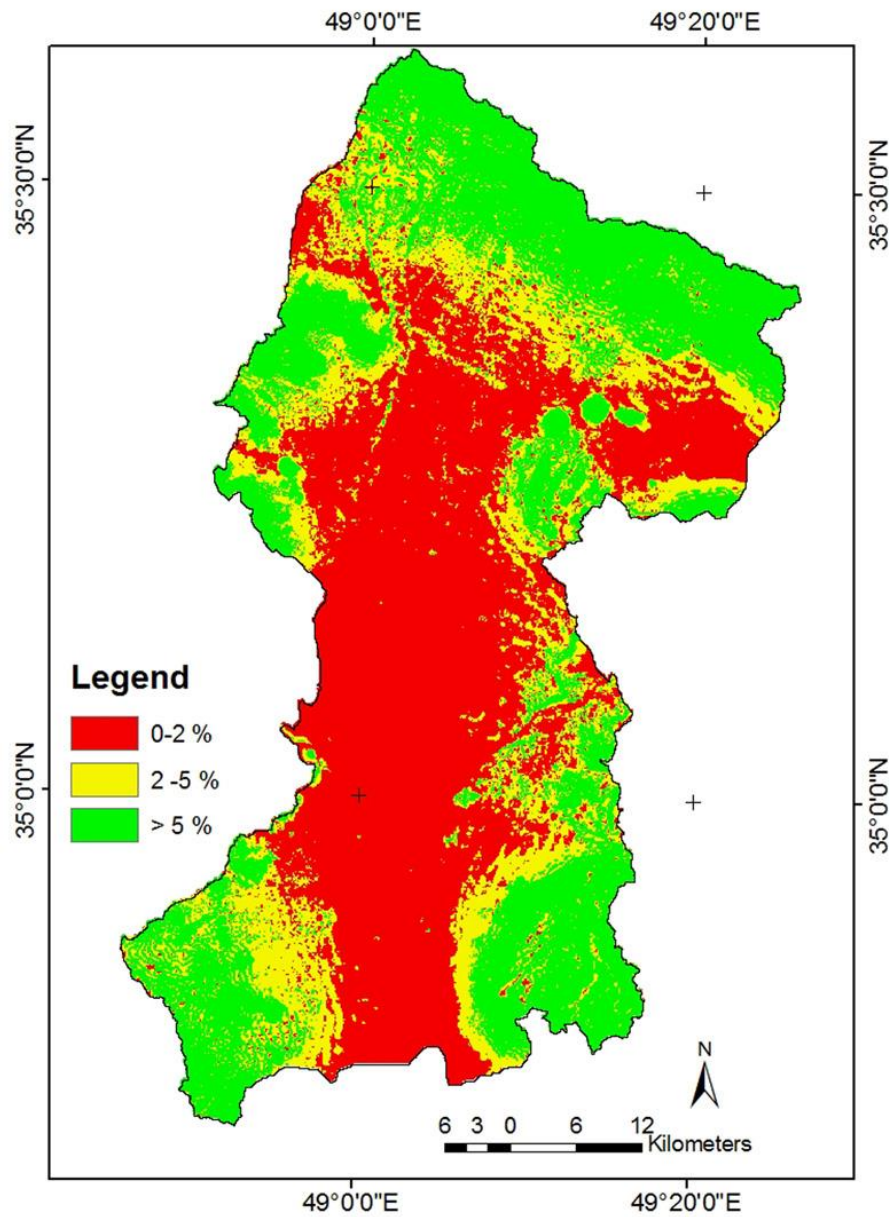


Figure 3-6. Slope map

Table 3-5. Information of Slope map

	Class	Area %
1	0-2%	48.89
2	2-5%	20.87
3	> 5%	30.24

3-3-2. Model Calibration

The Razan-Ghahavand watershed is calibrated using the parameters in Table 3-6. The parameters of Table 3-6 are including their initial and final ranges that are used in the calibration process. The first results of SWAT model did not present the stream flow correctly. The sensitivity analysis shows that some parameters are very sensitive against stream flow. Table 3-7 shows the most sensitive parameters based on their location in the watershed by assigning the sub-basin numbers to the parameters. The result from t-stat provides a measure of sensitivity (larger in absolute values are more sensitive) and p-values determine the significance of the sensitivity. A value closer to zero has more significance. According to sensitivity analysis, snow, soil, groundwater and infiltration parameters are the most sensitive parameters in the watershed. The most sensitive parameter (Curve number) is located in the sub basin with the hydrometric stations “Sirab Khomigan” (No. 41), and “Zehtaran” (No. 14) as their outlets. These stations are located in high elevation in comparison to Omarabad station (No.71) hydrometric station. Therefore CN2 is the most sensitive parameter at these stations. Second parameter after Curve Number is snow parameter (minimum melt rate for snow during the year). Snow melt is the most sensitive parameter due to the mountainous character of Razan-Ghahavand basin, where much of the stream flow is controlled by snow melt.

Figure 3-7 shows the results of calibration and validation for three hydrometric stations. The Calibration results for Q (m³/sec.) are shown for measured/observed data, the 95% prediction uncertainty (95PPU) and the best fit of optimization. The grey curves represent the 95PPUs of the discharge simulation together with observed discharges (blue line) and best discharge simulation (red line) at three hydrometric stations (Q_14, Q_41 and Q_71). The three hydrometric stations are located at different rivers (Zehtaran, Sirabe-Khomigan and Gharehchay) and represent a large area of the catchment. The general trend of the discharge both for calibration and validation simulations for all stations look pretty good. The model simulated the variation in time of peaks quit well but the uncertainty interval at peaks in some stations (for instance in March 2005 at the Q_14 station) is extremely large. In Table 3-8 the statistical results of this analysis are summarized, which show that the overall performance of the model is good. The R-factor at the outlet of the watershed is less than 1 shows a good calibration result. The p-factor is small revealed that the actual uncertainty is likely larger. Moreover the NS and R² for all three stations are bigger than 0.5 that is acceptable and shows good calibration results.

Table 3-6. Parameters for river discharge calibration and their initial and final ranges ^a

Parameter Name ^b	Definition	Initial range		Final range	
r__CN2.mgt	SCS runoff curve number for moisture condition II	-0.5	0.5	-0.13	0.14
v__GW_DELAY.gw	Groundwater delay time (days)	0.0	500	302	401
v__ALPHA_BF.gw	Baseflow alpha factor (days)	0	1	0.56	0.68
v__REVAPMN.gw	Threshold water in shallow aquifer	0	500	0.22	0.30
v__GW_REVAP.gw	Revap coefficient	0.02	0.2	0.18	0.20
v__RCHRG_DP.gw	Aquifer percolation coefficient	0	1	0.90	0.96
v__GWQMN.gw	Threshold water level in shallow aq. for baseflow	0	5000	3900	4050
r__SOL_AWC().sol	Available water capacity factor	-0.5	0.5	0.24	0.49
r__SOL_K().sol	Saturated hydraulic conductivity	-0.95	0.95	-0.90	-0.86
r__SOL_BD().sol	Soil bulk density	-0.5	0.5	-0.34	-0.29
v__SOL_ALB().sol	Moist soil albedo	0	0.25	0.14	0.16
v__EPCO.hru	plant uptake compensation factor	0.01	1	0.36	0.42
v__ESCO.hru	Soil evaporation compensation factor	0.01	1	0.01	0.42
v__SLSUBBSN.hru	Average slope length (m)	10	150	134	150
v__OV_N.hru	Manning's n value for overland flow	0	0.8	0.46	0.80
r__CH_N2.rte	Manning's n value for main channel	0	0.3	0.04	0.11
v__CH_K2.rte	Effective hydraulic conductivity in main channel alluvium	0	150	92	100
v__ALPHA_BNK.rte	Base flow alpha factor for bank storage (days)	0	1	0.22	0.48
r__HRU_SLP.hru	Average slope steepness	-0.95	0.95	0.19	0.68
v__SFTMP.bsn	Snowfall temperature	-5	5	-4.7	4
v__SMTMP.bsn	Snow melt base temperature (°C)	-5	5	3.3	5
v__SMFMX.bsn	Melt factor for snow on 21 Jun	0	10	1.8	5
v__SMFMN.bsn	Melt factor for snow on 21 Dec	0	10	0.004	5.5
v__TIMP.bsn	Snow pack temperature lag factor	0.01	1	0.05	0.70
v__SURLAG.bsn	Surface runoff lag coefficient	1	24	3.5	20

^a The final ranges are based on the parameters in the outlet station (Omarabad station)

^b r__: refers to rational changes; v__: refers to substitute changes

Table 3-7. The most Sensitive parameters including their t-value and p-value

Parameter Name	t-Value	p-Value
r__CN2.mgt_____23,26,27,28,29,32,33,34,37,38,41*	-44.67	0.00
r__CN2.mgt_____1,2,3,4,5,6,12,13,14	-15.06	0.00
v__SMFMN.bsn	-11.31	0.00
v__ALPHA_BNK.rte_____1,2,3,4,5,6,12,13,14	-9.39	0.00
v__ALPHA_BNK.rte_____23,26,27,28,29,32,33,34,37,38,41	-9.27	0.00
r__SOL_AWC().sol_____23,26,27,28,29,32,33,34,37,38,41	7.3	0.00
v__SMFMX.bsn	-4.93	0.00
v__TIMP.bsn	-4.89	0.00
v__CH_K2.rte_____23,26,27,28,29,32,33,34,37,38,41	2.47	0.01
V__GW_DELAY.gw_____1,2,3,4,5,6,12,13,14	2.34	0.02
v__GWQMN.gw_____23,26,27,28,29,32,33,34,37,38,41	2.02	0.04
r__SOL_AWC().sol_____1,2,3,4,5,6,12,13,14	1.97	0.05
v__GW_REVAP.gw_____23,26,27,28,29,32,33,34,37,38,41	1.78	0.07
r__CH_N2.rte_____1,2,3,4,5,6,12,13,14	-1.66	0.10
v__SMTMP.bsn	1.72	0.09
V__GW_DELAY.gw_____7-11,15- 22,24,25,30,31,35,36,39,40,42-138	1.64	0.10

* sub basin numbers

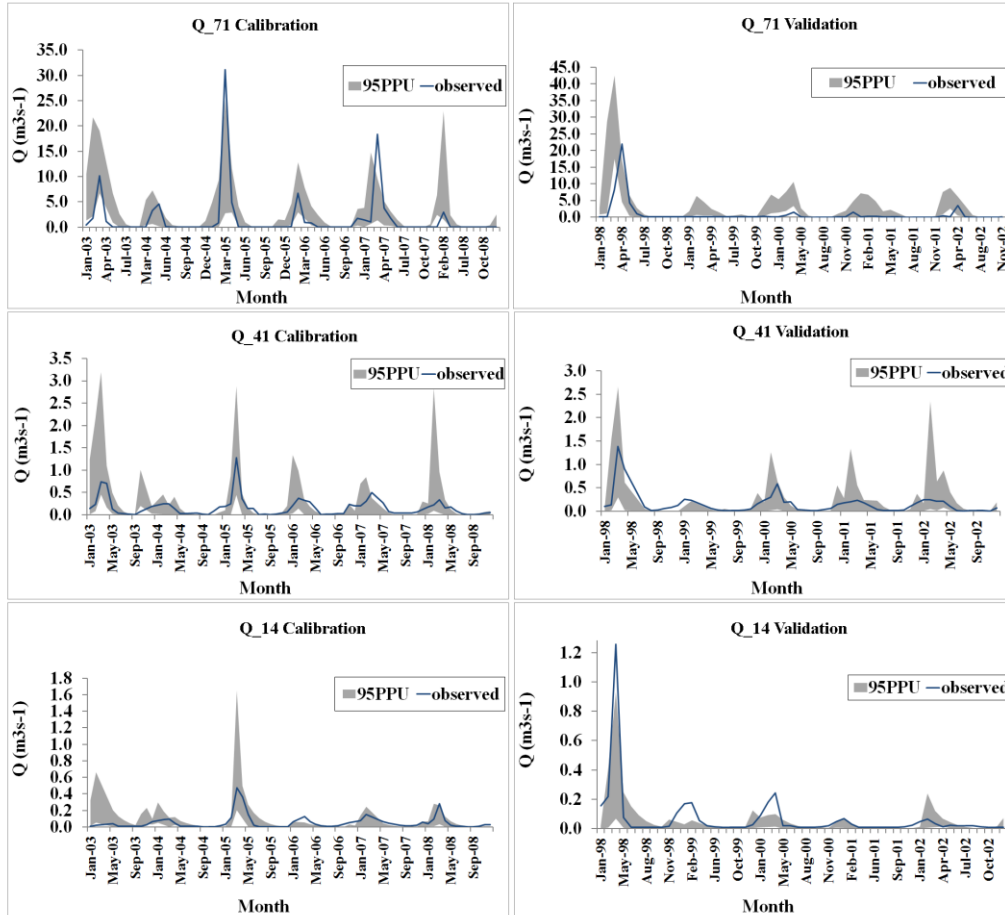


Figure 3-7. Calibration (2003-2008) and validation (1998-2002) of river discharge

Table 3-8. Statistical result of calibration and validation

Station	Calibration (2003-2008)				Validation (1998-2002)			
	P-factor	R-factor	R ²	NS	P-factor	R-factor	R ²	NS
14	0.66	1.41	0.68	0.63	0.44	0.36	0.91	0.72
41	0.60	1.99	0.70	0.53	0.51	1.33	0.78	0.42
71	0.30	0.79	0.62	0.60	0.45	1.02	0.69	0.66

3-3-3. Quantification of components

For the extraction of water components the average monthly 95PPUs of water components and average annual components (2003-2008) were simulated. As pointed out in figure 3-8, precipitation in April is highest with an amount around 50 mm and precipitation in September is lowest (0.2 mm).

Figure 3-8 (a-c) shows the average monthly values of actual evapotranspiration (AET), surface runoff (SURQ) and soil water content (SW). The trend of 95PPUs for actual evapotranspiration is similar to precipitation and their uncertainty values are not high. In April the rate of AET is high, due to highest precipitation and also because of more transpiration by crops due to growth and development of vegetation (both in arable and rangelands). In September AET is low, due to the end of growing season of crops and decreasing precipitation. On the other hand surface runoff is highest in January, February and March. Soil water content during summer is lowest and during winter is highest. Surface runoff in summer is lowest due to decreasing precipitation in this period of time. Moreover, soil water content in February is highest because of low evapotranspiration and pretty high precipitation.

The assessment of spatial distribution of evapotranspiration (ET) shows that the annual average values of ET vary from 238 mm in the South to 425 mm in the North of the watershed. The range of precipitation varies from 245 mm in the South to 413 mm in the North. The yearly average of surface runoff varies from 1 mm to 160 mm in various sub basins at which soil water varies from 13 mm to 206 mm in whole watershed. The highest average percolation is 134 mm in the North East of the watershed. In Figure 3-9 the spatial distribution of these components together with their spatial pattern in the watershed are presented.

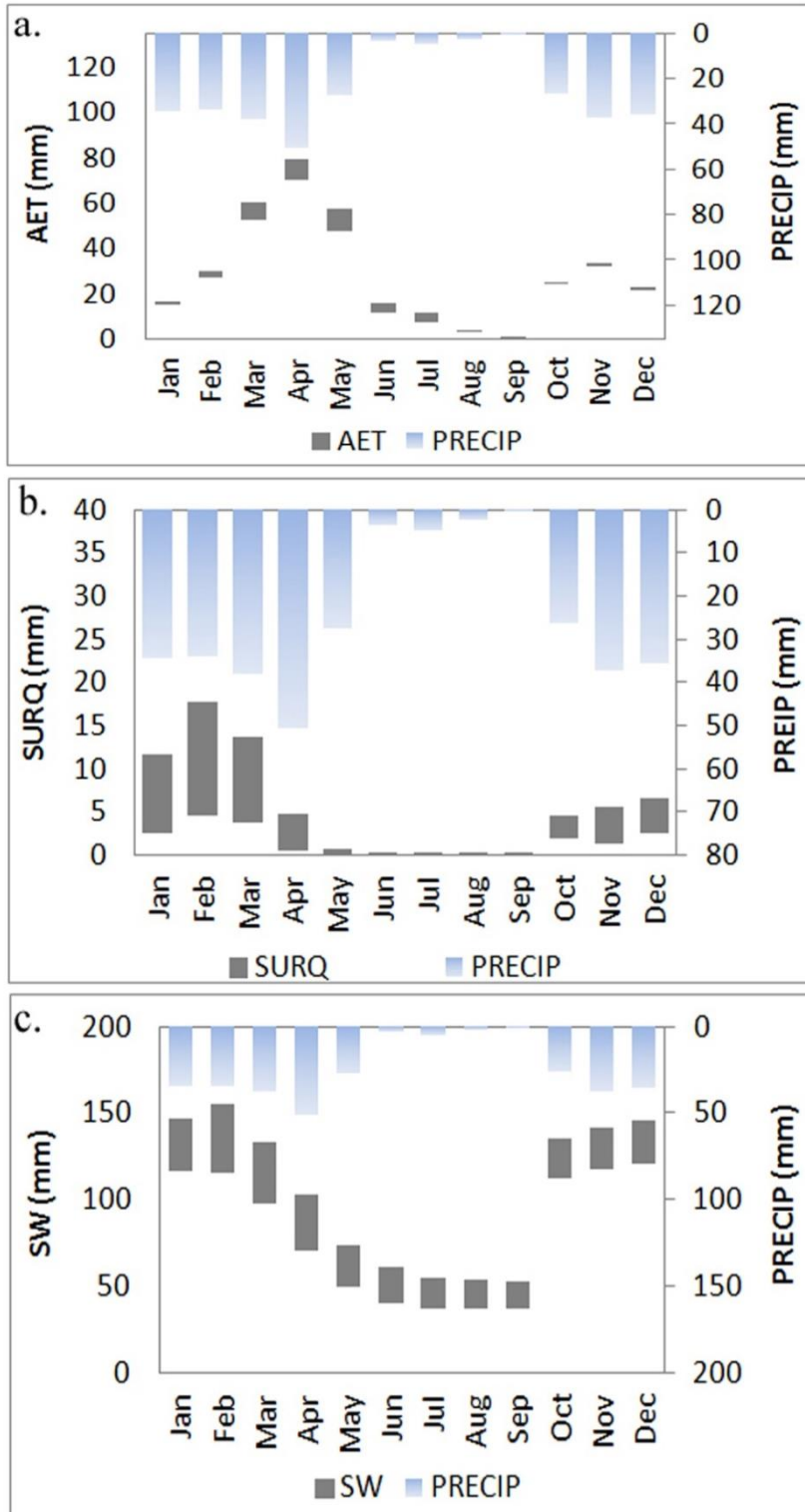


Figure 3-8-a,b,c. Average monthly 95PPU (2003-2008) of actual evapotranspiration (AET), surface runoff (SURQ) and soil water content (SW) against with precipitation (PERCIP)

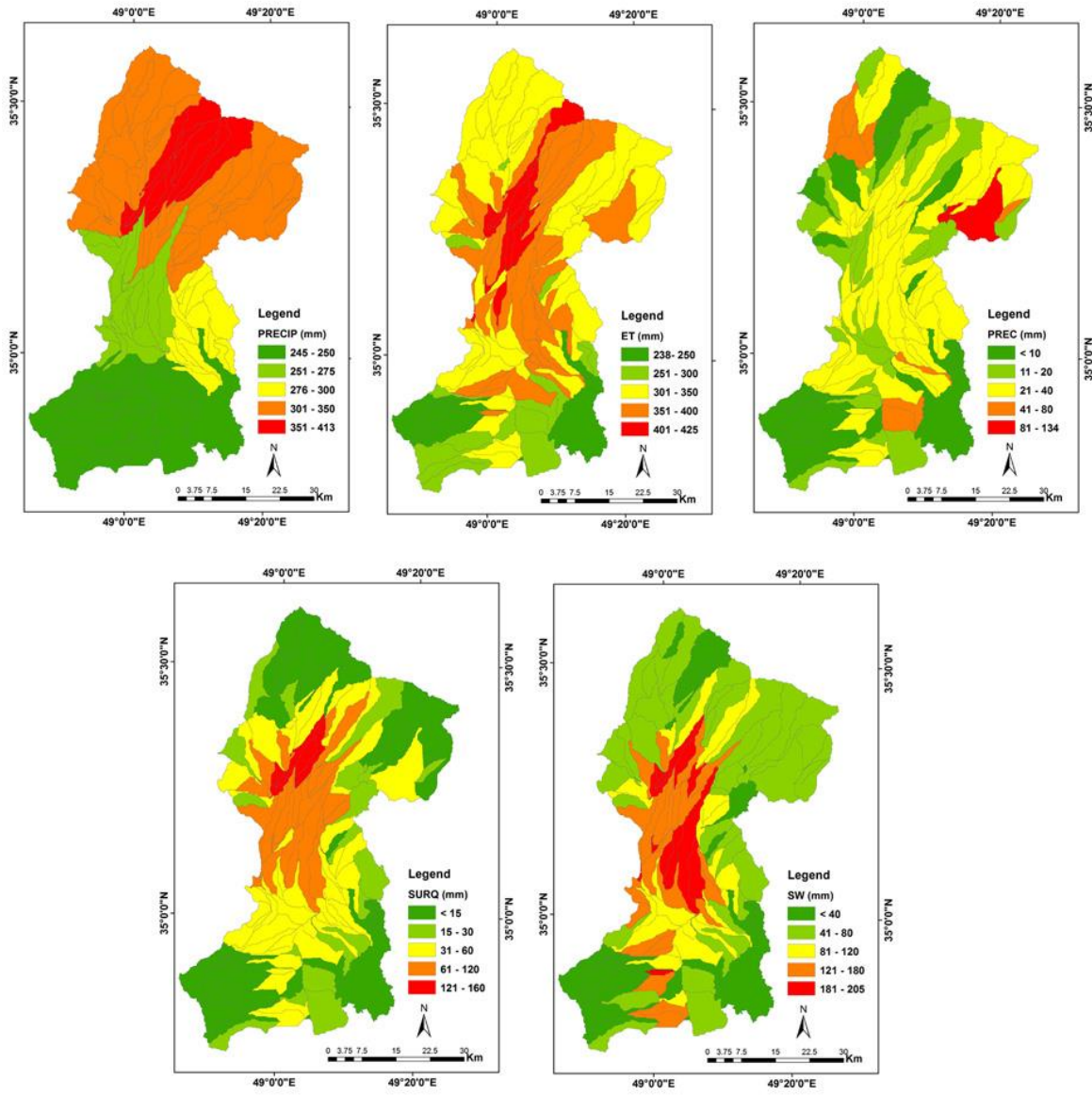


Figure 3-9. Average spatial distribution of yearly average of precipitation (PRECIP), actual evapotranspiration (AET), Percolation (PERC), Surface runoff (SURQ) and Soil water content (SW) for the years 2003 to 2008.

3-4. Conclusion

Based on Digital Elevation Model analysis inside GIS, land use classification and soil information the applicability of the SWAT model in this central drainage basin of Iran is tested. A GIS-based model for the Razan-Ghahavand watershed is now available and can be developed step by step into the future (e.g. integration of new and more precise base data). The river discharge data from 1997 to 2008 are used for model calibration and validation and the extraction of water balance components. The general trend of the discharge simulations (both for calibration and validation) looks pretty good for all stations, but the uncertainty interval at single stations is quite large. Overall, the research results show that water balance components like ET, Surface Runoff and Percolation can be modeled with a hydrological model like SWAT and the model output produces robust information for watershed management. This information can be used for adjusted planning and management of the watershed to meet the requirements for better water harvesting, finding initial suitable places for artificial aquifer recharge and future land rehabilitation by adapted rangeland management.

3-5. References

- Abbaspour KC (2011) User Manual for SWAT-CUP: SWAT Calibration and Uncertainty Analysis Programs. Swiss Federal Institute of Aquatic Science and Technology, Eawag, Duebendorf, Switzerland. 103 pp.
- Abbaspour KC, Yang J, Maximov I, Siber R, Bogner K, Mieleitner J, Zobrist J, Srinivasan R (2007) Modelling hydrology and water quality in the pre-alpine/alpine Thur watershed using SWAT, *Journal of Hydrology* 333: 413–430, DOI:10.1016/j.jhydrol.2006.09.014.
- Arnold JG, Srinivasan R, Muttiah RS, Williams JR (1998) Large area hydrologic modeling and assessment–Part 1: Model development. *Journal of the American Water Resources Association* 34: 73–89.

- Betrie GD, Mohamed YA, Van Griensven A, Srinivasan R (2011) Sediment management modelling in the Blue Nile Basin using SWAT model. *Hydrology and Earth System Sciences* 15: 807-818. doi:10.5194/hess-15-807-2011.
- Congalton RG (2004) *Remote Sensing and GIS Accuracy Assessment*, CRC Press, United States of America.
- Diallo Y, Hu G, Wen X (2009) Applications of Remote Sensing in Land Use/Land Cover Change Detection in Puer and Simao Counties, Yunnan Province. *Journal of American Science* 5: 157-166.
- Dunne T (1978) *Water in environmental planning*. W.H. Freeman and Company, New York, USA.
- Faramarzi M, Abbaspour KC, Schulin R, Yang H (2009) Modelling blue and green water resources availability in Iran. *Hydrological Process* 23: 486–501.
- Hargreaves G, Samani ZA (1985) Reference crop evapotranspiration from temperature, *Applied engineering in agriculture* 1: 96–99.
- IPCC (2013) *Climate Change 2013: The Physical Science Basis. Contribution of Working Group I to the Fifth Assessment Report of the Intergovernmental Panel on Climate Change* [Stocker TF, Qin D, Plattner GK, Tignor M, Allen SK, Boschung J, Nauels A, Xia Y, Bex V, Midgley PM(eds.)]. Cambridge University Press, Cambridge, United Kingdom and New York, NY, USA, 1535 pp.
- Mengistu DA, Salami AT (2007) Application of remote sensing and GIS inland use/land cover mapping and change detection in a part of south western Nigeria. *African Journal of Environmental Science and Technology* 1:99-109.
- Neitsch SL, Arnold JG, Kiniry JR, Williams JR (2009) *Soil and water assessment tools, Theoretical documentation*, ARS, Texas.
- Reis S (2008) Analyzing Land Use/Land Cover Changes Using Remote Sensing and GIS in Rize, North-East Turkey, *Sensors* 8: 6188-6202.

- Ritchie JT (1972) A model for predicting evaporation from a row crop with incomplete cover. *Water Resources Research* 8:1204-1213.
- Rostamian R, Jaleh A, Afyuni M, Mousavi SF, Heidarpour M, Jalalian A, Abbaspour KC (2008) Application of SWAT model for estimation runoff and sediment in two mountainous basins in central Iran. *Hydrological Sciences Journal* 53(5):977-988.
- Schmalz B, Tavares F, Fohrer N (2008) Modelling hydrological processes in mesoscale lowland river basins with SWAT—capabilities and challenges. *Hydrological Sciences Journal* 53(5): 989–1000
- Schmalz B, Fohrer N (2009) Comparing model sensitivities of different landscapes using the ecohydrological SWAT model. *Advances in Geosciences* 21:91–98, 2009.
- Schuol J, Abbaspour K C, Srinivasan R, Yang H (2008) Estimation of freshwater availability in the West African sub-continent using the SWAT hydrologic Model. *Journal of Hydrology* 352: 30– 49.
- Srinivasan R, Zhang X, Arnold J (2010) SWAT Ungauged: Hydrological Budget and Crop Yield Predictions in the Upper Mississippi River Basin. *Transactions of the ASABE* 53(5): 1533-1546.
- Soil Survey Staff (2010) *Keys to Soil Taxonomy*, 11th ed. USDA-Natural Resources Conservation Service, Washington, DC.
- USDA SCS (Soil Conservation Service) (1972) *SCS National Engineering Handbook*. Section 4, Hydrology. Washington, DC: USDA.
- Yang J, Reichert P, Abbaspour KC, Xia J, Yang H (2008) Comparing uncertainty analysis techniques for a SWAT application to the Chaohe Basin in China. *Journal of Hydrology*. doi:10.1016/j.jhydrol.2008.05.012.
- Zhi L, Wen-zhao L, Xun-chang Z, Fen-li Z (2009) Impact of land use change and climate variability on hydrology in an agricultural catchment on the Loess Plateau of China. *Journal of Hydrology* 377: 35-42. <http://dx.doi.org/10.1016/j.jhydrol.2009.08.007>

Estimation of groundwater recharge and its relation with land degradation: Case study of a semi-arid river basin in Iran ²

Abstract

Groundwater extraction is one of the most important criteria of land degradation especially land subsidence in arid and semi-arid areas. Understanding the relationship between water extraction and recharge of groundwater can lead to better watershed management. For the estimation of groundwater recharge in Razan-Ghahavand watershed in Central Iran the Soil and Water Assessment Tools (SWAT) was used. Model calibration was done by using SUFI-2 based on monthly river discharge and annual crop yield, where crop yield was used to better estimate the evapotranspiration term, which consequently increased our knowledge on estimating aquifer recharge. The calibration results were satisfactory: The Nash-Sutcliffe model efficiency ranged from 0.53 to 0.63 for calibration and from 0.42 to 0.72 for validation. The results showed that, although the groundwater level was decreasing about 1 meter per year, the groundwater recharge did not change significantly leading to a net withdrawal causing land subsidence over time.

² This paper is under review in "Environmental Earth Sciences Journal". Springer, Inc.

4-1. Introduction

Groundwater is the main source of water supply in arid and semi-arid regions (Awan & Ismaeel, 2014). Exploitation of ground water resource exceeding the recharge, and consequently decrease in the water table is a major cause of land degradation, especially land subsidence and ecological problems such as change of vegetation composition in these regions. An estimation of groundwater recharge can help stakeholders and policy-makers to develop sustainable management of semi-arid regions in Iran. However, the precise prediction of ground water recharge in this area is very complex. Therefore, we simulated the groundwater recharge in a semi-arid region of Iran by SWAT model and we used an innovative technique to calibrate the model.

Although the same hydrological rules apply in both semi-arid and humid areas, physical characteristics are often different (Wisler & Brater, 1959). In arid and semi-arid regions the unsaturated zone has a key role on the rate of groundwater recharge. Generally, the separation of rainfall into surface runoff and infiltration is controlled by the unsaturated zone (Raneesh & Thampi, 2013). The infiltration of water may move the unsaturated zone through evapotranspiration, and may also percolate through aquifer as a groundwater recharge. To develop good estimate of groundwater recharge, the physical soil properties of unsaturated zone, land use/cover characteristics as well as the climate conditions must be considered.

Groundwater recharge can be simulated by various methods including physical, chemical, isotope or numerical techniques (Scanlon & Alan, 2002). A hydrologic model (rainfall/runoff) as a numerical model is used to estimate recharge rates over large areas. Gehrels et al. (2001) revealed that groundwater recharge is an important variable in hydrological models. Singh (1995) reviewed many hydrologic models, which generally estimate groundwater recharge as a residual term in the water-budget equation. Furthermore, various researchers have discussed processes of groundwater recharge estimation based on the water balance concept (Arnold & Allen, 1999; Yeh et al., 2007; Barthel et al., 2012). However, the spatial resolution of recharge estimation is different in various watershed models (Scanlon & Alan, 2002). Some of them called lumped models provide a single recharge estimation for the entire catchment (Kite, 1995), while others are spatially distributed into hydrological response units (HRU's) (Arnold et al., 2000).

Desertification today is seen as a broad phenomenon of environmental degradation and its interaction with human populations (Kappas et al., 2013). Land degradation is defined the loss of biological or economic productivity and is based on the framework of ecosystems services (Adeel et al., 2005). Drivers of land degradation are different from regions to regions. Therefore, land degradation may be appearing in different forms in various areas (e.g. salinization, land subsidence, soil erosion, and biodiversity loss) (Lu et al., 2007). Land degradation could also change hydrological conditions. Removing vegetation cover leads to soil surface expose to the impact of raindrops. The rainfall infiltration into the soil then reduces, soil moisture decreases, runoff increases, flooding occur, water quality deteriorates and groundwater level drops. Desertification is a major hazard for Iran. Three-fourth of the country has experienced desertification (Amiraslani & Dragovich, 2011). Groundwater resources supply over 50 percent of water demand in Iran (Motagh et al., 2008). The rate of aquifer depletion in Iran is high due to over-pumping of aquifers (Brown, 2005). The central drainage basin of Iran is seriously affected by increasing water demand and recurrent drought (Beheshti, 2011). Motagh et al., (2008) reported that the average of water level in Iranian aquifers have declined about 50 cm annually. He revealed that decrease in the groundwater levels leads to land-surface deformation. The relationship between groundwater and land degradation has been investigated by many previous researchers (Zhao et al., 2005); Gullison & Bourque, 2001). Many recent studies have focused on the decline of groundwater level and water quality (Qi & Luo, 2005), the salinity of groundwater and land degradation (Wen et al., 2005), groundwater and vegetation degradation (Ji et al., 2006; Guo et al., 2009), groundwater and change of land cover (Zhang et al., 2005). Stromberg et al. (1996) revealed that depletion of groundwater threatens riparian ecosystems in arid and semi-arid regions. Chen et al. (2003) mentioned that in northwest China the oasis-ecosystem depend on the groundwater level variability. Any change on water level in this area can significantly affect vegetation growth. Guo et al. (2009) reported that a decrease in groundwater table led to ecological deterioration and desertification in the northwest of China. Therefore, a balance between groundwater recharge and groundwater exploitation is important to prevent land degradation.

In arid and semi-arid countries like Iran, exploitation and diversion of water resources in aquifers and rivers are common activities and arise from low rate, high variability, and uneven distribution of precipitation (Abrishamchi & Tajrishi, 2005). Growing population, increasing per

capita water use, and irrigation are some causes of severe pressure on water resources in such countries. In Razan-Ghahavand semi-arid's watershed, part of central drainage basin in Iran, intensive agriculture and traditional irrigation methods lead to large amounts of water withdrawal. Groundwater, the main sources of water harvesting in this area, is exploited due to increasing demand and recurrent droughts. Ecological deteriorations such as decreasing of biomass in rangelands, decreasing crop yields, and deterioration of soil are taking place in south of the watershed due to water scarcity. Additionally, mismanagement of groundwater may have led to land subsidence, a dominant land degradation phenomenon in the west of the area, and salinization in central part of the area. Therefore, knowledge about water resources components and in this case groundwater recharge can leads to sustainable management of available resources and also result in best management practice in Razan-Ghahavand area.

The main objective of this research was to estimate the groundwater recharge by means of a hydrologic model. We used an innovative technique to calibrate our hydrologic model in order to precise estimating of groundwater recharge. We assessed the relationship between groundwater recharge and groundwater level fluctuation in order to interpret land degradation phenomena such as land subsidence occurrence in the area.

We used the Soil and Water Assessment Tool (SWAT) (Arnold et al., 1998) to achieve this goal. SWAT was selected because it is a continuous time and spatially distributed model, in which components such as weather, crop growth and irrigation, reach routing, water transfer, and agricultural management practices are considered. The advantage of hydrological models is that all water balance components can be estimated over an infinite time series, and distributed hydrological models can account for spatial heterogeneities and provide more detail information of the hydrological processes in a watershed.

4-2. Materials and method

4-2-1. Study area

The Razan-Ghavand watershed is located in central drainage basin of Iran and has an area of about 3100 km² (Figure 4-1). The outlet of the watershed is Omarabad in the east. The long-term average daily discharge at this station is 6.7 m³ s⁻¹. The altitude of the basin ranges from 1,577 m

in the eastern lowland part of the basin to 2,843 m in the hilly part of the basin in northern areas. The climate is semi-arid, and the average annual precipitation, temperature and potential evapotranspiration are about 295 mm, 11°C, and 1,320 mm, respectively. The area is mainly farmland (irrigated and rain fed) and rangeland. Most of the water withdrawal is used for the irrigation of farmlands and for power generation in the Mofatah power plant. In the northern part of the watershed good ecological condition exists with good rangeland and high biomass production, while most of the rangelands degradation and salinization are taking place in the southern part. Land subsidence is prevalent in the western part of the watershed. Geological formation consists of parent rocks such as limestone, shale and conglomerate. The aquifer's area is 1,750 km² with a thickness about 70-100 meters (Amiri, 2005). The transmissivity of the watershed ranges from 100 to 750 m² day⁻¹, and the average specific yield of the aquifer is 4.5%. There are 81 piezometric wells well distributed over the area (Figure 4-2). Despite the piezometric wells, there are more than 1400 operation wells in the study area, which are extracting groundwater for agriculture, industries and domestic use. The average water level is 30 meter in this aquifer, decreasing with an average rate of about 1 meter per year.

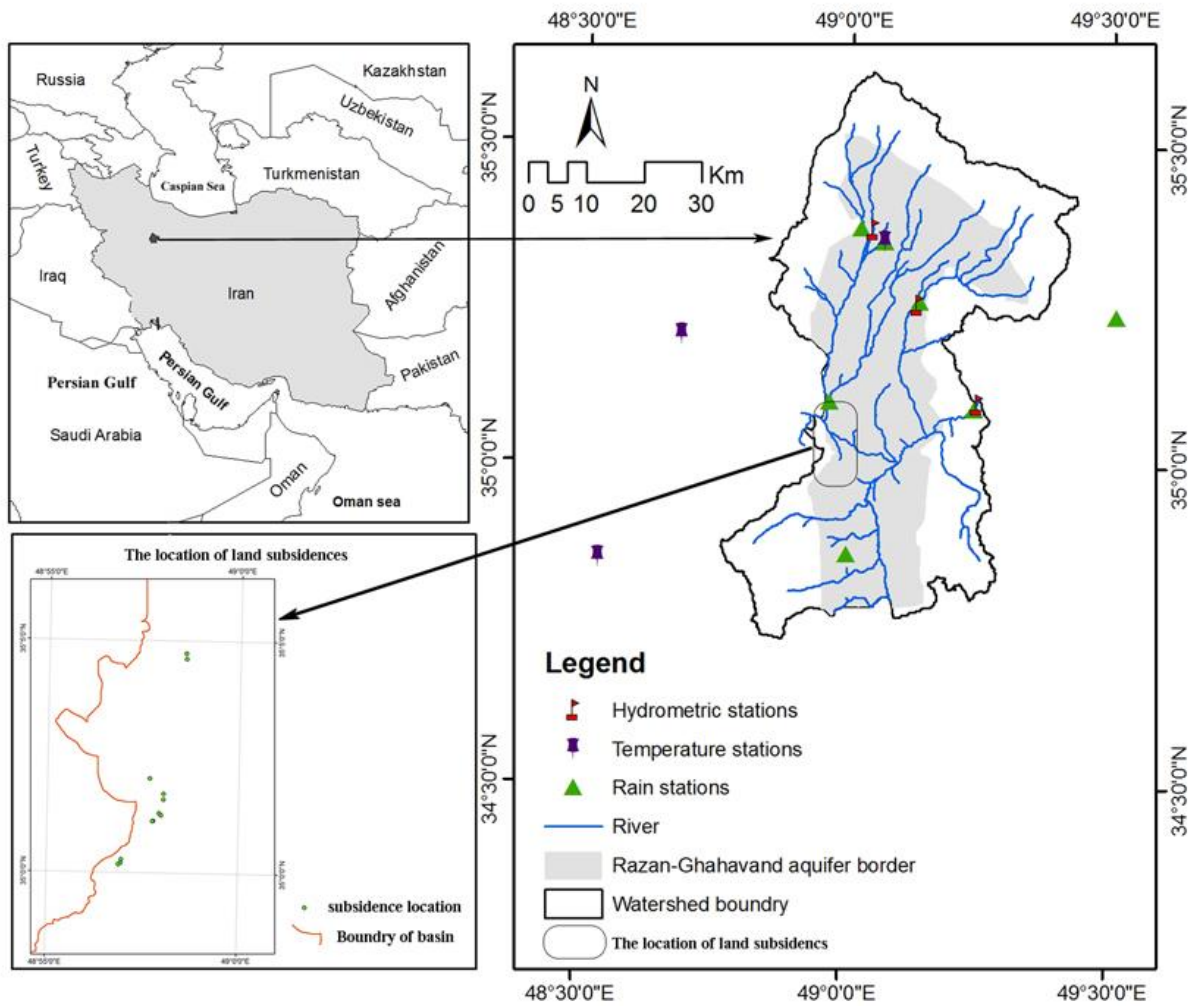


Figure 4-1. Location of the study area in northwestern part of central drainage basin of Iran (Razan-Ghavand watershed). The location of land subsidence, a dominate land degradation phenomenon in western area, has been shown in the map. The distribution of rain gages and temperature stations and also hydrometric stations has been shown in the map.

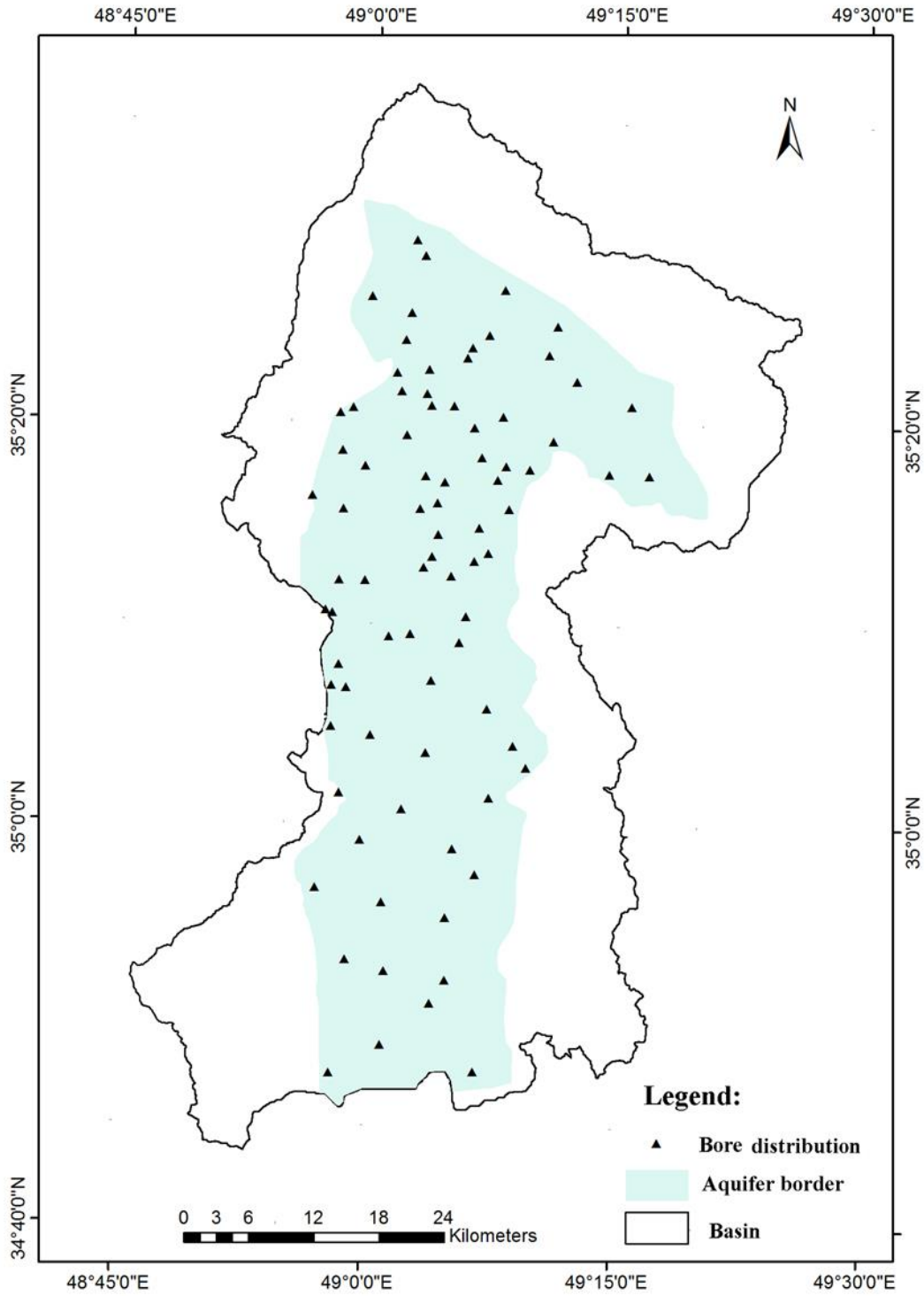


Figure 4-2. The location of piezometric wells in the study area

4-2-2. Groundwater recharge

Estimation of groundwater recharge is complex and depends on groundwater parameters (e.g. hydraulic conductivity), soil parameters, vegetation and land use characteristics, and climate parameters (Arnold et al., 2000). Among various models employed in water balance studies, we used SWAT, Soil and Water Assessment Tools, to estimate groundwater recharge. SWAT simulates the groundwater recharge as a residual of the water balance model. Hydrological response units (HRUs) which are hydrological homogenous were used as the basis of groundwater recharge calculation. Both shallow (2-20 m) and deep aquifer recharge (>20m) can be simulated by SWAT at the HRU level. Figure 4-3 shows the conceptual model of SWAT. The percolation water in the soil profile may percolate as groundwater recharge or loss as lateral flow or evapotranspiration. In shallow aquifer, the water can return through the unsaturated vadose zone by capillary activities to replace the deficit of water for plant evapotranspiration (REVAP), or may also move as a groundwater flow/bypass, the rest move into deep aquifer recharge and become groundwater.

In this study, the groundwater recharge refers to the amount of water leached from the root zone into deep aquifer. In other words, deep aquifer recharge is a fraction of total groundwater recharge:

$$W_{deep} = \beta_{deep} \times W_{rchrg}$$

Where W_{deep} is deep aquifer recharge (mm), β_{deep} is aquifer percolation coefficient, and W_{rchrg} is the amount of total groundwater recharge calculated as:

$$w_{rchrg,i} = (1 - \exp[-1/\delta_{gw}]) \cdot w_{seep} + \exp[-1/\delta_{gw}] \cdot w_{rchrg,i-1}$$

Where δ_{gw} is the delay time (day), w_{seep} is the total amount of water exiting the bottom of soil profile on day i (mm), and $w_{rchrg,i-1}$ is the amount of recharge entering the aquifers on day $i-1$ (mm). w_{seep} is calculated:

$$W_{seep} = W_{perc,ly=n} + W_{crk,btm}$$

Where $W_{perc,ly=n}$ is the amount of water percolation out of the lowest layer (n) in the soil profile on day i (mm), and $W_{crk,btm}$ is the amount of water flow past the lower boundary of soil profile due to bypass flow on day i (mm). Percolation is modeled with a layered storage routing

technique combined with a crack flow model. Groundwater recharge was simulated at the HRU level and then compared with groundwater level fluctuations.

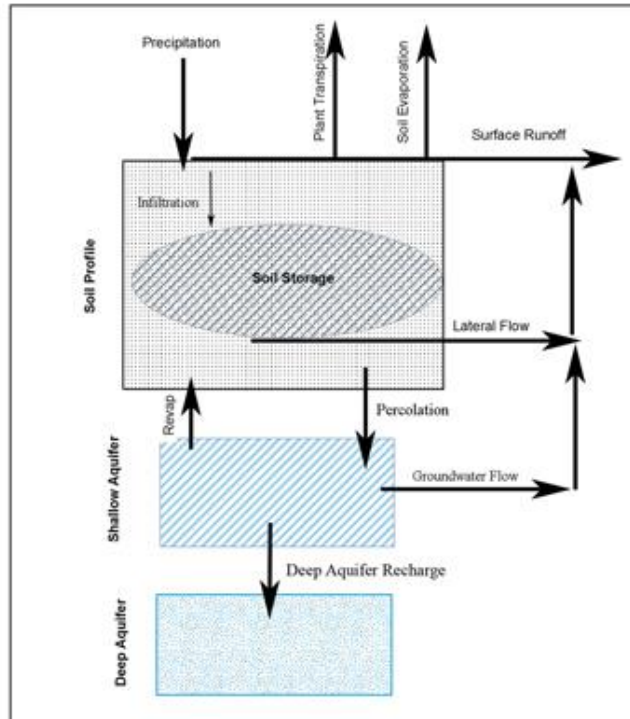


Figure 4-3. Conceptual of SWAT model (Adapted from Neitsch et al., 2005)

4-2-3. Model input

Running SWAT a variety of input data (weather data, soil data) is needed. Weather input data such as daily precipitation, daily minimum and maximum temperature, and daily solar radiations were obtained from the Public Weather Service of the Iranian Meteorological Organization (WSIMO), which had four synoptic, and climatology stations, and 22 rain gauge stations for a period of 31 years from 1977 to 2008. A weather generator model, WXGEN, (Sharpley & Williams, 1990) was used to fill the data gap. River discharge data were collected from Iran Water Resources Management Company (IWRMC), and Hamedan Regional Water Co. (HMRW) for 3 outlet stations, Omar Abad, Zehtaran, and Sirabe Khomigan,, and one inlet station for the period of 1977–2008. Winter wheat is a dominant crop in the study area and was obtained from 1998 to 2008 in central plain of Razan-Ghavand from Hamedan agricultural organization. Digital elevation model (DEM) and digital stream network map were extracted

from topography map of National Cartographic Center of Iran (NCC) with a resolution of 15 m. Land use/land cover map was created from satellite images (Landsat TM) dated in 2009 according to supervised classification (Rafiei Emam et al., 2015). The landuse/land cover map includes 7 classes including irrigated agriculture, rain fed agriculture, good rangeland, moderate rangeland, weak rangeland, bare lands and urban. A five-layer soil map was generated using soil profile information including 13 types of soil (Soil & Water Research Institute). Physical parameters of each layer such as texture, available water content, field capacity, wilting point, hydraulic conductivity, and bulk density, were estimated by Soil-Plant-Air-Water model, SPAW, (Saxton & Willey, 2005), and based on silt, sand, and clay content of each layer. The slope map was produced using the DEM algorithm in ArcGIS whereat the slope range was divided into three classes: 0-2%, 2-5% and >5%.

4-2-4. Model setup

The first step inside SWAT to set up the model is to create hydrologic response units (HRUs) which are the basis of groundwater recharge calculation in this study. The hydrologic response units (HRUs) are produced by integrating the single sub-basins (by delineation of the watershed according to the DEM and the stream network system), soil, land use, and slope maps. A model is constructed using dominant HRUs (dominant soil and land use types defining the soil and land use of the sub-basins). A second model is constructed using multiple HRUs (To define HRU, 10 % threshold of land use and soil was selected); in the first step 138 HRUs (or sub-basins) are created and in the second attempt 831 HRUs in the watershed are derived.

Agricultures especially irrigated farmlands have significantly influence on groundwater recharge. We simulated the crop growth in order to estimate crop yields in SWAT model. The crop yields further were used in the calibration of the hydrologic model. Winter wheat was chosen as the representative crop in Razan-Ghahavand watershed. For rain-fed and irrigated lands two agricultural schedules are defined according to the information obtained from farmers and the Hamedan Agricultural Organization. Fertilization operations and auto-irrigation, based on water stress thresholds, are used to simulate crop growth due to lack of water use data in irrigation. The Hargreaves method (Hargreaves & Samani, 1985) is used to estimate evapotranspiration, which only requires minimum and maximum temperature. Variable storage routing method is selected to route water through the channel network. To adapt SWAT to the

conditions of the study area, the curve number (CN) is adjusted based on the slope characteristics. While in SWAT, the default curve number is calculated for a slope value of 5%. We also defined elevation bands for sub-basins with more than 100 m elevation difference and define TLAPS (Temperature lapse rate [$^{\circ}\text{C}/\text{km}$]) and PLAPS (Precipitation lapse rate [$\text{mm H}_2\text{O}/\text{km}$]) for these sub-basins. For more detailed information about SWAT see Neitsch et al. (2011).

4-2-5. Model Calibration

The model is calibrated and validated at the sub-basin level based on monthly observed river discharges and annually observed crop yield across the watershed. Data from 1997 to 2002 are used for validation and data from 2001 to 2008 are used for calibration including 2 years of warm up phase.

For calibration of the model and uncertainty analysis, the Sequential Uncertainty Fitting program, SUFI-2 (Abbaspour, 2011) is chosen. SUFI-2 is an algorithm for sensitivity, calibration, validation, and uncertainty analysis. SUFI-2 has been used in many studies before for calibration and uncertainty analysis (Abbaspour et al., 2009; Schuol et al., 2008; Faramarzi et al., 2009).

In SUFI-2 algorithm, uncertainties including parameter, conceptual model, and input (e.g. precipitation) are mapped on the parameter ranges. The objective of the procedure was to capture most of the measured data within the 95% prediction uncertainty (Abbaspour et al., 2007). Model output is expressed as 95% prediction uncertainty (95PPU), which was calculated at the 2.5% and 97.5% levels of the cumulative distribution of an output variable obtained through Latin Hypercube sampling. The P-factor and R-factor were used to quantify the strength of calibration and uncertainty performance. The P-factor is the percentage of measured data bracketed by the 95PPU band, and the R-factor is the average width of the 95PPU band divided by the standard deviation of the measured data. Ideally, we would like to bracket most of the measured data within the 95PPU band while having the narrowest band. Nash–Sutcliffe model efficiency (NS) and coefficient of determination (R^2) were used to assess the SWAT model. For crop yield, MSE (mean square errors) was used as the objective function (Akhavan et al., 2010; Faramarzi et al., 2010; Abbaspour et al., 2009).

We identified the most sensitive parameters for each hydrometric station separately by changing specific parameters such as CN within their allowable range to obtain the best range. After calibrating the model for hydrology, crop parameters were calibrated including heat unit (HU), bio target (BIO-TARG), harvest index (HI) and auto water stress (AUTO_WSTRS). Heat unit shows growing degree days needed to bring plant to maturity. Bio target controls biomass produced by the plant every year, and harvest index is the weight of the harvested portion of the plant biomass divided by the weight of the total aboveground plant biomass. Auto water stress is limiting the need to prescribe exact amounts and timing for irrigation.

4-3. Results and Discussion

There are many published works on the estimation of groundwater recharge as well as the trend of water level and land degradation in semi-arid regions. The principal differences exist between various methods to estimate groundwater recharge. However, numerical method is widely used to estimate groundwater recharge (Arnold & Allen, 1999; Gehrels et al., 2001; Manghi et al., 2009; Xu et al., 2011; Barthel et al., 2012). Most of the researchers focused on the estimation of shallow groundwater recharge, which means water that percolates into shallow aquifer. However, we revealed deep aquifer recharge, water percolate into the deep aquifer with depth more than 20 meter, while water harvesting from deep aquifer using excavating of deep wells is usual in our study area. Based on an initial sensitivity analysis, a number of parameters such as soil parameters, groundwater parameters, snow parameters, crop parameters were chosen to calibrate the hydrologic model. These parameters were then regionalized based on their location in the watershed by assigning the sub basin numbers to the parameter (Table 4-1). The measure of sensitivity and the significance of sensitive parameters were provided by the t-stat and the p-value, respectively. The initial and final ranges of these parameters are also indicated in Table 4-1.

Table 4-1. The most sensitive parameters and their initial and final ranges

Parameter ^a	t-value	p-value	Initial range	Final range
r_CN2.mgt_____23,26,27,28,29,32,33,34,37,38,41 ^b	-44.67	0.00	-0.5 0.5	-0.27 -0.02
r_CN2.mgt_____1,2,3,4,5,6,12,13,14	-15.06	0.00	-0.5 0.5	-0.29 -0.15
v_SMFMN.bsn	-11.31	0.00	0 10	0.0 5.5
v_ALPHA_BNK.rte_____1,2,3,4,5,6,12,13,14	-9.39	0.00	0.01 1.00	0.02 0.17
v_ALPHA_BNK.rte_____23,26,27,28,29,32,33,34,37,38,41	-9.27	0.00	0.01 1.00	0.06 0.48
r_SOL_AWC().sol_____23,26,27,28,29,32,33,34,37,38,41	7.33	0.00	-0.5 0.5	-0.35 -0.10
v_SMFMX.bsn	-4.93	0.00	0 10	1.8 5
v_TIMP.bsn	-4.89	0.00	0.01 1	0.05 0.70
v_GWQMN.gw_____23,26,27,28,29,32,33,34,37,38,41	2.02	0.04	0 5000	2028 4830
V_GW_DELAY.gw_____1,2,3,4,5,6,12,13,14	2.34	0.02	0 500	322 407
v_CH_K2.rte_____23,26,27,28,29,32,33,34,37,38,41	2.47	0.01	0 150	20 65
r_SOL_AWC().sol_____1,2,3,4,5,6,12,13,14	1.97	0.05	-0.5 0.5	-0.26 -0.12
v_GW_REVAP.gw_____23,26,27,28,29,32,33,34,37,38,41	1.78	0.07	0.02 2	0.17 0.20
V_GW_DELAY.gw_____7-11,15- 22,24,25,30,31,35,36,39,40,42-138	1.64	0.10	0 500	302 401

^a r: parameter value is multiplied by 1+ given value, v: parameter value is replaced by a value from the given range

^b Sub basin numbers

Generally, Hydrological models are sensitive to various kinds of input variables related to vegetation, land management, soil, weather, aquifer, and channels (Arnold et al., 2000). Finch (1998) revealed that the variables related to soil components (e.g. water capacity) are the most crucial land surface parameters for estimating groundwater recharge. We found the same result in our study. We revealed that the curve number (CN) and the groundwater delay time (GW-DELAY) are the most crucial parameters, which are related to both soil and vegetation.

Our study showed that the curve number (CN2) is the most sensitive parameter in the mountainous areas; this could be probably due to relatively low rainfall rate in the watershed and steepness of the area. Vaghefi et al. (2014) mentioned that the most sensitive parameter of mountainous Karkheh river basin is CN2. The same result was reported by a number of other studies (Akhavn et al., 2010; Famarzi et al., 2009; Schmalz et al., 2008). The sensitivity of CN2 parameter is shown in Figure 4-4, where an increase in the CN2 values leads to raising runoff and consequently decreasing groundwater recharge and infiltration estimation. The second

sensitive parameter in highlands was minimum melt rate for snow in December (SMFMN); this is because snowmelt controls much of the stream flow in the mountainous region. Akhavan et al. (2010) also reported the same result.

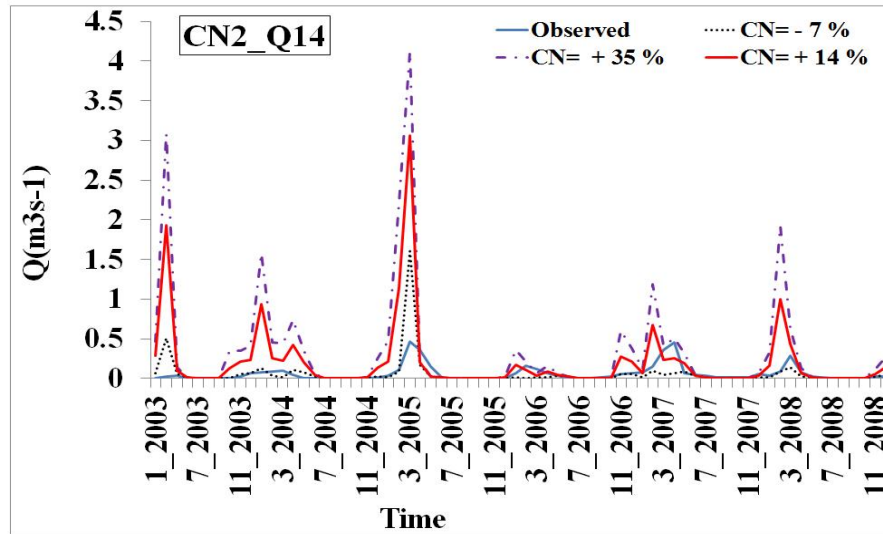


Figure 4-4. The sensitivity analysis of CN2 parameter by decreasing 7 percent, and increasing 14 and 35 percents of CN2 value against surface runoff production.

The most sensitive parameter in lowlands was groundwater delay time (GW_DELAY) which describes the delay time of water that moves past the lowest depth of the soil profile by percolation or bypass flow before becoming shallow aquifer recharge. This parameter depends on the depth of the water table and the hydraulic properties of the geological formation in the vadose and groundwater zone. Schmalz et al. (2008) revealed the same result for groundwater parameters in low land areas.

The results of model calibration and validation for river discharge were quite satisfactory (Figure 4-5). At all stations, the flow dynamics was simulated quite well (R^2 higher than 0.62). The model simulated the time of runoff peak very well, except in some months. For instance, at Omarabad station in April 2004 and 2007 the model simulated the runoff earlier than the actual time, which is probably due to an earlier simulated snow melt (Figure 4-5a). Eckhardt & Ulbrich (2003) mentioned that the rising temperature and the earlier beginning of the growing season may have result in this uncertainty. Another possibility could be the paucity of data on water use in the farmlands. This result is comparable to the work of Akhavan et al. (2010) and Rostamian

et al. (2008). They also mentioned that SWAT cannot simulate the snow melt precisely; the evidence of this came from the model weakness to simulate peak flow rates in their study, which also has been revealed in some months in our calibration as well. The validation results (Figure 4-5b), however, are satisfactory, represented by high NS (66%) and R^2 (0.69). At Zehtaran station (No.41), Figures 4-5 c & d, a P -factor of more than 0.5 shows that the model simulates the runoff very well at this station. In Sirab-Khomigan (No.14), Figures 4-5 e & f, the results of calibration and validation showed a high accuracy of simulation.

After calibration, we compared the statistical results of dominant (with 138 HRU) and multiple or non-dominant (with 831 HRU) models (Figure 4-6). The results showed that multiple HRUs model, i.e. non-dominant HRU models, were more accurate and reliable than the dominant HRU models. We used the more accurate model for further analysis. Many researchers used HRU as a basis of groundwater recharge estimation. (Awan et al., 2013) revealed that the HRUs can be used not only to facilitate the identification of the sub-unit's characteristics, but also help to estimate the recharge into the entire basin. Arnold et al. (2000) simulated daily water balance in the HRUs in order to simulate groundwater recharge.

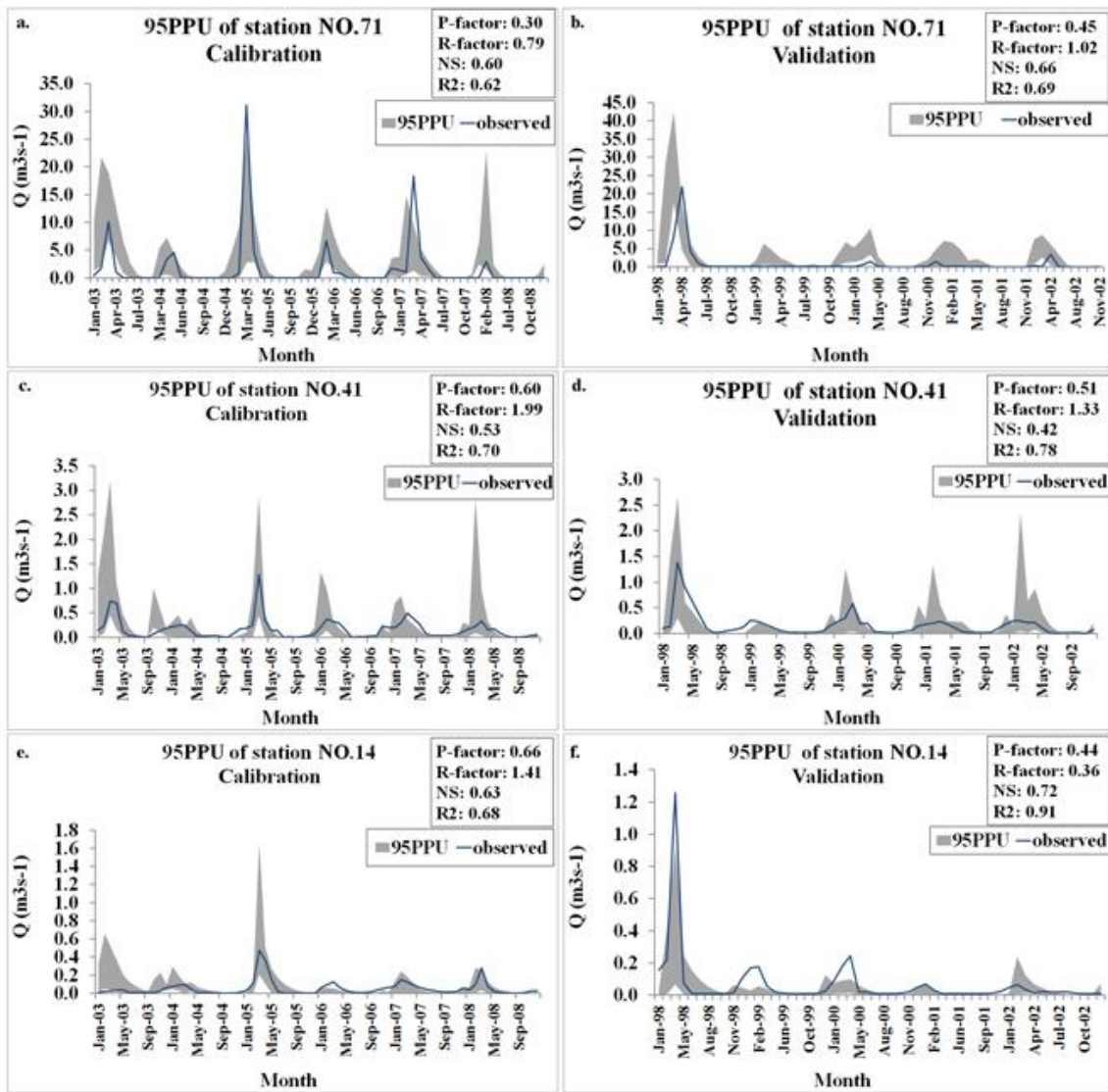


Figure 4-5. Result of calibration and validation in a & b: Omarabad station (No.71); c & d: Sirab khomigan station (No.41) and e & f: Zehtaran station (No.14)

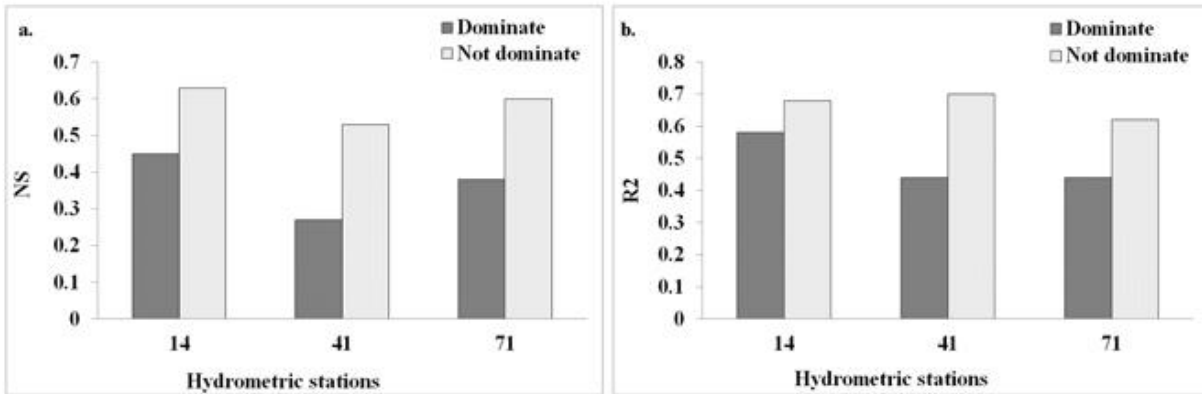


Figure 4-6-a,b. Statistical results of dominate and non-dominate HRU in SWAT model

4-3-1. Calibration of model for crop yield

After the calibration of the model by discharge, we calibrated the crop parameters. A good calibration with crop yield would result in a good calibration of evapotranspiration (ET) adding more confidence to simulation of soil moisture and groundwater recharge (Faramarzi et al. 2009). Model uncertainties for irrigated wheat are larger than for rain fed wheat in both calibration and validation results (Figure 4-7). For irrigated fields the yield varies from 2430 kg ha⁻¹ to 3780 kg ha⁻¹, and for rain fed fields the yield varies from 890 kg ha⁻¹ to 1362 kg ha⁻¹. For irrigated and rain fed yield, the p-factor was quite satisfactory and varies from 0.67 to 0.92. The r-factor was quite small for rain fed rather than irrigated yield which indicates low uncertainties of prediction. Vaghefi et al. (2014) mentioned that a p-factor larger than 0.73 for irrigated yield is satisfactory in a semi-arid river basin of Karkheh in Iran.

The RMSE for rain fed yield was just 70 kg ha⁻¹ and 250 kg ha⁻¹ in calibration and validation period, respectively, what documented high accuracy of rain fed calibration. In irrigated lands the RMSE varies from 190 kg ha⁻¹ to 691 kg ha⁻¹ both for validation and calibration. Akhavan et al. (2010) mentioned the high ranged of RMSE (80 to 4220 kg ha⁻¹) for calibration and validation of crop yield (e.g. wheat and potato) in Hamedan area, Iran. They revealed that the large RMSE could be owing to the lack of data concerning to management practices (e.g. tillage operation, irrigation operation, planting date), which can be accounted also in our study area. The same limitation is also reported by Framarzi et al. (2010). Overall, the calibration and validation

of crop yield in our study was satisfactory due to low RMSE and pretty high value of p-factor both in calibration and validation period.

4-3-2. Groundwater recharge, water level and land subsidence

The process of runoff and crop simulation in the study area did not only lead to model parameters being defined, but also allowed the delineation of the recharge rate. In other words, with calibration and prediction of surface runoff and crop yield, the recharge rate can be estimated with high confidence. Sun & Cornish (2005) reported the same result. Githui et al. (2012) used river discharge and evapotranspiration data in order to calibrate the SWAT model for groundwater recharge estimation. Immerzeel & Droogers (2008) also mentioned that ET is useful to better simulate the water balance components such as groundwater recharge. Estimated groundwater recharge was analyzed for an 11-year period from 1998 to 2008. The estimated annual average recharge for this period (1998-2008) was 4.8 mm/yr. Figure 4-8 shows that recharge has been dominated by the period surrounding 2003. A rather meaningful relationship is seen between groundwater recharge, simulated by SWAT, and observed groundwater level (Figure 4-8). A sharp decline in water level from 1998 to 2002 is accompanied by a decreasing groundwater recharge. As groundwater recharge increased from 2001 to 2003, groundwater level remained rather constant until 2005, which started to decrease again as groundwater recharge decreased.

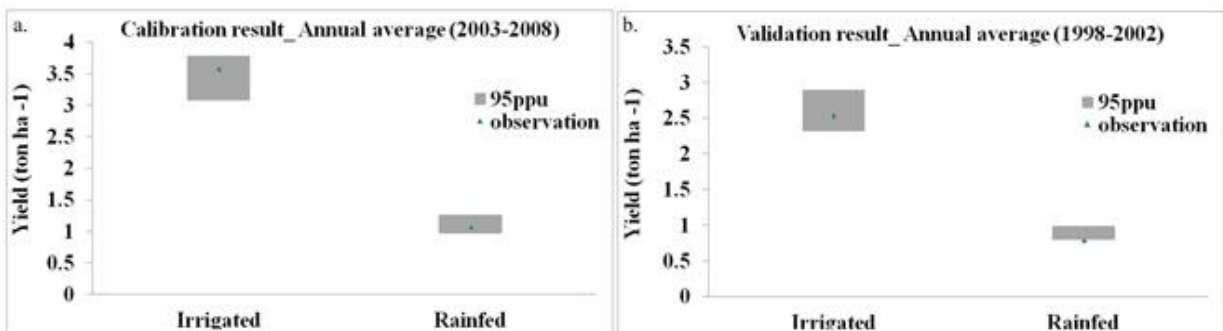


Figure 4-7-a,b. Calibration (left graph) and validation (right graph) results of annual average (2003–2008 for calibration and 1998–2002 for validation) crop yield for rainfed and irrigated wheat in study region. The green point is observation, and the gray band expresses the 95% prediction uncertainty (95PPU).

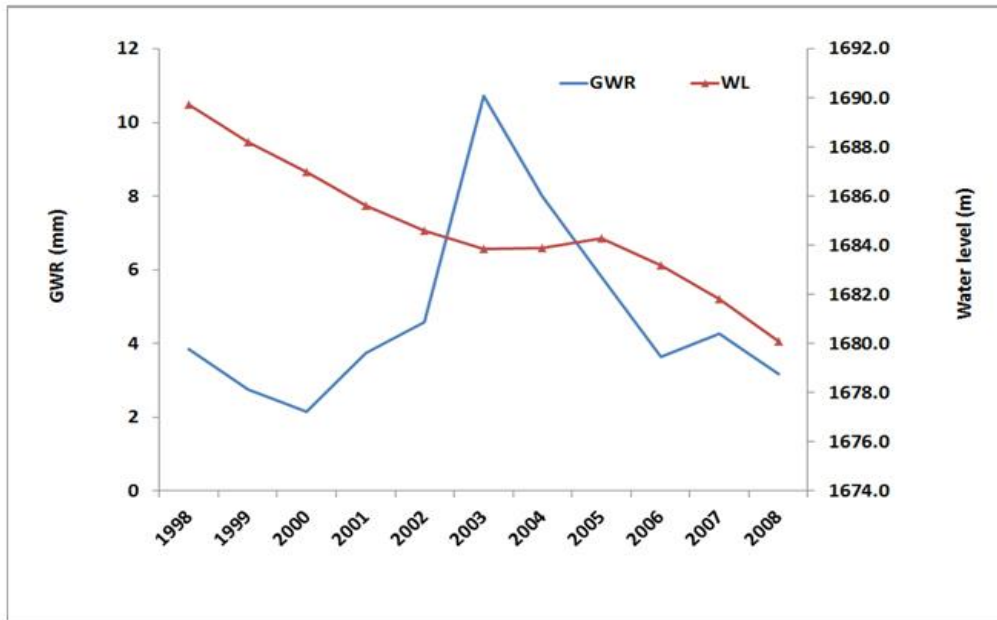


Figure 4-8. Relation between mean annual groundwater recharge and groundwater level from 1998 to 2008

Figure 4-9 shows the groundwater and precipitation distribution in the watershed. The result of water balance showed that precipitation in the north of the watershed is higher than in the southern part. In the south, the average precipitation is below 265 mm per year. Ghahavand desert is located in this part. These areas are degraded because of huge groundwater extraction for irrigation and also for using in power production at Mofatah power plant in previous years and now most of the area is salinized with large occurrences of land subsidence. In the north of the watershed, precipitation is higher than 300 mm per year with good rangeland and ecological condition. Groundwater recharge is high in the north, especially in northeast portion of basin. Apart from the amount of precipitation, Land use/Land cover (LULC) and soil type had significantly effect on groundwater recharge. In the northeast of the basin, there is coarse soil texture, which leads to high groundwater recharge. Whereas in the central and south part of the area, there is finer soil texture which resulted in low GWR. Awan and Ismaeel (2014) mentioned that HRUs that have built-up settlements have no groundwater recharge. They revealed that sandy loam textures have the largest amount of groundwater recharge in compare to other type of texture in the study area in Punjab province, Pakistan.

The estimation of temporal precipitation showed an increase in average annual precipitation in 2002 and 2003 (Figure 4-10) and resulted in raising groundwater recharge in 2003. More than 16 percent of precipitation (62 mm) in 2002 occurred in December, which significantly affected the hydrological process in 2003.

Borehole data from 1998 to 2008 were investigated comprehensively using 81 borehole sites. The water level in the north of the aquifer is more or less constant while in the west of the aquifer water levels varied in different places. The depth of groundwater level is from 0.5 m in the north to 140 m in the west of the aquifer. Among all, six piezometric wells were selected around the aquifer to assess the water level fluctuations (Figure 4-11). The groundwater level assessment showed that a minimum groundwater decrease was observed in wells No. 1, 2 and 3 in north and eastern part of the study area, and the maximum groundwater level decrease was observed in well No. 5 and 6 (in the West and South West of the region). Groundwater levels in the west and south west of the aquifer have experienced a steady decline as a result of increasing groundwater extraction for agricultural irrigation purposes and also of water use of the Mofatah power plant. In the north and east of the region there is no significantly declining of the groundwater level.

Most of the land subsidence occurred in the west of the watershed which has been shown in Figure 4-1. This area is under intensive agriculture use. The comparability of groundwater recharges and point measurements of groundwater level in the sub basin assigning land subsidence in the west of the watershed is shown in Figure 4-12. The figure shows that groundwater level decreased by about 40 m during this time but the recharge did not change significantly. The trend of groundwater level was not the same as the groundwater recharge. Water extraction exceeded that of recharge which caused the groundwater level to decrease. Timothy (2006) mentioned that more than 80% of serious land subsidence problems are associated with huge withdrawal of groundwater, making it a growing problem throughout the world. On the other hand, poorly managed irrigation systems and high removal of groundwater for irrigation purposes lead to increasing critical groundwater levels, enhancing secondary salinity (UNDP, 2007). We also generally projected the same result in our study area (e.g. in central and east of the basin salinization appeared in farmlands). Land degradations turn out to be

costly in the agricultural lands. Awan et al. (2002) cited that land salinization and degradation of farmlands in Uzbekistan led to costs of US\$31 million annually.

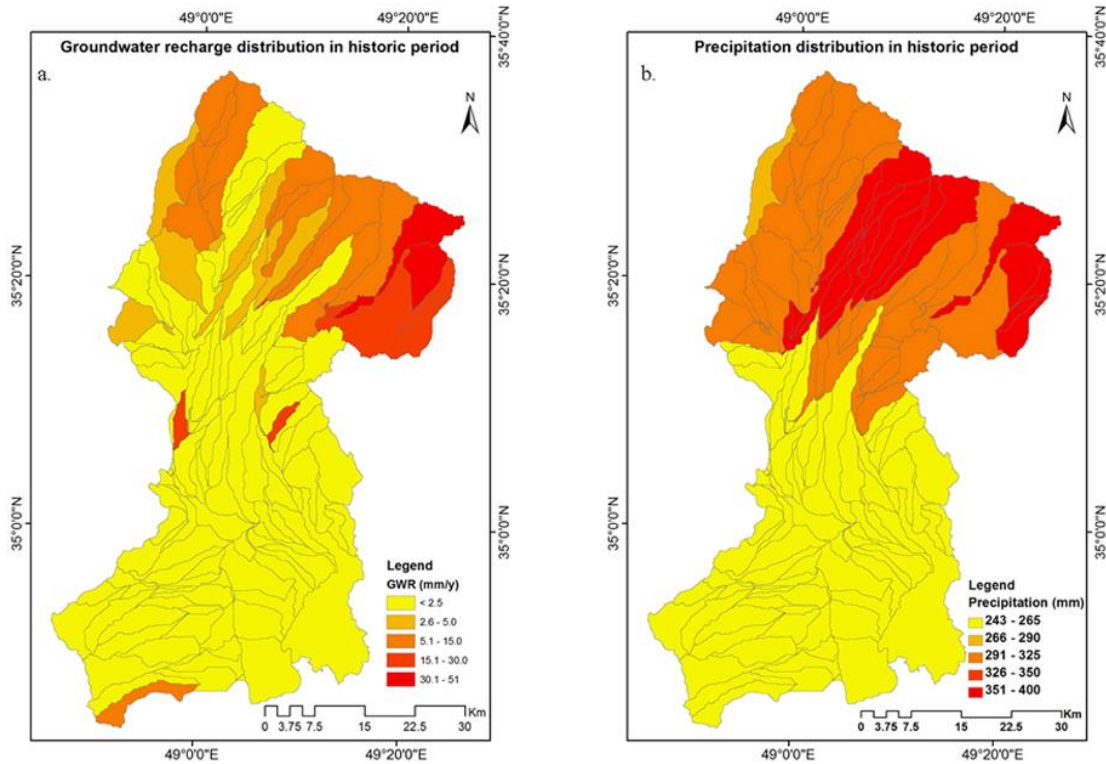


Figure 4-9. Average yearly of groundwater recharge and precipitation distributions in each sub basin in the watershed

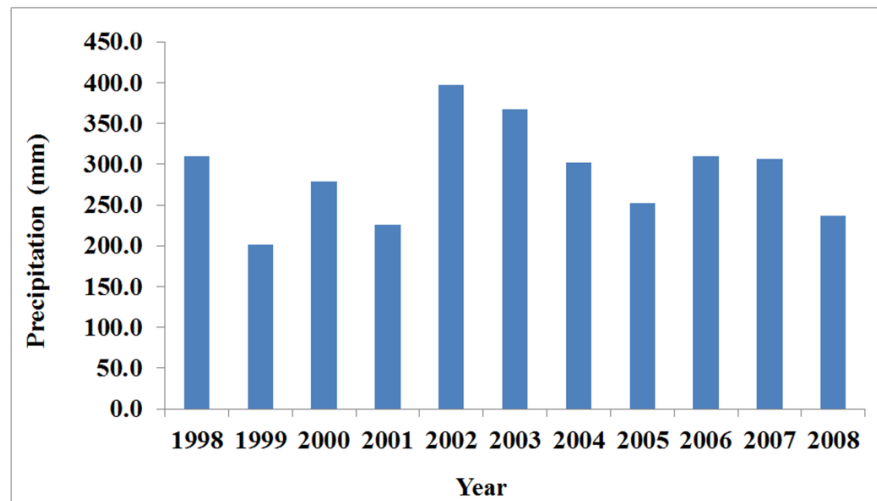


Figure 4-10. Mean annual precipitation in Razan-Ghahavand study area, showing drought cycles from 1999 to 2008. An increase precipitation in 2002 and 2003 may have significantly increased on groundwater recharge in 2003.

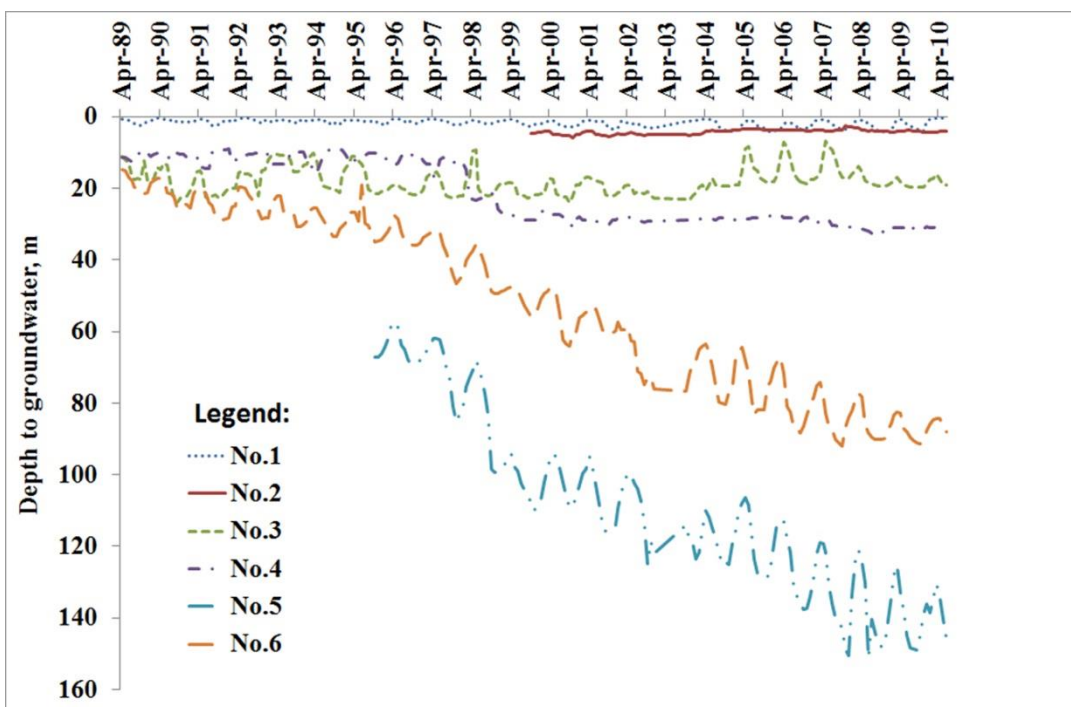


Figure 4-11. Depth to groundwater at different locations in the study area. Bores No.1, 2, and 3 are located in North of area. Bore No. 4 in East, and bores No. 5 and 6 are located in West of area

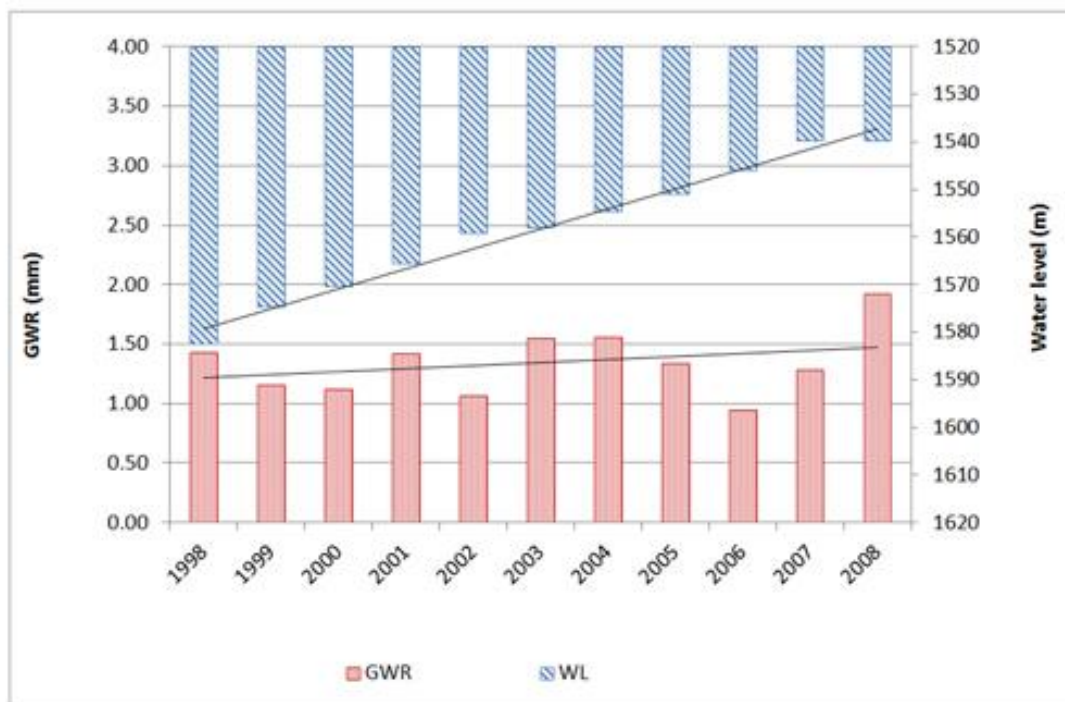


Figure 4-12. Trend of groundwater recharge and groundwater level in west of the watershed, where land subsidences has been occurred.

4-4. Summary and Conclusions

The concept of HRU that was used in this research, made it possible to recognize the influence of variables on groundwater recharge. In this study, we demonstrated that the more detailed HRU use in the model (Multiple HRU model approach) had the better performance of the model in a semi-arid region of Razan-Ghahavand. The definition of model parameters played a key role in precise estimation of groundwater recharge by the SWAT water balance model. The model was calibrated both by surface runoff and crop yield with uncertainty analysis. SWAT has been extensively tested for a variety of climates, however little is known about its performance in semi-arid regions where river discharge is too low normally with high peak flow in flood events, or even there are just seasonal streams which make the model too complex for precise calibration. Lack of data on the amount of water used in irrigated lands was another limitation of this research.

Temporal and spatial estimation of groundwater recharge can provide detail information for decision makers and stakeholder to regulate groundwater recharge for sustainable development. The annual average of groundwater recharge was verified by independently observed borehole data in the study area. Awan et al. (2013) presented the same method. In general, temporal assessment showed that groundwater recharge did not change significantly during the time step from 1998 to 2008, except in 2003 due to highest precipitation, while the water table declined about 1 meter per year. In particular, the water level was decreased about 3.6 meters in year in the west of the watershed with no significantly change in recharge. Overexploitation of groundwater was the main reason of the declining water level.

Groundwater is the main source of water in the study area and more than 90 percent of groundwater was used for agriculture while the rest went for industry and drinking. As the amount of water withdrawal is more than the water recharge and the bedrock in the west of the basin is limestone, overexploitation of water lead to joints and fracture systems in the bedrock, which is one of the main causes of land subsidence in this area.

4-5. References

- Abbaspour KC (2011) User Manual for SWAT-CUP: SWAT Calibration and Uncertainty Analysis Programs. Swiss Federal Institute of Aquatic Science and Technology, Eawag, Duebendorf, Switzerland. 103 pp.
- Abbaspour KC, Faramarzi M, Ghasemi SS, Yang H (2009) Assessing the impact of climate change on water resources in Iran. *Journal of water resources research* 45:1-16. DOI: 10.1029/2008WR007615.
- Abbaspour KC, Yang J, Maximov I, Siber R, Bogner K, Mieleitner J, Zobrist J, Srinivasan R (2007) Modelling hydrology and water quality in the pre-alpine/alpine Thur watershed using SWAT, *Journal of Hydrology* 333: 413–430, DOI:10.1016/j.jhydrol.2006.09.014.
- Abrishamchi A, Tajrishi M (2005) Inter basin water transfer in Iran. In *Water conservation, reuse, and recycling: proceeding of an Iranian American workshop*, The National Academies Press: Washington, D.C.;252–271.
- Adeel Z, Safriel U, Niemeijer D, White R (2005) *Ecosystems and Human Well-Being: Desertification Synthesis*, World Resource Institute, Washington, D.C.
- Akhavan S, Abedi-Koupai J, Mousavi SF, Afyuni M, Eslamian SS, Abbaspour KC (2010) Application of SWAT model to investigate nitrate leaching in Hamadan–Bahar Watershed, Iran. *Agriculture, Ecosystems and Environment journal* 139: 675–688.
- Amiraslani F, Dragovich D (2011) Combating desertification in Iran over the last 50 years: An overview of changing approaches. *Journal of Environmental Management* 92:1-13.
- Amiri M (2005) Relationship between Sinkholes of Famenin - Kabudrahang- Ghahavand Plain and the Bed Rock of the Area. *Geosciences journal* 58: 134-147.(Persian language)
- Arnold JG, Allen PM (1999) Automated Methods for Estimating Baseflow and Ground Water Recharge from Streamflow Records. *Journal of the American Water Resources Association* 35:411–424.

- Arnold JG, Muttiah RS, Srinivasan PM, Allen PM (2000) Regional Estimation of Base Flow and Groundwater Recharge in the Upper Mississippi River Basin. *Journal of Hydrology* 227:21–40.
- Arnold JG, Srinivasan R, Muttiah RS, Williams JR (1998) Large area hydrologic modeling and assessment–Part 1: Model development. *Journal of the American Water Resources Association* 34: 73–89.
- Awan UK, and Ismaeel A (2014) A new technique to map groundwater recharge in irrigated areas using a SWAT model under changing climate. *Journal of Hydrology* 519, Part B(0): 1368-1382.
- Awan UK, Tischbein B, Martius C (2013) Combining hydrological modeling and GIS approaches to determine the spatial distribution of groundwater recharge in an arid irrigation scheme. *Irrigation Science* 31(4): 793-806.
- Barthel R, Reichenau TG, Krimly TD, Schneider K, Mauser W (2012) Integrated modeling of global change impacts on agriculture and groundwater resources. *Water Resources Management* 26:1929–1951. DOI:10.1007/s11269-012-0001-9.
- Beheshti H (2011) The prospective environmental impacts of Iran nuclear energy expansion . *Energy Policy* 39: 6351–6359.
- Brown L (2005) Stabilizing water tables: falling water tables. In: Brown, L. (Ed.), *Outgrowing the Earth: The Food Security Challenge in an Age of Falling Water Tables and Rising Temperatures*. UK: Earth Scan, pp. 101.
- Chen YN, Li WH, Xu HL, Liu JZ, Zhang HF, Chen YP (2003) The influence of groundwater on vegetation in the lower reaches of Tarim River. *Acta Geographica Sinica* 58:542–549.
- Eckhardt K, Ulbrich U (2003) Potential impacts of climate change on groundwater recharge and streamflow in a central European low mountain range. *Journal of Hydrology* 284: 244–252.

- Faramarzi M, Abbaspour KC, Schulin R, Yang H (2009) Modelling blue and green water resources availability in Iran. *Hydrological Process* 23: 486–501.
- Faramarzi M, Yang H, Schulin R, Abbaspour KC (2010) Modeling wheat yield and crop water productivity in Iran: implications of agricultural water management for wheat production. *Agricultural Water Management* 97: 1861–1875.
- Finch JW (1998) Estimating direct groundwater recharge using a simple water balance model—sensitivity to land surface parameters. *Journal of Hydrology* 211: 112–125.
- Gehrels H, Peters NE, Hoehn E (2001) *Impact of Human Activity on Groundwater Dynamics*. IAHS Publication,
- Githui F, Selle B, Thayalakumaran T (2012) Recharge estimation using remotely sensed evapotranspiration in an irrigated catchment in southeast Australia. *Hydrological Processes* 26(9): 1379-1389.
- Gullison JJ, Bourque CPA (2001) Spatial prediction of tree and shrub succession in a small watershed in Northern Cape Breton Island, Nova Scotia, *Ecological Modelling* 137: 181–189.
- Guo Q, Feng Q, Li J (2009) Environmental changes after ecological water conveyance in the lower reaches of Heihe River, northwest China. *Environmental Geology* 58(7):1387-1396.
- Hargreaves G, Samani ZA (1985) Reference crop evapotranspiration from temperature, *Applied engineering in agriculture* 1: 96–99.
- Immerzeel WW, Droogers P (2008) Calibration of a distributed hydrological model based on satellite evapotranspiration. *Journal of Hydrology* 349: 411–424.
- Ji XB, Kang ES, Chen RSh, Zhao WZh, Zhang Zh H, Jin BW (2006) The impact of the development of water resources on environment in arid inland river basins of Hexi region, Northwestern China. *Environmental Geology* 50:793–801.

- Kappas M, Propastin P (2013) Monitoring and Assessment of Dryland Ecosystems with Remote Sensing. In: Chen, Jiquan, Wan, Shiqiang, Henebry, Geoffrey, Qi, Jianguo, Gutman, Garik, Sun, Ge, Kappas, Martin. (eds.). Dryland East Asia. Land Dynamics Amid Social and Climate Change. De Gruyter/Higher Education Press, pp. 309-349
- Kite GW (1995) The SLURP model. In: V.P. Singh (Editor), Computer Models of Watershed Hydrology. Water Resources Publications, p. 521-562.
- Lu D, Batistella M, Mausel P, Moran E (2007) Mapping and monitoring land degradation risks in the Western Brazilian Amazon using multitemporal Landsat TM/ETM+ images. Land Degradation & Development, 18(1): 41-54.
- Manghi F, Mortazavi B, Crother C, Hamdi MR (2009) Estimating regional groundwater recharge using a hydrological budget method. Water Resources Management 23:2475–2489. doi:10.1007/s11269-008-9391-0
- Motagh M, Walter T R, Sharifi MA, Fielding E, Schenk A, Anderssohn J, Zschau J (2008) Land subsidence in Iran caused by widespread water reservoir overexploitation. Geophysical research letters 35, L16403, doi:10.1029/2008GL033814, 2008
- Neitsch SL, Arnold JG, Kiniry JR, Williams JR, King KW (2011) Soil and water assessment tool. Theoretical documentation. TWRI TR-191. College Station, Texas: Texas Water Resources Institute.
- Qi SZ, Luo F (2005) Water environmental degradation of the Heihe River basin in arid northwestern china. Environmental Monitoring and Assessment 108:205–215.
- Rafiei Emam A, Kappas M, Abbaspour KC (2015) Simulation of water balance components in a watershed located in central drainage basin of Iran. In: Remote Sensing of the Terrestrial Water Cycle, Geophysical Monograph 206 (V. Lakshmi, ed.). American Geophysical Union. Wiley & Sons press. ISBN: 9781118872031. In press.

- Raneesh KY, Thampi SG (2013) A Simple Semi-distributed Hydrologic Model to Estimate Groundwater Recharge in a Humid Tropical Basin. *Water Resources Management* 27:1517–1532.
- Rostamian R, Jaleh A, Afyuni M, Mousavi SF, Heidarpour M, Jalalian A, Abbapour KC (2008) Application of SWAT model for estimation runoff and sediment in two mountainous basins in central Iran. *Hydrological Science Journal* 53(5):977-988.
- Saxton KE, Willey PH (2005) Watershed Models: Pages 400–435; The SPAW Model for Agricultural Field and Pond Hydrologic Simulation, CRC Press.
- Scanlon BR, Alan D (2002) Groundwater Recharge in Texas. Kansas Geological Survey, Lawrence, KS.
- Schmalz B, Tavares F, Fohrer N (2008) Modeling hydrological processes in mesoscale lowland river basins with SWAT— capabilities and challenges. *Hydrological Science Journal* 53(5): 989–1000.
- Schuol J, Abbaspour KC, Srinivasan R, Yang H (2008) Estimation of freshwater availability in the West African sub-continent using the SWAT hydrologic Model. *Journal of Hydrology* 352: 30– 49.
- Sharpley AN, Williams JR (1990) EPIC-Erosion Productivity Impact Calculator: 1. model documentation. U.S. Department of Agriculture, Agricultural Research Service, Tech. Bull. 1768.
- Singh VP (1995) Computer models of watershed hydrology. Water Resources Publications, Highlands Ranch, Colorado, 1130 p.
- Stromberg JC, Tiller R, Richter B (1996) Effects of Groundwater Decline on Riparian Vegetation of Semiarid Regions: The San Pedro, Arizona. *Ecological Applications* 6:113–131.
- Sun H, Cornish PS (2005) Estimating shallow groundwater recharge in the headwaters of the Liverpool Plains using SWAT. *Hydrological Process* 19:795–807.

- Timothy HD (2006) Space geodesy: Subsidence and flooding in New Orleans. *Nature* 441: 587-588.
- UNDP (2007) Water: critical resource for Uzbekistan's future. United Nations Development Program, Tashkent
- Vaghefi S, Abbaspour K, Mousavi S, Srinivasan R, Yang H (2014) Analyses of the impact of climate change on water resources components, drought and wheat yield in the semi-arid Karkheh River Basin in Iran. *Hydrological processes* 28(4): 2018-2032
- Wen X, Wu Y, Su J, Zhang Y, Liu F (2005) Hydrochemical characteristics and salinity of groundwater in the Ejina Basin, Northwestern China. *Environmental Geology* 48:665–675.
- Wisler CO, Brater EF (1959) *Hydrology*. New York : Wiley press.
- Xu X, Huang G, Qu Z, Pereira LS (2011) Using MODFLOW and GIS to assess changes in groundwater dynamics in response to water saving measures in irrigation districts of the Upper Yellow River Basin. *Water Resources Management* 25:2035–2059. doi:10.1007/s11269-011-9793-2
- Yeh HF, Lee CH, Chen JF, Chen WP (2007) Estimation of groundwater recharge using water balance model. *Water Resources* 34(2):153–162.
- Zhang XY, Gong JD, Zhao X, Zhou MX (2005) The change of land cover/land use in Ejina oasis over 20 years. *Advances Earth Sciences* 20(12):1300–1305.
- Zhao C, Wang Y, Chen X, Li B (2005) Simulation of the effects of groundwater level on vegetation change by combining FEFLOW software. *Ecological Modelling* 187: 341-351

Assessing the impact of climate change on water resources, crop production and land degradation in a semi-arid river basin ³

Abstract

The semi-arid regions of Iran have experienced severe water resources stress due to natural (e.g. drought) and anthropogenic (e.g. depletion of water in various sectors) factors. Assessing the impact of climate change on water resources and crop production could significantly help to better water management and hence prevention of land degradation in this area. A hydrological model of the Razan-Ghahavand basin was used as a representative case study of a semi-arid region of Iran. Future climate scenarios in the mid-21st century were generated from four global circulation models (GCMs) with three scenarios under the fourth assessment report (AR4) of Intergovernmental Panel on Climate Change (IPCC) emission projections. The GCMs have been downscaled based on observed data at ten climate stations across the basin. The results showed that for the basin as whole, the mean annual precipitation is likely to decrease while the maximum temperature increases. The changes in these two climate variables resulted in substantial reduction in groundwater recharge as the main source of water supply in this area. Furthermore, soil water content was decreased which resulted in the reduction of crop yield in rain-fed areas. Indeed, the risk of drought in the south and flooding in the north was high.

³ This paper is accepted to publish in peer-reviewed "Hydrology Research Journal". IWA, Inc.

5-1. Introduction

Semi-arid regions suffer from shortage of water. Climate variation alongside anthropogenic factors such as population growth, land-use changes, and overuse of water resources especially for irrigation, are significant concerns. Climate change and its impact on water resources have further challenge in the sensitive and fragile ecosystems like the semi-arid regions of Iran. The availability of water resources, crop production and the process of land degradation should be future considerations in this area in order to build up a sustainable ecosystem and to improve food security. However, the uncertainty of Global Circulation Models (GCMs) may lead to different results in the same area (Gosain et al., 2011; Singh & Bengtsson, 2005; WWF, 2010). Therefore, we developed an ensemble of GCMs model to predict the water availability and also the capacity of crop production in the semi-arid region of Iran.

Hijioka et al. (2014) in IPCC-AR5 mentioned that increasing water demand and mismanagement of water resources give rise to water scarcity as a major challenge for most regions in Asia. According to IPCC (2007a) climate change has a pernicious effect on water resources and freshwater availability in most of the regions of the world. It can also have a significant impact on the hydrological cycle (Piao et al., 2009; Wu et al., 2012). IPCC (2013) in their AR5 report revealed that human influence in global warming and changing of water cycle has grown since AR4. The quantum of damages, however, can differ from one place to another. The Variation of precipitation and temperature characteristics can lead to land degradation especially in fragile arid and semi-arid ecosystems (Meadows & Hoffman, 2003). The variation of intensity and variability of precipitation lead to increasing risks of droughts and floods in most of the regions. Furthermore, alteration in floods and droughts and a rise in water temperature are changing the water quality (IPCC, 2007b). IPCC (2014) reported that drought frequency would likely raise in presently dry regions by the end of the 21st century. Shifts in precipitation and temperature results in variations of groundwater recharge and also causes water table fluctuations (Changnon et al., 1988; Zektser & Loaiciga, 1993). Additionally, changes in groundwater recharge can have an influence on evapotranspiration, groundwater flow direction, groundwater level and surface water-groundwater interaction (Ali et al., 2012).

Land use changes (particularly urbanization) could alter the hydrological response of an area by changing the amount of rainwater that goes into surface discharge and groundwater recharge (Baker & Miller, 2013). However, the impact of Land Use / Land Cover change (LULCC) varies

with the climatic conditions (Kim et al., 2013). Human activities and climate variability can influence on the hydrological processes (e.g. annual runoff, stream flow) especially in semi-arid regions (Zhan et al., 2013; Xu et al., 2013). Zhou et al. (2013) revealed that surface runoff and base flow are very sensitive to urbanization, whereas evapotranspiration and annual streamflow are less sensitive. Many previous studies identified a combined effect of climate and land use change on water components (e.g. surface runoff) (Kim et al., 2013; Tu, 2009; Tong et al., 2012).

Food-producing capacity and livestock production can be significantly affected by climate change for years to come. While some areas may experience a decrease in crop production, others are likely to increase. CO₂ concentration and temperature are two important factors affecting crop production. While increasing CO₂ concentration as the main driver of climate change could raise production of some crops (e.g. wheat), the changing climate in general is likely to have a negative effect on the length and quality of the growing season. Additionally, getting higher intensity of droughts and floods could have countless consequences for crop production. On the other hand, a temperature increase of a few degrees is expected to generally raise crop production in temperate areas; however, greater warming may decrease crop yields (Adams et al., 1998; Raleigh & Urdal, 2007).

Assessing the impact of climate change on hydrological processes can be used with various hydrological models (e.g., Kirshen, 2002; Rosenberg et al., 1999). For instance, the Hydrologic Unit Model of the US (HUMUS) was used to assess the impact of global warming on the hydrology of the Ogallala area in the United States, where the comparison of different GCMs shows an influence on the reduction of groundwater recharge (Rosenberg et al., 1999). Eckhardt and Ulbrich (2003) used a revised version of SWAT (Soil and Water Assessment Tools) to investigate the impact of climate change on groundwater recharge and stream flow in a central European low mountain range. The results of their studies show little effect of climate change on mean annual groundwater recharge and stream flow. In this research we used SWAT eco-hydrologic model (Arnold et al., 1998) to study the impact of climate change on water resources and crop productions. Various investigations show the benefit of SWAT to assess the impact of climate change (Fontaine et al., 2001; Young et al., 2009; Faramarzi et al., 2013).

As water resources in Iran become scarcer due to recurrent droughts and rising demand, accurate knowledge of the available resources in the future is mandatory for successful management. The fresh water availability in the semi-arid region of Razan-Ghahavand has

experienced severe reduction due to increasing demand for sanitation, drinking water, manufacturing and agriculture. All of these factors trigger the expansion of land degradation in this area. To improve water resource management, water use efficiency, sustainability of agriculture, and land management to combat degradation in the future, precise knowledge of water resources is needed. There is a close relationship between water resources, industry, agriculture and urban dynamics in this area. Therefore, it is essential to study the climate change impact on hydrology and water resources.

The main objective of this research is to investigate the impact of climate change on water resources components such as groundwater recharge, soil water content, surface runoff and actual evapotranspiration (AET) for 2046-2065. This period was chosen because we would like to know the changes in the mid of 21st century, and on the other hand, the uncertainty of data in this period is less than the end of century. The effect of land use change (e.g. urbanization) on surface runoff, estimation of crop yields and an analysis of future land degradation are the other objectives of this research. We used the ensemble of four global climate models to quantify the impact of climate change on water resources and crop productions in the mid-21st century.

5-2. Material and methods

5-2-1. Study area

The study area called Razan-Ghahavand is located in the central drainage basin of Iran. The area is approximately 3100 km². The range of the highest and lowest elevation inside the watershed is roughly 1265 m. A variety of species has evolved from the highest to the lowest elevation following this gradient. The climate of this region is semi-arid with an annual average temperature around 11⁰C and annual average precipitation of about 295 mm. The main river in the watershed, called Gharehchay, enters the watershed from the east whereas the watershed's outlet is controlled by the Omarabad hydrometric station in the west part of the watershed. Additionally, two other streams, Sirab Khomigan and Zehtaran respectively, join the main river from the north part of the basin. In table 5-1 the watershed area covered by the single hydrometric stations and their sub basins is shown. According to the land use map about 52 % of the area is grazing land covered by species that occur in different numbers and with a varying capacity for livestock rearing. Irrigation farming covers 26% and rain-fed cultivation cover 5 % of the watershed area.

Because of traditional irrigation methods and water conveying systems, the efficiency of water use is only 35 % and substantial amounts of water are lost (Abrishamchi & Tajrishi, 2005). Figure 5-1 shows the location of the study area inside Iran including all available hydrometric and meteorological stations. There are various features of land degradation phenomena in this basin. In the south of the area rangelands have deteriorated. In the west of the basin, the groundwater level has decreased and land subsidence has occurred. In the eastern part arable lands are salinized (Figure 5-2).

Table 5-1- Sub basins affected to flow in each station including the rate of discharge

NO.	Stations Name	Location (in the sub basin)	Sub basins	Area (km²)	Discharge m³s⁻¹
I	Sirab-Khomigan	14	1,2,3,4,5,6,12,13,14*	255	0.33
II	Zehtaran	41	23,26, 27,28,29,32,33,34, 37,38,41	420	0.66
III	Omarabad	71	All sub basin	3100	6.68

* Sub basin numbers

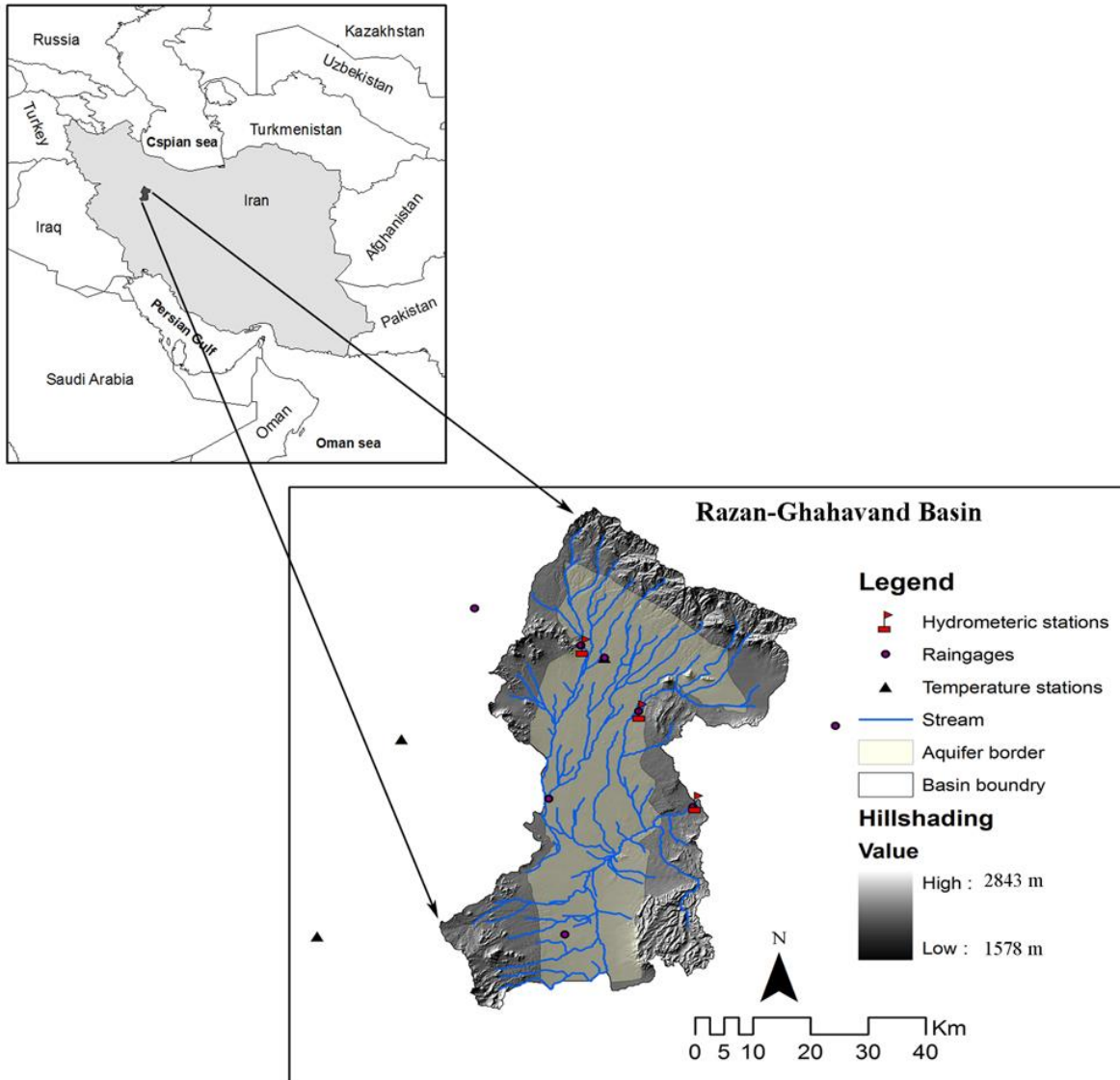


Figure 5-1. Region of Razan-Ghahavand watershed showing the hypsometric map, distribution of river and streams, hydrometric and climatic stations (e.g. rain gage and synoptic)



Figure 5-2. Some features of land degradation in the area (e.g. soil salinization in arable lands, rangeland degradation, and land subsidence)

5-2-2. The SWAT Simulator, model setup, calibration and uncertainty analysis

We used Soil and Water Assessment Tools (SWAT) (Arnold et al., 1998) to assess the influence of climate change on water resources and crop production. SWAT is a hydrologic model to study the quality and quantity of surface and ground water resources and predict the impact of land use, land management and climate change on water resources. It is a physical, distributed and continuous time model that operated on a daily time assessment. The main components of SWAT include hydrology, climate, nutrient cycle, sediment movement, crop growth and agricultural management. Hydrological processes in SWAT simulate surface runoff, potential

evapotranspiration, percolation, lateral subsurface flow, groundwater flow to streams from shallow aquifers, snowmelt, transmission losses from streams, and water storage and losses from ponds (Neitsch et al., 2011). Hydrological response units (HRUs) including homogenous land use, soil and slope characteristics are the units of water balance calculations. The water in each HRU is stored in four storage volumes including snow, soil profile (0-2m), shallow aquifer (2-20 m), and deep aquifer (>20 m).

Basic input data include climate data, soil information, a digital elevation map, a river map, a land use classification plus crop and agricultural management data. All data are needed to set up a SWAT hydrologic model run. Climate data consist of daily precipitation, daily minimum and maximum temperature and daily solar radiation obtained from the weather service of the Iranian meteorological organization (WSIMO) from 1977 to 2008. Because the watershed is not located at the headwater of a particular basin, the inlet was defined for catchment. In other words, inlet is defined to estimate the amount of water entering the basin. The surface runoff inside the catchment is estimated by the SCS curve number method based on daily precipitation, soil hydrologic groups, antecedent soil moisture plus different mapped land use. To adapt the model to the specific study area's condition, the curve number (CN) is modified in relation to changing slope factors. To define the impact of elevation difference on the model, elevation bands are defined for sub-basins an elevation difference of more than 100 m using a specific TLAPS (Temperature lapse rate [$^{\circ}\text{C}/\text{km}$]) and PLAPS (Precipitation lapse rate [$\text{mm H}_2\text{O}/\text{km}$]) value. To route water through the channel network, a variable storage routing method is chosen. The crop growth is simulated based on the EPIC method (Williams et al., 1984) by determining leaf area development (LAI), light interception, and radiation use efficiency. Winter wheat is selected as the dominant crop in agricultural lands both for rain fed and irrigated lands. Schedule planning (e.g. time of planting, irrigation, fertilization, harvesting) was defined both for irrigated and rain fed farmlands according to real information obtained from farmers and the Hamedan Agricultural Organization (HAO). Irrigation application is simulated based on an auto-irrigation routine, because it is difficult to know the volume and specific time of irrigation by farmers during simulation periods. Auto-irrigate triggers irrigation events based on water stress threshold. To estimate potential evapotranspiration (PET) the Hargreaves method (Hargreaves & Samani, 1985) is used. Actual evapotranspiration is obtained based on the Ritchie methodology (Ritchie, 1972).

Several researchers have reported an uncertainty quantification of the hydrological models (Jin et al., 2010; Li et al., 2010; Li et al., 2013). Li & Xu (2014) used Bayesian and Generalized Likelihood Uncertainty Estimation (GLUE) methods to estimate the uncertainty of a hydrological model. Abbaspour (2011) developed a SUFI-2(Sequential Uncertainty Fitting) method to analysis the uncertainty of the hydrological models.

After setting up a SWAT model run, a Sufi-2 algorithm is used to uncertainty analysis and to calibrate the model based on the monthly river discharge and yearly crop yield. The Sufi-2 represents all modelling sources of uncertainties such as input data, conceptual model and parameter selections. The uncertainties are mapped based on the parameter ranges. The algorithm tries to bracket most of the measured data within the 95 percent prediction uncertainty band (95PPU) which is calculated at 2.5 % and 97.5% of the cumulative distribution of an output variable obtained through Latin hypercube sampling. To quantify the goodness of calibration and uncertainty performance two indices (P-factor and R-factor) are used. The P-factor is the percentage of data bracketed by the 95PPU band and the R-factor is the average width of the 95PPU band divided by the standard deviation of the measured data. To compare the measured and simulated monthly discharge and annual crop yield, Nash-Sutcliffe (NS) and Root Mean Square Error (RMSE) objective functions are used, respectively. In this research, we used a previously calibrated SWAT model of the Razan-Ghahavand river system. A detailed description about calibration, validation, uncertainty and sensitivity analysis is presented by Rafiei Emam et al. (2015a).

5-2-3. Climate change model

An increasing CO₂ concentration will have a severe effect on vegetation, especially on leaf area index development and stomata conductance (Wand et al., 1999) and additionally it can lead to changes in evapotranspiration resulting in change to other water components.

The impact of climate change on water resources and crop production was assessed by developing a set of GCMs (General circulation models) parameterized based on three IPCC-AR4 emission scenarios (A1B, B1, and A2) in the middle of the 21st century (2046-2065) defined by the Intergovernmental Panel on Climate Change (IPCC, 2007a). The approved new set of scenarios is described in the IPCC Special Report on Emission Scenarios (SRES). Four different narrative storylines were developed to consistently describe the relationships between the forces

driving emissions and their evolution and to add context for the scenario quantification. The resulting scenarios cover a wide range of the main demographic, economic and technological driving forces of future greenhouse gas and sulphur emissions. The B1 storyline and scenario family describes a convergent world with the same global population, that peaks in mid-century and declines thereafter, as in the A1 storyline, but with rapid change in economic structures toward a service and information economy, with reductions in material intensity and the introduction of clean and resource-efficient technologies. The emphasis is on global solutions to economic, social and environmental sustainability, including improved equity, but without additional climate initiatives. The three A1 groups are distinguished by their technological emphasis: fossil intensive (A1FI), non-fossil energy sources (A1T), or a balance across all sources (A1B) (where balanced is defined as not relying too heavily on one particular energy source, on the assumption that similar improvement rates apply to all energy supply and end-use technologies). The A2 storyline and scenario family describes a very heterogeneous world. The underlying theme is self-reliance and preservation of local identities. Fertility patterns across regions converge very slowly, which results in a continuously increasing population. Economic development is primarily regionally oriented and per capita economic growth and technological change more fragmented and slower than other storylines.

Spatial resolution of GCM output is coarse; therefore we applied a downscaling program (LARS-WG) developed by Semenov and Stratonovitch (2010) in order to generate fine resolution climate data to use the output in the hydrological model. LARS-WG is a model simulating time-series of daily weather at a single site. It utilizes semi empirical distribution to obtain statistical parameters such as length of wet and dry periods, daily precipitation, daily minimum and maximum temperature and daily solar radiation based on daily observed climate data at local stations of the catchment. For the minimum and maximum temperature, auto- and cross- correlation calculated monthly were used by semi empirical distribution calculation. For solar radiation, semi-empirical distributions with equal interval sizes are used. LARS-WG has been successfully tested in several case studies with diverse climate types (e.g. Lawless & Semenov, 2005; Sunyer et al., 2012; Zarghami et al., 2011). The new version of LARS-WG includes the data for different GCM models. A number of statistical tests such as t-test, F-test and chi-squared test were implemented by LARS-WG in order to verify the results of the simulation by comparing the synthetic data with the observed data.

Our climate model provided downscaled output from four GCMs (CCSM3, CSIRO-MK3, MPEH5 and HADGEM). These GCM models are high resolutions (finer than 1.9 degree) therefore we selected them. We developed a multi model ensemble from these GCMs. An ensemble of climate models exhibit more reliable representation of regional and local uncertainties than results from individual GCMs by decreasing the biases from single models (Abbaspour et al., 2009; Gaiser et al., 2011; Wu et al., 2012). After downscaling GCM's data, the daily climate data were put into the SWAT calibrated eco-hydrologic model to simulate the future impacts on water components. Parameter ranges in the hydrologic model represent the uncertainty of the model run. According to the calibrated model, 69 set of eco-hydrologic parameters were used to capture the uncertainty of model (e.g. CN2, alpha_bf). The model was then run for a baseline scenario (1998-2008) and future climate scenarios (2046-2065). The CO₂ concentration was defined 492ppm, 54ppm and 545ppm for the selected climate scenarios B1, A1B and A2, respectively (Semenov & Stratonovitch, 2010).

5-2-4. Land use change (Urbanization)

We estimated the impact of urbanization on surface runoff in our study area. To examine the land-use change, two series of satellite images in 1989 and 2009 were used. The land use of 2009 was adopted for the SWAT model. Based on changes in land use during 20 years (1989-2009), future land use (2050) was predicted. Moreover, population and growth rates were used as a driver in land-use prediction 2046-2065.

5-3. Results and discussion

We used a previously calibrated SWAT model of the Razan-Ghahavand area (Rafiei Emam *et al.* 2015b). The model's performance was satisfactory for both calibration and validation periods. The Nash-Sutcliff model efficiency was ranged from 0.53 to 0.63 for calibration and from 0.42 to 0.72 for validation for river discharge. Santhi et al. (2001) and Moriasi et al. (2007) mentioned that the model performances can be evaluated as satisfactory if NS and R² are greater than 0.5. The root mean square error (RMSE) for crop (rain-fed wheat) calibration and validation was 0.07 and 0.25 ton ha⁻¹, respectively. In irrigated wheat the RMSE was estimated 0.19 and 0.691 ton ha⁻¹, respectively, showing a good performance of the model. Generally, a good calibration with

crop yield leads to a good calibration of evapotranspiration (ET) adding more confidence to simulation of soil moisture and groundwater recharge. Figure 5-3 shows the calibration and validation performance of the SWAT model based on the river discharge at the Omarabad station. More details on calibration, uncertainty analysis and model results can be found in Rafiei Emam et al. (2015a) and Rafiei Emam et al. (2015b).

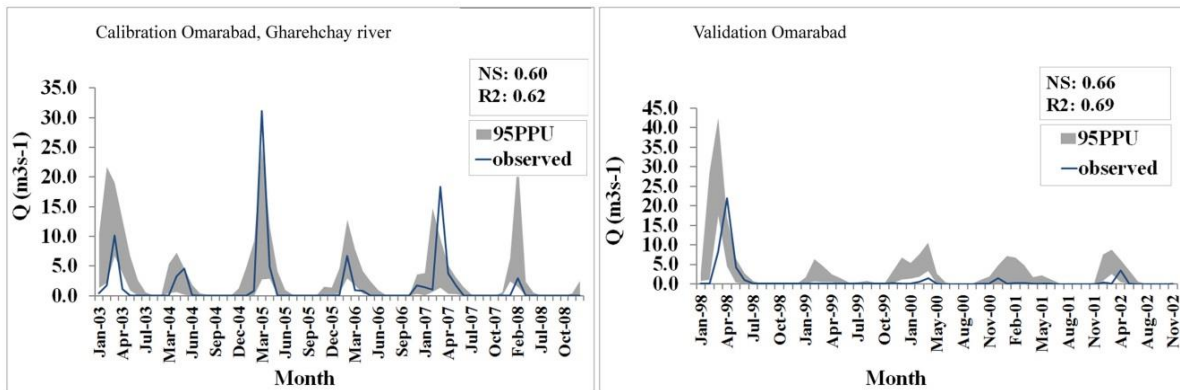


Figure 5-3. Results of SWAT calibration-validation for one selected hydrometric station

5-3-1. Downscaling results

To assess the reliability of the downscaling result, the mean and standard deviation (sd) of observed and generated values of rainfall and temperature from 1983 to 2009 were calculated for the Ghahavand station in the south of the area (Figure 5-4a,b). The results showed that the simulated and observed mean and sd of temperature and rainfall are close together which indicates the high reliability of the simulation.

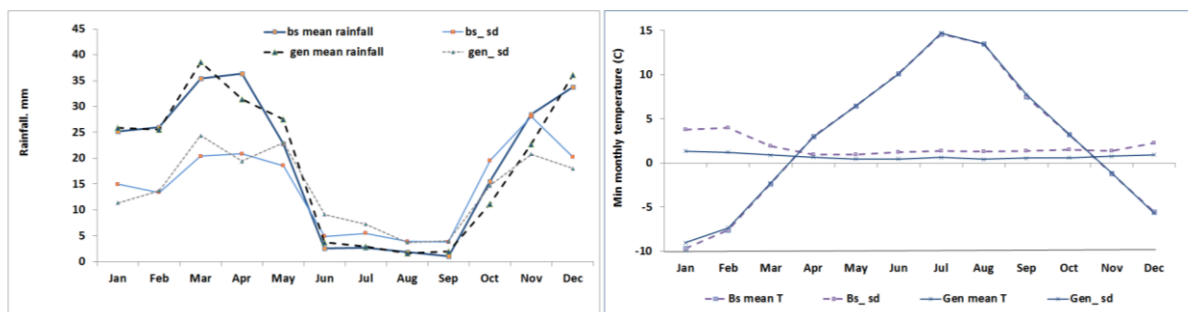


Figure 5-4. -a,b. Comparison of the observed and generated mean and standard deviation of monthly rainfall and minimum temperatures at the Ghahavand station (1983-2009). bs: base line, gen: generated, sd: standard deviation

5-3-2. Impact of climate change on precipitation and temperature

The results revealed that the annual precipitation decreased between 8 to 35 mm in different scenarios. The same result of reduced annual precipitation in the period of 2046-2065 was reported by Zarghami et al. (2011) in the northwest of Iran. Figure 5-5 compares the prediction of monthly mean precipitation for the period from 2046 to 2065 using the GCMs model and base line in the study area. The three scenarios have a tendency to raise monthly mean precipitation at the end of autumn but are less pronounced during spring and summer. This shortfall in precipitation especially in spring will increase the water stress. The water stress has an effect on crop production and rangeland species especially in the south of the watershed. The monthly mean precipitation will be decreased in scenario A1B more than A2 and B1.

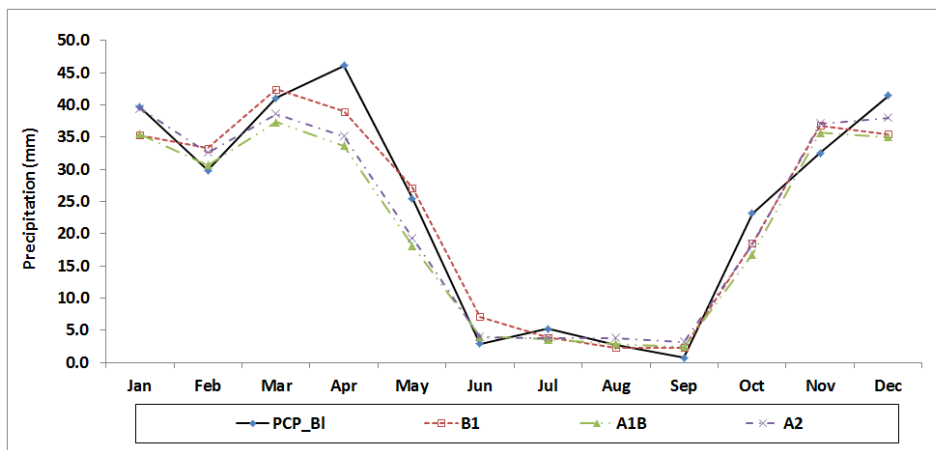


Figure 5-5. Mean monthly precipitation in baseline (1997-2008), and future (2046-2065) in three different emission scenarios according to the ensemble multi models.

The spatial distribution of annual precipitation in the historic period (1998-2008), percent changes of precipitation based on the future (2046-2065) and historic data are shown in figure 5-6(a-d). The precipitation will decrease in the south, east and northeast of the watershed up to 18 percent for scenario A1B. In scenarios A2, precipitation will decrease from 5 to 10 percent in the south of the watershed while in scenario B1 precipitation in this part will be decreased only up to 5 percent for the duration of 2046-2065. The spatial patterns show that in the west of the study area the precipitation is rising up to 27 percent in scenario B1.

Because precipitation is already low in the southern lowlands of the watershed, the decline of precipitation may have a significant influence on increasing drought in the future. Hence, crop

production and rangeland productivity in this area will be at a lower level which may lead to more land degradation and desertification. Rangelands in the northern and southern part of the watershed are directly affected by precipitation and soil moisture distribution. The rangelands in the southern portion of the area are more sensitive than in the northern part due to lower precipitation and hence lower soil moisture.

Figure 5-7 shows the absolute alteration of the surface temperature for three different emission scenarios (A1B, A2 and B1) at Dargazin station located in the north of the watershed. The figure revealed that the average temperature will rise by approximately 2.3 °C. In total, the emission scenarios have a tendency to raise the maximum (Tmax) and minimum (Tmin) temperatures throughout the year. The highest increase was found with the A2 scenario for Tmin (about 58 % change), whereas the lowest increase occurred with the B1 scenario for Tmax (change of 5.2 %).

Figure 5-6e-h shows an historic patterns of the average maximum temperature (Figure 5-6e) and anomalies of the absolute difference between the maximum temperature prediction of the three scenarios and the average over the future(2046-2065) and historic (1998-2008) period. The results showed the changes of maximum temperature in A1B and A2 is more than B1 emission scenario. In scenarios A1B and A2, most of the north and central watershed experience an increase of about 2°C in temperature (in scenario B1 about 1°C) while in the south of the watershed the increase is mostly about 2.5°C (in B1 scenario about 1.5 °C).

The diurnal temperature range is calculated as the difference between maximum and minimum temperature. For the historic period it is between 14°C-16.5 °C over the watershed area. This difference in the southern area is more than center and the northern basin. However, the diurnal temperature will decrease in the north and central part of the watershed while it will increase in the south of the watershed during 2046-2065. Hence, the minimum temperature increase is stronger in the north and central part of watershed and lower in most parts of the southern water catchment.

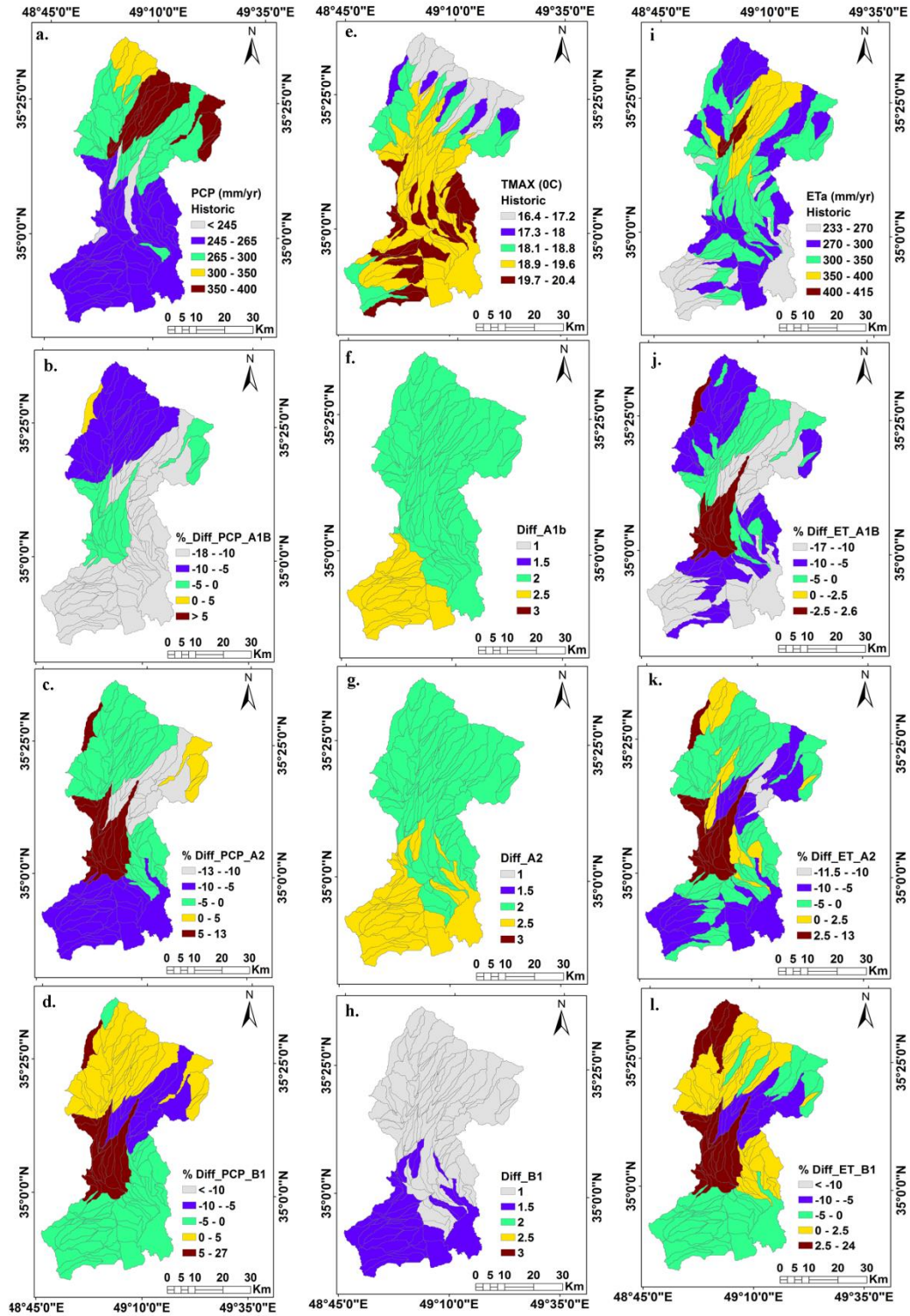


Figure 5-6. Spatial pattern of average annual precipitation (a), maximum temperature (e) and actual evapotranspiration(i) for the historic period (1998-2008). Percent difference calculated of precipitation based on future and historic data (b-d),% difference maximum temperature (f-h) and the pattern of percent difference calculated of ET based on future and historic data (j-l).

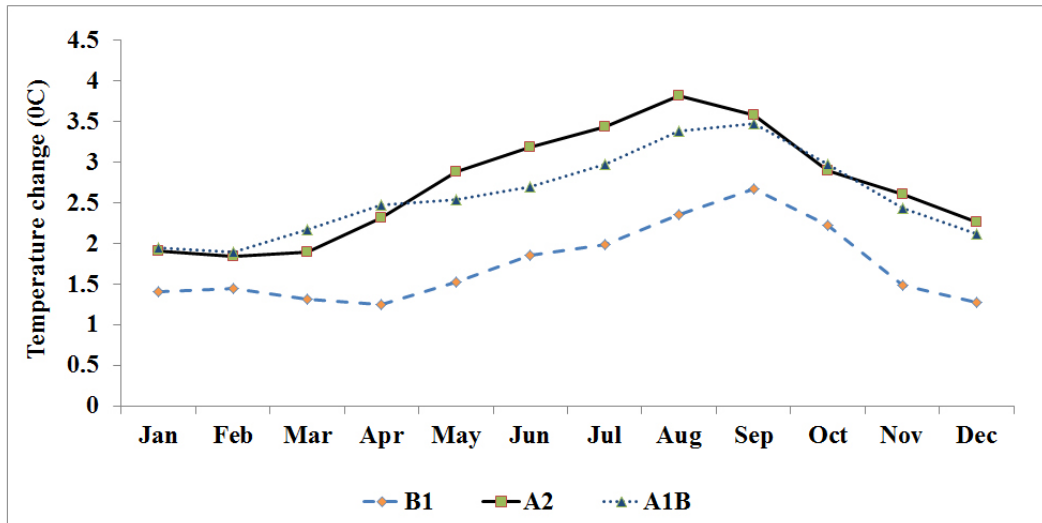


Figure 5-7. The absolute surface temperature changes (°C) in north of study area in GCM period with respect to the baseline period for three different emission scenarios, according to the CCSM3 model.

5-3-3. Impact of climate change on water balance components

Evapotranspiration varies considerably across the area due to soil and land cover variations. The annual actual ET varies from 233 to 415 mm with the highest evapotranspiration in the northern part and lowest in the southern part of the watershed (Figure 5-6i). Approximately 294 mm of the water budget is lost by annual evapotranspiration (ET), which revealed that evapotranspiration has the largest portion of the watersheds' overall water budget. The percentage difference calculated between ET based on the emission scenarios and the baseline scenario show that in most parts of the watershed the evapotranspiration will decrease by up to 17 %. However, an increase of ET is seen in the west of the watershed throughout all scenarios (Figure 5-6j-k). The B1 scenario indicated an increase in ET in the north and central part of the watershed while scenario A1B illustrated a further decrease in ET.

Groundwater recharge is affected not only by hydrological processes, but also by physical characteristics of the land surface and soil types. The average annual groundwater recharge rate is approximately about 5 mm/yr. The groundwater recharge rate responds not only to variation in land use but also to variation of hydraulic soil characteristics and variations in climatic conditions across the watershed. On the other hand, the area is a semi-arid region with low precipitation and high temperature, therefore most of the precipitation will not infiltrate deep into the soils due to high evapotranspiration. The northern part of the watershed has significantly

higher recharge rates than the southern part. The areas with high groundwater recharge may illustrate regions where the underlying aquifers are facing higher contamination vulnerability. This may have a considerable impact on land use planning, where land is being converted into residential areas and/or industrial regions (Jyrkama & Sykes, 2006). The groundwater recharge varies significantly over time. In summer the monthly recharge rate is lower than in other months of the year due to high temperatures and low precipitation. There also is no return flow from irrigation in the summer. The results also show that the increase in groundwater recharge in B1 scenario in the west of the basin is much more than in other scenarios. In scenario A1B the groundwater recharge shows a greater decrease in the north of the area more than in other scenarios (Figure 5-8a-d).

Figure 5-8e-h shows the annual spatial pattern of surface runoff in the study area. The northeast and the southwest of the watershed have significantly higher surface runoff due to the existence of low permeability soils. In scenario B1 the surface runoff rate is much higher than in other scenarios especially in the north, center and the south west of the watershed; the increase of surface runoff runs up to 65 % in these regions. In the southeast, and some parts of the north of the watershed the surface runoff decreased to 56 %. However, in mountainous areas of the north portion of the basin the runoff will increase.

The historical data show a soil moisture rate varying from 10 mm in the southwest to 80 mm in the north portion of the watershed. According to the emission scenarios, soil moisture in the north and south portion of the watershed has significantly decreased whereas the center and western part of the area showed an increase of water content. The A1B scenario shows the highest decrease in soil moisture compared to the other scenarios (Figure 5-8i-1).

5-3-4. Land-use change scenario

Land use change monitoring indicates that urban or built-up land expanded by about 100 % in Razan-Ghahavand during the 1989-2009 periods. The urban land was increased mostly due to the contraction of croplands. Based on this information and according to the mean annual population growth rate in the area reported by the Statistical Center of Iran (2011) of 2.63 % during 1986-2006, we assumed the urban or built-up growth is about 190 % during the 2046-2065 periods. The results indicated that the average annual runoff volume increased by more

than 60 % from 2045 to 2064 due to urbanization. The increase of surface runoff by urbanization have already mentioned in other studies (Weng, 2001).

5-3-5. Impact of climate change on crop production

Figure 5-9 depicts anomaly graphs of irrigated and rain-fed wheat yield in the future. The results of the ensemble model show the increase of production in irrigated areas, however in rain-fed areas the production decreased. The reasons for rising wheat yield in irrigated areas are increasing CO₂ concentration and rising temperature, especially minimum temperature, while the cereals suffered from temperature stress during historical period (1998-2008). In general, heat stress decreased in all GCMs scenarios in comparison to the base line both for irrigated and rain-fed lands (Figure 5-10). Within the watershed, the heat stress in the south of region is predicted 26 percent less than in the north part of the plain, which is due to the mean monthly temperature in the south being higher than in the north part. The reason for the decreasing rain-fed yield especially in A1B scenario is due to decreasing precipitation (-10%) resulting in a decline of soil moisture (-13%). The analysis of water stress shows that it will increase in the future in all scenarios in rain-fed areas as a result of a decrease in predicted rain-fed yield. In irrigated lands, water stress doesn't change significantly and M95PPU recorded around 75 days stress (Figure 5-11). The analysis of monthly water stress shows an increase from April to June (both for irrigated and rain-fed lands) which has a pernicious effect on crop production (e.g. Figure 5-12 revealed the anomaly graph of water stress in the A1B scenario both for irrigated and rain fed).

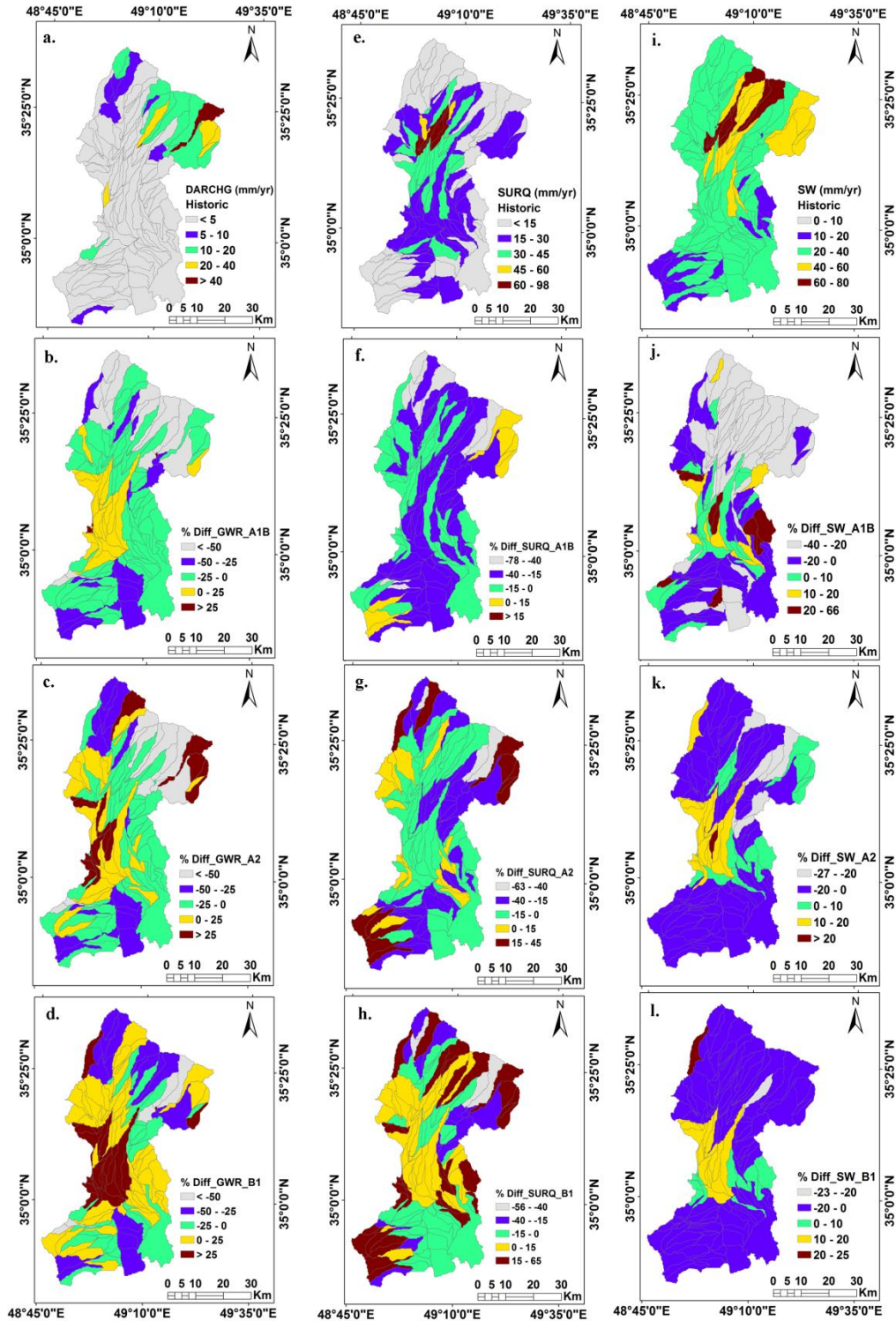


Figure 5-8. Spatial pattern of deep aquifer recharge, surface runoff, and soil water content in historical (1998-2008) and future (2046-2065) periods. The pattern of deep aquifer recharge (a) and % difference calculated of DARCH based on future and historic data (b-d). The distribution of average annual surface runoff (e) and % difference calculated of SURQ based on future and historic data (f-h). The spatial pattern of soil water content (i) and % difference calculated of SW based on future and historic data (j-l)

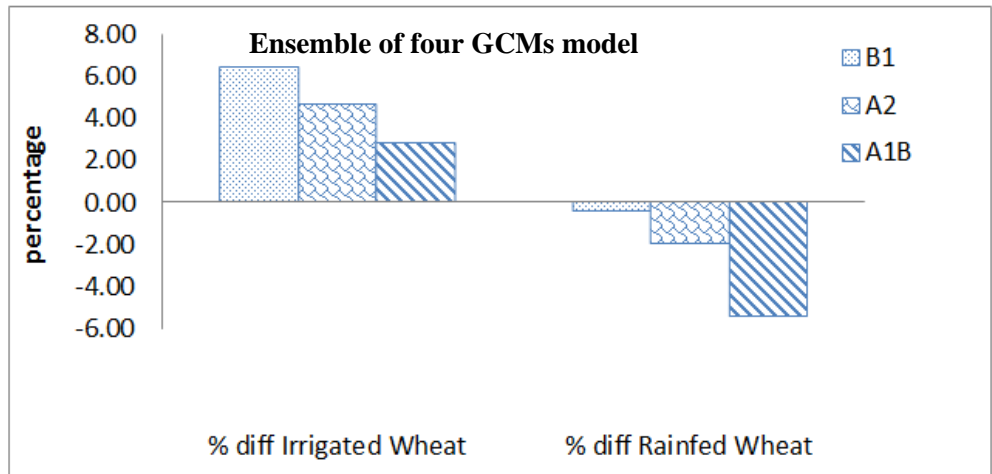


Figure 5-9. Anomaly graph of irrigated and rain-fed wheat yield in the GCMs scenarios

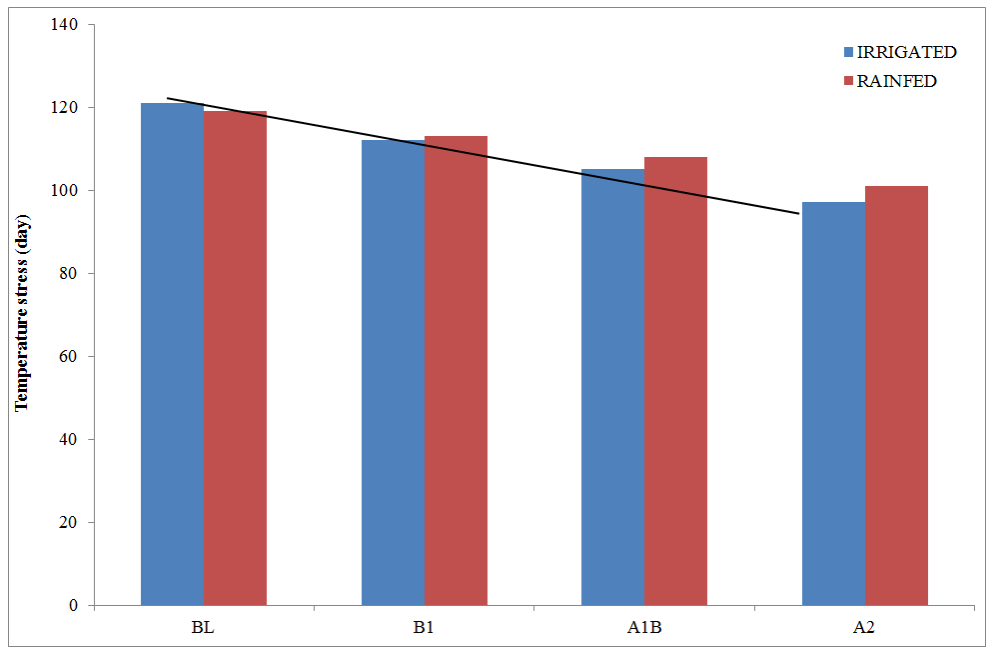


Figure 5-10. Temperature stress during growing season for rain-fed and irrigated lands

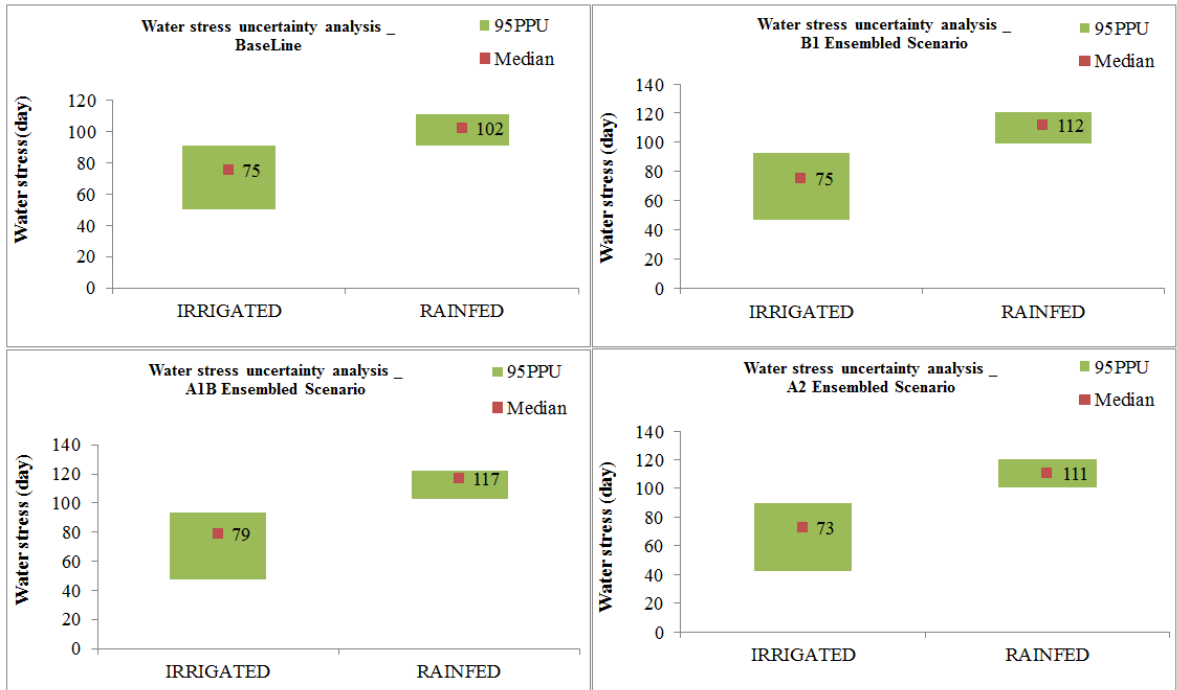


Figure 5-11. Water stress uncertainty analysis in different scenarios both for irrigated and rain-fed areas

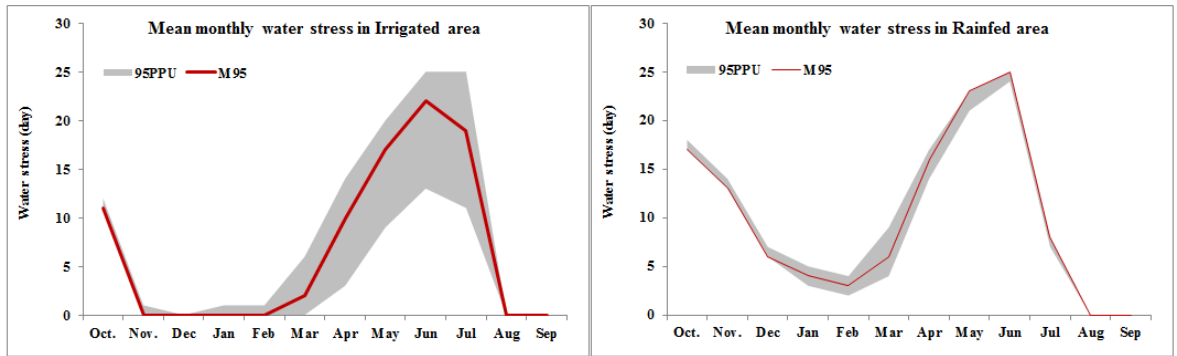


Figure 5-12. Means monthly water stress in irrigated and rain-fed lands. 95PPU: 95 percent prediction uncertainty, M95: Median of iteration

5-3-6. Land degradation and water table

There are various land degradation phenomena in the study area. The evidence of these land degradations are salinization in the east and center, rangeland degradation in the south and subsidence in the west of the watershed. Land subsidence in the study area responds directly to groundwater resources. Because of shortage of precipitation, groundwater is the main source of water resources for agriculture, industry and domestic purposes. In the west part of the watershed due to the over-extraction of groundwater, and sensitivity of the bedrock, land subsidences are happening on a large scale.

The hydrograph of the aquifer was mapped based on piezometric well data (Figure 5-13a). It revealed the trend of the water level falling about 20 meters during the 21 years from 1988 to 2008. In other words, the water table is declining about 95 cm per year. The biggest decrease in the water level appeared in the west of the aquifer with approximately 3.5 meter per year (Figure 5-13b). This huge fluctuation caused land degradation such as land subsidence and collapse and also salinization and other ecosystem deterioration. If the decline of the groundwater table continues to the same degree in the future, then the groundwater resources will be exhausted. To predict the water level of the aquifer in the future (2046-2065), we used the Auto-Regressive Integrated Moving Average model (ARIMA). ARIMA is usually used to predict future points in the time series course. The result shows a decrease of the water level up to 32 m in 2050 (Figure 5-14). The use of ARIMA for the prediction of groundwater levels is documented by other studies such as Changnon et al., (1988).

Table 5-2 shows the estimation of average annual recharge in the historic period (1998-2008) and the percentage difference between the future groundwater recharge (2046-2065) and the baseline groundwater recharge. The highest decrease (24 %) is based on the A1B scenario and the lowest decline (8 %) is found for scenario B1. The field observations show that most land subsidence is happening in HRU 515 and 571 in the west of the basin. Therefore, the groundwater recharge was estimated in these areas specifically. The results show an increase of recharge in those places up to 52 % for scenario B1. The reason for a rising recharge is due to increasing precipitation in this part of the basin. Overall, we can conclude that for the future the whole basin is facing both declining ground water table and decreasing groundwater recharge.

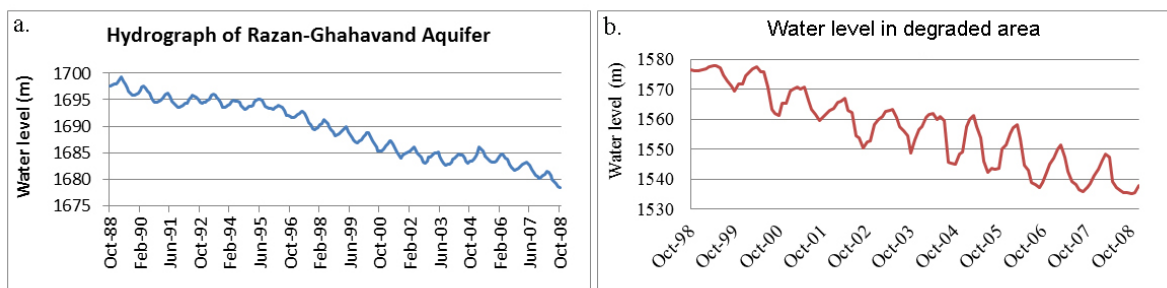


Figure 5-13-a: The hydrographs of Razan-Ghahavand Aquifer, b: the hydrograph of degraded area in the western part of basin.

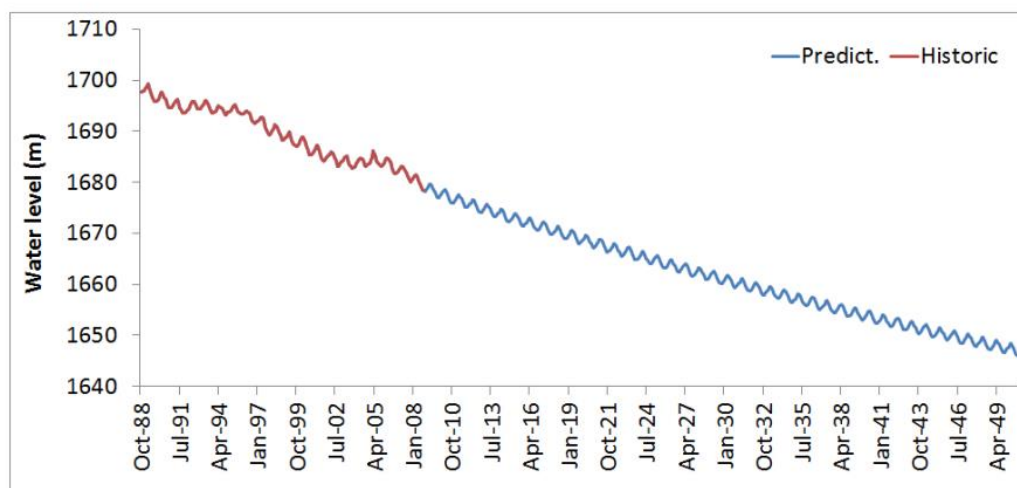


Figure 5-14. The hydrograph of Razan-Ghahavand Aquifer from historic period (1988) to 2050, predicted by ARIMA model

Table 5-2. The rate of groundwater recharge in HRUs 515, 571 (in the west of basin) and whole basin in base line and percent difference calculated of GWR based on the future (2046-2065) and historic (1998-2008) data.

Scenario	HRU:571	HRU: 515	Watershed
B1	52%	51%	-14.1 %
A1B	44%	42%	-16.6%
A2	32%	39%	-26.7%
Bs	1.2 mm	1.3 mm	4.78 mm

5-4. Summary and conclusions

This study investigated the ensemble climate change effect on hydrology, crop production and land degradation based on four GCMs model in three emission scenarios. Additionally, the impact of land use changes (urbanization) on runoff production was evaluated.

The Razan-Ghahavand basin is currently under high pressure due to growing water demand for drinking, agriculture and industrial purposes. The population has grown rapidly in the last 20 years. A future climate is likely to affect the water resources differently in the north and south of the basin. The spatial pattern of climate change models show that with increasing CO₂ the temperature is increased and it leads to more evapotranspiration and less groundwater recharge. A similar result is reported by Bouraoui et al. (2004). We found that precipitation in the south and central part of the basin will decline while the north and the west parts will face more precipitation. The increase of precipitation in the west is the reason for rising groundwater recharge in HRUs with land subsidence phenomena; therefore the water table in this part of the basin will increase. In other words, with good water management in this area further land subsidence could be controlled. However, the rangelands in the southern part of the basin are under water stress which will continue even in the future due to the decrease in precipitation. However, we can conclude that the watershed will have less rain and hot summer temperatures. Therefore, a sustainable strategy needs to consider for future water resources development.

On the other hand, wheat is the representative crop in the basin and suffered from heat stress during the historical period. Therefore, with rising temperatures in the future, the production will increase especially in irrigated lands. Nevertheless, production in rain fed areas will decrease due to water stress. The water stress in rain fed areas is more than in irrigated areas however the uncertainty in irrigated lands is more due to unaccounted for water use in the model due to lack of data. Hence, increasing of water use efficiency will be mandatory in the future cropping systems in order to sustainable water use.

Urbanization growth has a significant effect on surface runoff. It is important to note that to develop a water resources management plan, LULC certain changes (e.g. urbanization) as well as associated flood patterns should be considered.

Finally, it is important to note that, the predictions of hydrological components in the future were based on the use of same soil parameters for baseline. In this study the change of soil parameters was not considered in the future. Change of soil parameters may have an effect on

soil water content as well as surface runoff in the basin. Therefore, further research on climate change assessment while considering soil parameters changes would raise the confidence on the outcomes. The same limitation have already discussed by (Faramarzi et al., 2013).

We used a set of four GCMs model in this study, however considering the effect of other GCMs or even RCMs model may have different outcomes which should be study in further research.

5-5. References

- Abbaspour KC (2011) User Manual for SWAT-CUP: SWAT Calibration and Uncertainty Analysis Programs. Swiss Federal Institute of Aquatic Science and Technology, Eawag, Duebendorf, Switzerland. 103 pp.
- Abbaspour KC, Faramarzi M, Ghasemi SS, Yang H (2009) Assessing the impact of climate change on water resources in Iran. *Water Resources Research* 45(10): 1-16.
- Abrishamchi A, Tajrishi M (2005) Inter basin water transfer in Iran. In *Water conservation, reuse, and recycling. Proceeding of an Iranian American workshop*, The National Academies Press: Washington, D.C., pp.252–271.
- Adams RM, Hurd BH, Lenhart S, Leary N (1998) Effects of global climate change on agriculture: an interpretative review. *Climate Research* 11: 19-30.
- Ali R, McFarlane D, Varma S, Dawes W, Emelyanova I, Hodgson G, Charles S (2012) Potential climate change impacts on groundwater resources of south-western Australia. *Journal of Hydrology* 475: 456-472.
- Arnold JG, Srinivasan R, Muttiah RS, Williams JR (1998) Large area hydrologic modeling and assessment–Part 1: Model development. *American Water Resources Association* 34: 73–89.

- Baker TJ, Miller SN, (2013) Using the Soil and Water Assessment Tool (SWAT) to assess land use impact on water resources in an East African watershed *Journal of Hydrology* 486: 100-111.
- Bouraoui F, Grizzetti B, Granlund K, Rekolainen S, Bidoglio G (2004) Impact of climate change on the water cycle and nutrient losses in a Finnish Catchment. *Climatic Change* 66: 109–126.
- Changnon SA, Huff FA, Hsu CF (1988) Relations between precipitation and shallow groundwater in Illinois. *J. Climate* 1,1239–1250. DOI:10.1175/1520-0442(1988)001<1239:RBPASG>2.0.CO;2.
- Eckhardt K, Ulbrich U (2003) Potential impacts of climate change on groundwater recharge and streamflow in a central European low mountain range. *Journal of Hydrology* 284(1-4): 244-252.
- Faramarzi M, Abbaspour KC, Ashraf Vaghefi S, Farzaneh MR, Zehnder AJB, Srinivasan R, Yang H (2013) Modeling impacts of climate change on freshwater availability in Africa. *Journal of Hydrology* 480: 85-101.
- Fontaine TA, Klassen JF, Cruickshank TS, Hotchkiss RH (2001) Hydrological response to climate change in the Black Hills of South Dakota, USA. *Hydrological Sciences Journal* 46: 27–40.
- Gaiser T, Judex M, Igue AM, Paeth H, Hiepe C (2011) Future productivity off allow systems in sub-Saharan Africa: is the effect of demographic pressure and fallow reduction more significant than climate change?. *Agricultural and Forest Meteorology* 151: 1120–1130.
- Gosain AK, Rao S, Arora A (2011) Climate change impact assessment of water resources. *Current Science* 101(3): 356–71.
- Hargreaves G, Samani ZA (1985) Reference crop evapotranspiration from temperature, *Applied engineering in agriculture* 1: 96–99.

- Hijioaka Y, Lin E, Pereira JJ, Corlett RT, Cui X, Insarov GE, Lasco RD, Lindgren E, Surjan A (2014) Asia. In: Climate Change 2014: Impacts, Adaptation, and Vulnerability. Part B: Regional Aspects. Contribution of Working Group II to the Fifth Assessment Report of the Intergovernmental Panel on Climate Change [Barros, V.R., C.B. Field, D.J. Dokken, M.D. Mastrandrea, K.J. Mach, T.E. Bilir, M. Chatterjee, K.L. Ebi, Y.O. Estrada, R.C. Genova, B. Girma, E.S. Kissel, A.N. Levy, S. MacCracken, P.R. Mastrandrea, and L.L.White (eds.)]. Cambridge University Press, Cambridge, United Kingdom and New York, NY, USA, pp. 1327-1370
- IPCC (2007a) The physical science basis – summary for policymakers. Contribution of WGI to the Fourth Assessment Report of the Intergovernmental Panel on Climate Change. <http://www.ipcc.ch/ipccreports/ar4-wg1.htm>.
- IPCC (2007b) Climate Change 2007: The Scientific Basis. IPCC Contribution of Working Group I to the Fourth Assessment Report of the Intergovernmental Panel on Climate Change. Cambridge University Press, Cambridge.
- IPCC (2013) Climate Change 2013: The Physical Science Basis. Contribution of Working Group I to the Fifth Assessment Report of the Intergovernmental Panel on Climate Change [Stocker, T.F., D. Qin, G.-K. Plattner, M. Tignor, S.K. Allen, J. Boschung, A. Nauels, Y. Xia, V. Bex and P.M. Midgley (eds.)]. Cambridge University Press, Cambridge, United Kingdom and New York, NY, USA, 1535 pp.
- Jin X-L, Xu C-Y, Zhang Q, Singh VP (2010) Parameter and modeling uncertainty simulated by GLUE and a formal Bayesian method for a conceptual hydrological model. *Journal of Hydrology* 383: 147-155.
- Jyrkama MI, Sykes JF (2006) *The Handbook of Groundwater Engineering: The Impact of Climate Change on Groundwater*. University of Waterloo.
- Kim J, Choi J, Choi C, Park S (2013) Impacts of changes in climate and land use/land cover under IPCC RCP scenarios on streamflow in the Hoeya River Basin, Korea. *Science of the Total Environment* journal 452-453: 181-95.

- Kirshen PH (2002) Potential impacts of global warming on groundwater in eastern Massachusetts. *Journal of Water Resources Planning and Management* 128: 216–226.
- Lawless C, Semenov MA (2005) Assessing lead-time for predicting wheat growth using a crop simulation model. *Agricultural and Forest Meteorology* 135: 302–313.
- Li L, Xia J, Xu C-Y, Singh VP (2010) Evaluation of the subjective factors of the GLUE method and comparison with the formal Bayesian method in uncertainty assessment of hydrological models. *Journal of Hydrology* 390: 210-221.
- Li L, Xu C-Y (2014) The comparison of sensitivity analysis of hydrological uncertainty estimates by GLUE and Bayesian method under the impact of precipitation errors. *Stochastic Environmental Research and Risk Assessment* 28(3): 491-504.
- Li L, Xu C-Y, Engeland K (2013) Development and comparison in uncertainty assessment based Bayesian modularization method in hydrological modeling. *Journal of Hydrology* 486: 384-394.
- Meadows ME, Hoffman TM (2003) Land degradation and climate change in South Africa. *The Geographical Journal* 169 (2): 168-177.
- Moriasi DN, Arnold JG, Van Liew MW, Bringer RL, Harmel RD, Veith TL (2007) Model evaluation guidelines for systematic quantification of accuracy in watershed simulations. *American Society of Agricultural and Biological Engineers* 50(3): 885-900.
- Neitsch SL, Arnold JG, Kiniry JR, Williams JR, King KW (2011) Soil and water assessment tool. Theoretical documentation: Version 2000. TWRI TR-191. College Station, Texas: Texas Water Resources Institute.
- Piao S, Friedlingstein P, Ciais P, Peylin P, Zhu B, Reichstein M (2009) Footprint of temperature changes in the temperate and boreal forest carbon balance. *Geophysical Research Letters* 36, L07404. doi: 10.1029/2009gl037381.
- Rafiei Emam A, Kappas M, Abbaspour KC (2015a) Simulation of water balance components in a watershed located in central drainage basin of Iran. In: *Remote Sensing of*

the Terrestrial Water Cycle, Geophysical Monograph 206 (V. Lakshmi, ed.). American Geophysical Union. Wiley & Sons press. ISBN: 9781118872031.

- Rafiei Emam A, Kappas M, Akhavan S, Hosseini SZ, Abbaspour KC (2015b) Estimation of groundwater recharge and its relation with land degradation: Case study of a semi-arid river basin in Iran. *Environmental Earth Sciences*
- Raleigh C, Urdal H (2007) Climate change, environmental degradation and armed conflict. *Political Geography* 26(6): 674–694.
- Ritchie JT (1972) A model for predicting evaporation from a row crop with incomplete cover. *Water Resources Research* 8: 1204-1213.
- Rosenberg NJ, Epstein DJ, Wang D, Vail L, Srinivasan R, Arnold JG (1999) Possible impacts of global warming on the hydrology of the Ogallala Aquifer Region. *Climatic Change* 42: 677–692.
- Santhi C, Arnold JG, Williams JR, Dugas WA, Srinivasan R, Hauck LM (2001) Validation of the SWAT model on a large river basin with point and nonpoint sources. *American Water Resources association* 37 (5): 1169–1188.
- Semenov MA, Stratonovitch P (2010) Use of multi-model ensembles from global climate models for assessment of climate change impacts. *Climate Research* 41: 1–14.
- Singh P, Bengtsson L (2005) Impact of warmer climate on melt and evaporation for the rainfed, snowfed and glacierfed basins in the Himalayan region. *Journal of Hydrology* 300: 140–54.
- Statistical Center of Iran (2011) Report of population rate.
- Sunyer MA, Madsen H, Ang PH (2012) A comparison of different regional climate models and statistical downscaling methods for extreme rainfall estimation under climate change. *Atmospheric Research* 103: 119–128.

- Tong STY, Sun Y, Ranatunga T, He J, Yang YJ (2012) Predicting plausible impacts of sets of climate and land use change scenarios on water resources. *Applied Geography* 32: 477–89.
- Tu J (2009) Combined impact climate and land use changes on streamflow and water quality in eastern Massachusetts, USA. *Journal of Hydrology* 379: 268–83.
- Wand SJE, Midgley GF, Jones MH, Curtis PS (1999) Responses of wild C4 and C3 grass (Poaceae) species to elevated atmospheric CO2 concentration: a meta-analytic test of current theories and perceptions. *Global Change Biology* 5: 723–741.
- Weng Q (2001) Modeling Urban Growth Effects on Surface Runoff with the Integration of Remote Sensing and GIS. *Journal of Environmental Management* 28: 737-748.
- Williams JR, Jones CA, Dyke PT (1984) A modeling approach to determining the relationship between erosion and soil productivity. *Transactions of the ASAE* 27 (1): 129–144.
- World Wide Fund (WWF) (2010) Impacts of climate change on growth and yield of rice and wheat in the Upper Ganga Basin. <http://awassets.wwfindia.org/downloads/>
- Wu Y, Liu S, Gallant AL (2012) Predicting impacts of increased CO2 and climate change on the water cycle and water quality in the semiarid James River Basin of the Midwestern USA. *Science of the Total Environment* 430: 150-160.
- Xu XY, Yang HB, Yang DW, Ma H (2013) Assessing the impact of climate variability and human activities on annual runoff in the Luan River basin, China. *Hydrological Research* 44(5): 940-952.
- Young CA, Escobar-Arias MI, Fernandes M, Joyce B, Kiparsky M, Mount JF (2009) Modeling the hydrology of climate change in California's Sierra Nevada for subwatershed scale adaptation. *Journal of American Water Resources Association* 45: 1409–23.
- Zarghami M, Abdi A, Babaeian I, Hassanzadeh Y, Kanani R (2011) Impacts of climate change on runoffs in East Azerbaijan, Iran. *Global Planet Change* 78: 137–146.

- Zektser IS, Loaiciga HJ (1993) Groundwater fluxes in the global hydrologic cycle: past, present, and future. *Journal of Hydrology* 144: 405-442.
- Zhan CS, Niu CW, Song XF, Xu C-Y (2013) The impacts of climate variability and human activities on streamflow in Bai River basin, northern China. *Hydrological Research* 44(5): 875-885. doi:10.2166/nh.2012.146
- Zhou F, Xu Y-P, Chen Y, Xu C-Y, Gao YQ, Du JK (2013) Hydrological Response to Urbanization at Different Spatio-temporal Scales simulated by coupling of CLUE-S and the SWAT model in the Yangtze River Delta region. *Journal of Hydrology* 485: 113-125.

Estimating actual evapotranspiration from MODIS time series compared to a hydrological model in a semi-arid catchment in Iran⁴

Abstract

The accurate estimation of actual evapotranspiration (ET_a) is of crucial importance for management of water resources, especially in arid and semi-arid areas. Remote sensing data can be used as proxy data for the calibration of hydrological models in areas with low data availability. In this study, the Surface Energy Balance Algorithms for Land (SEBAL) model was used to estimate ET_a over the semi-arid region of the Razan-Ghavand watershed located in the central drainage basin of Iran. Eight overpasses MODIS data during 150-day growing season from January 2008 to May 2008 were selected for this purpose. In addition, a SWAT (Soil and water assessment tools) hydrological model was used to estimate ET_a based on a water balance equation. The SEBAL model was internally calibrated for the aerodynamic resistance to heat transport (r_{ah}) using Monin-Obukhov theory, while the SWAT model was calibrated using river discharge and crop yield. Here, crop yield leads to more precise estimates of evapotranspiration. The performance of the SWAT hydrological model was evaluated by Nash Sutcliffe (NS) and R^2 , which calculated greater than 0.5 showing satisfactory results. Furthermore, the average of monthly ET_a was estimated from 4.5 mm to 46 mm between January 2008 and May 2008 by the SEBAL model. The ET_a estimates between both the SEBAL and SWAT models were found to be comparable. Therefore, the evapotranspiration estimates based on remote sensing data can be useful for calibration of hydrological models in an area with low data availability.

⁴ This paper is prepared to submit to an international peer-review journal

6-1. Introduction

The management of water resources is one of the biggest challenges in arid and semi-arid areas. The evapotranspiration (ET) process is one of the most important components within the hydrological cycle (Wang et al., 2014). It can release a large amount of water from the land surface by soil evaporation and vegetation transpiration. Quantifying ET is important for water resource planning and management. However, a point measurement of ET cannot be extended to a large area due to the dynamic of the heat transfer process (Wang et al., 2014). Therefore, we studied ET spatially by surface energy balance techniques derived from remotely sensed data. The results were compared with the output of surface water balance approaches adapted from a hydrological model.

Satellite data are very useful in terms of producing information in the spatial and temporal scales, especially in arid and semi-arid regions. Remote sensing is an important source of data and information for hydrological modeling. Additionally, it can help precise calibration of hydrological models (Awan & Ismaeel, 2014). Remote sensing techniques also enable estimation of some variables for hydrology (e.g. soil moisture, evapotranspiration) (Engman, 1991). Generally, actual evapotranspiration is estimated as a residual of the surface energy balance derived from remotely sensed data (Bastiaanssen et al., 1998a; Su, 2002; Allen et al., 2007a). The widely used residual model is Surface Energy Balance Algorithm for Land (SEBAL) developed by Bastiaanssen et al. (1998a). SEBAL estimates actual evapotranspiration based on the land surface temperature derived from thermal remotely sensed data (RS-ET). Several researchers revealed the good performance of the SEBAL in various areas (Spiliotopoulos et al., 2008; Teixeira et al., 2009; Tang et al., 2013). However, it is not easy to validate RS-ET (Norman et al. (2006). Allen et al. (2011) reported a validation study of RS-ET model using weighing lysimeters as the most direct and accurate field measurement approach. However, in some researches the eddy covariance and Bowen ratio measurements have been applied for validation purposes (Kalma et al., 2008; Ruhoff et al., 2013).

In addition to the remote sensory method, hydrological models are useful approaches to estimate evapotranspiration. The models can be divided into various groups: white box (i.e. Distributed physically based models), gray box (i.e. Lumped conceptual models), and black box (i.e. Empirical models). Some hydrological models that consider the evapotranspiration in spatial and temporal scales belong to distributed models. SWAT (Arnold et al., 1998) is a kind of physical

distributed model and has been tested by different researchers (Tobin & Bennett, 2013; Schuol et al., 2008; Faramarzi et al., 2009). In the SWAT model, all water balance computations are done in homogenous units obtained through soil, land-use and slope maps. ET is a residual of the surface energy balance in the SWAT model.

Water supplies are difficult in semi-arid regions of Iran. Groundwater is the source of water supply for irrigation purposes (Awan & Ismaeel, 2014) and as the groundwater recharge is less than the discharge (Rafiei Emam et al., 2015b), aquifers are eventually depleted. The average efficiency of water use in farmlands is less than 35%, which reveals the huge volume of water wasted by percolation or evapotranspiration processes. The information about spatial evapotranspiration in the RGB is too sparse.

Although remotely sensed approaches and distributed hydrological models are useful techniques for spatial estimation of ET, the validation of the RS-ET models and the calibration of the hydrological models, especially in areas with low data availability, are not easy.

The main objective of this research is to estimate the actual evapotranspiration by surface energy balance technique (SEBAL) using MODIS time series data in a spatial scale. Some equations of the METRIC model are used to mitigate the effects of topography. A comparison between ET_a estimated by SEBAL and ET_a estimated by SWAT is another goal of this research leading to validation of the SEBAL model. If the ET_a estimated by remote sensing and by the hydrological model is the same, the former technique could be used for further calibration of hydrological models especially in area with low data availability.

6-2. Material and Methods

6-2-1. Study area

The study was carried out in the central drainage basin of Iran, called Razan-Ghahavand Basin (RGB) (Figure 6-1). The climate in the study area can be characterized as being semi-arid, with an annual average precipitation of approximately 290 mm and temperature of 11 °C. The elevation of the study area ranges from 1577 m to 2843 m from the eastern to northern part of the basin. More than 30 percent of the area is agriculture (e.g. Wheat, alfalfa), and the remaining 70% comprises of rangelands, bare lands, and residential area.

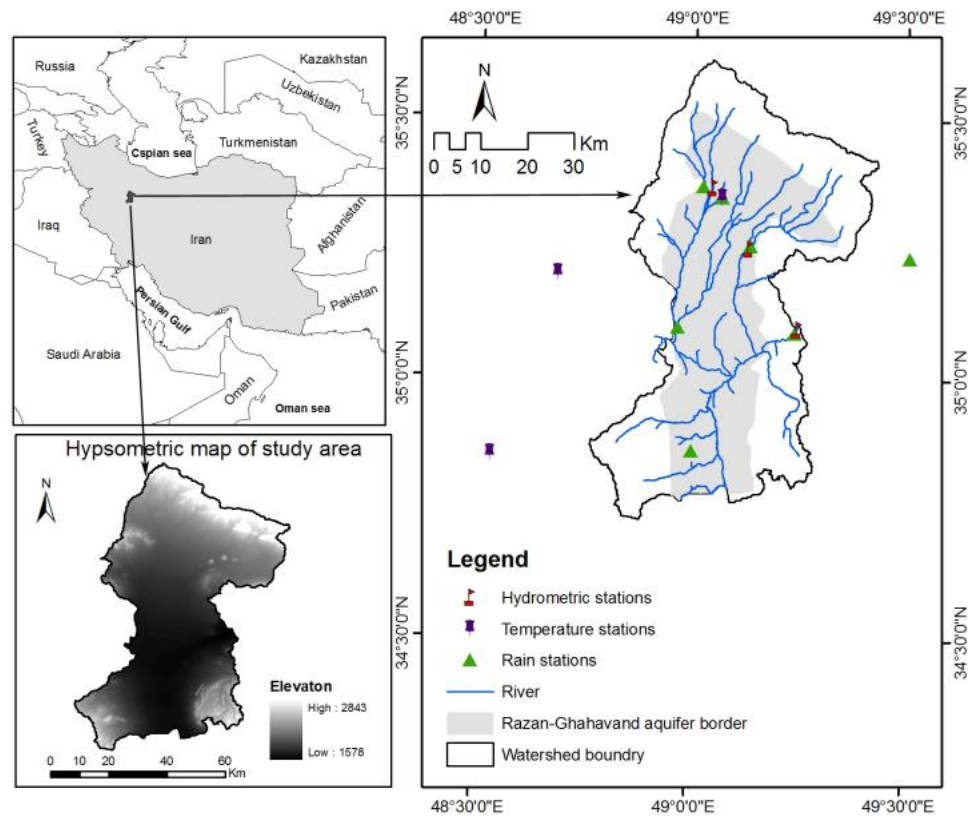


Figure 6-1. Map of study area, including streams, hydrometric, temperature and rain gages

6-2-2. Satellite and meteorological data

One of the main products that are needed for evapotranspiration (ET) estimation by means of remotely sensed energy balance is Thermal Infrared Radiation (TIR). TIR refers to electromagnetic waves from 3 to 20 micrometer. Most of remote sensing applications use ranges between 8 and 14 micrometer. Therefore, all earth observation satellite systems consisting of thermal bands can be used for surface energy balance modeling. In this research, different MODIS data products were used (e.g. LST, NDVI). The same data is used by Du et al. (2013) and Anderson (2008) for surface energy balance model. MODIS data from January 2008 to May 2008 was used in different temporal (daily, 8_day, 16_day) and spatial (250 m, 500 m, and 1000 m) resolution. A summary of the available MODIS products for this study is given in Table 6-1. In addition to the satellite data, hourly climatic data (e.g. solar radiation, wind speed, temperature, relative humidity and atmospheric pressure) were extracted from a synoptic station in the southern part of the study area.

We selected at least one cloud-free image per month in order to estimate instantaneous evapotranspiration at the satellite overpass time. The LST images (MOD11A1) used in this study are listed in table 6-2 including the overpass time.

Table 6-1. Specification of MODIS products used in ET modeling

Data Product	Layer	Spatial resolution	Temporal resolution
MOD11A1	LST/Emissivity	1 km	Daily
MOD13A2	NDVI	1 km	16-days
MCD43B3	Albedo	1 km	16-days
MCD15A3	LAI	1 km	8-days
MOD09GA	Reflectance	500m	8-days

Table 6-2. Overpass date and time of terra sensor

No.	Overpass Date	Overpass time	DOY*
1	14 January 2008	11:24	14
2	5 February 2008	10:06	36
3	8 March 2008	10:25	68
4	20 March 2008	10:30	80
5	13 April 2008	11:12	104
6	24 April 2008	11:30	115
7	15 May 2008	11:18	136
8	25 May 2008	10:24	146

* DOY: Day Of Year

6-2-3. Mapping of Land use/land cover

The land use/Land cover (LULC) map is needed in both the surface energy balance method (e.g. to compute momentum roughness length (Z_{om})) (Waters et al., 2002), and for the water balance technique (e.g. to create hydrological response unit (HRU)) in order to estimate evapotranspiration. To create the LULC map, Landsat TM data in 2009 was used, and LULC classification was done by means of supervised classification.

6-2-4. Surface energy balance algorithm

The method described here to estimate actual evapotranspiration is based on a surface energy balance model (Bastiaanssen et al., 1998a; Bastiaanssen, 2000) (Figure 6-2). By using the SEBAL algorithm to estimate surface energy balance, ET_a is calculated as a residual of the surface energy equation:

$$LE = Rn - G - H \quad (1)$$

Where LE refers to latent energy representing actual evapotranspiration, Rn indicates net energy, G refers to sensible heat flux which is conducted into the ground, and H indicates sensible heat flux converted into the air. The units of all parameters are [$W\ m^{-2}$]. Rn is calculated as a sum of all heat energy flux, shortwave and long wave radiations, at the surface:

$$Rn = (1 - a)R_s \downarrow - R_L \uparrow + \varepsilon_0 R_L \downarrow \quad (2)$$

Where a is a land surface albedo, $R_s \downarrow$ is an incoming short wave radiation, $R_L \uparrow$ is an outgoing long wave radiation, ε_0 is a land surface emissivity, and $R_L \downarrow$ is an incoming long wave radiation. Incoming short wave radiation is calculated as follows:

$$R_s \downarrow = (G_{sc} \times \cos \theta \times \tau_{sw}) / dr^2 \quad (3)$$

Where G_{sc} refers to the solar constant ($1367\ Wm^{-2}$), θ is a solar incident angle, τ_{sw} is the atmospheric transmissivity, and dr indicates relative distance between the earth and sun in the astronomical units. For mountains lands, θ is calculated based on slope and aspect according to the equation presented in the METRIC model (Allen et al. 2007a). However, in the flat surface, where slope and aspect are ignored, solar incident angle is equivalent to the solar zenith angle (i.e. $\pi/2$ minus the solar elevation angle). τ_{sw} is calculated by empirical model of SDCE-EWRI (2005) cited by Allen et al. (2007b) by using atmospheric pressure, elevation above sea level, amount of water in the atmosphere, near surface vapor pressure, solar zenith angle, and turbidity coefficient. The outgoing long wave radiation is calculated as:

$$R_L \uparrow = \varepsilon_0 \times \sigma \times T_s^4 \quad (4)$$

Where ε_0 refers to the land surface emissivity, σ is the Stefan-Boltzman constant ($5.67 \times 10^{-8}\ W.m^2.k^{-4}$), and T_s is the land surface temperature (K). Incoming long wave radiation is calculated as:

$$R_L \downarrow = \varepsilon_a \times \sigma \times T_a^4 \quad (5)$$

Where ε_a indicates an atmospheric emissivity, and T_a refers to the near surface air temperature (K) usually assumed equal to cold pixel value. To calculate heat transfer into the soil (G) Bastiaanssen

et al., (1998b) suggested the following equation based on the soil surface temperature in °K (T_s), albedo (a), and vegetation index (NDVI):

$$G = (T_s - 273.15) \cdot (0.0038 + 0.0074 a) \cdot (1 - 0.98 \times NDVI^4) \cdot R_n \quad (6)$$

Heat transfer into the air (H) is the most critical factor to consider regarding surface balance energy. It depends on surface temperature, surface roughness length (Z_{om}), and wind speed using buoyancy corrections.

$$H = \rho_a \cdot C_p \frac{dT}{r_{ah}} \quad (7)$$

Where ρ_a is air density ($\text{kg}\cdot\text{m}^{-3}$), C_p refers to the specific heat of the air ($1004 \text{ J}/(\text{kg}\cdot\text{K})$), r_{ah} refers to the aerodynamic resistance of wind speed between two near surface heights ($\text{m}\cdot\text{s}^{-1}$), dT represents the temperature difference between the two near surface heights (e.g. $Z_1=0.1\text{m}$ and $Z_2=2\text{m}$). To compute heat transport into the air, one first needs to calculate r_{ah} and dT . In the first attempt, the aerodynamic resistance to heat transport (r_{ah}) is calculated for neutral stability, so the H in neutral atmospheric conditions can be estimated. The stability of atmospheric conditions has a significant effect on the aerodynamic resistance (r_{ah}) and takes into account the estimation of sensible heat flux (H), especially when evaluating dry conditions (Waters et al., 2002). The computation of H by SEBAL repeats through a number of iterations until r_{ah} stabilizes. For this aim the Monin-Obukhov theory is used in iterative processes to correct buoyancy effects generated by surface heating. r_{ah} is calculated by equation (8):

$$r_{ah} = \frac{1}{u_* \times k} \left[\ln \left(\frac{z_2}{z_1} \right) - \Psi_{h(z_2, L)} + \Psi_{h(z_1, L)} \right] \quad (8)$$

where, u_* is the friction velocity at the blending layer of 200 m; k is the von Karman constant (dimensionless, = 0.4); $\Psi_{h(z_2)}$ is the stability correction of atmosphere for heat transport based on Monin-Obukhov length (L) (equals to $-\rho c_p u_*^3 T_s / K g H$), g is gravitational constant (9.81 ms^{-2})

dT , the near surface temperature difference, is computed by assuming a linear relationship between dT and T_s :

$$dT = b + aT_s \quad (9)$$

To define a and b as a correlation coefficient, SEBAL is used the two anchor pixels in “cold” and “hot” areas. The cold areas refer to the well-irrigated fields containing low surface temperature. In these areas all available energy is assumed to be evapotranspired. The hot areas indicate the

enough dry regions with high surface temperature. One can assume that in hot areas $LE = 0$, means there is no evapotranspiration in these areas.

Then H and dT is calculated in cold and hot pixels by means of the following equations:

$$H_{cold} = R_n - G - \lambda ET_{cold} \quad (10)$$

$$dT_{cold} = H_{cold} * r_{ah} / (\rho C_p) \quad (11)$$

$$H_{hot} = R_n - G \quad (12)$$

$$dT_{hot} = H_{hot} * r_{ah} / (\rho C_p) \quad (13)$$

By stabilizing r_{ah} in iterative process, the final value of H is estimated. The flowchart of the process is shown in Figure 6-2 (After Waters et al., 2002; Bastiaanssen et al., 2000). After the final computation of H , the LE is computed for each pixel by equation 1. Then, the instantaneous ET at each pixel is calculated as:

$$ET_{inst} = 3600 \frac{LE}{\lambda} \quad (14)$$

Where ET_{inst} refers to the instantaneous ET (mmhr^{-1}), 3600 is the time conversion from second to hours, LE is the latent heat flux for evapotranspiration (Wm^2), λ indicates the latent heat of vaporization (JKg^{-1}) and is computed as following equation represented by Allen et al., (2011):

$$\lambda = [2.501 - 0.00236(T_s - 273.15)] * 10^6 \quad (15)$$

To extrapolate the ET -ins to a period of time (e.g. daily, monthly), ET fraction ($ETrF$) should be calculated. $ETrF$ is same as Kc in the traditional ET computation model. The evapotranspiration fraction and ET_{24} is computed as:

$$ETrF = \frac{ET_{inst}}{ET_r} \quad (16)$$

$$ET_{24} = ETrF * ET_{r,24} \quad (17)$$

Where ET_r is reference evapotranspiration, and $ET_{r,24}$ is calculated as cumulative of 24-hour ET_r for the day of the specific chosen image:

$$ET_{r-24} = \sum ET_{r-h} \quad (18)$$

Monthly ET is calculated as:

$$ET_{monthly} = ETrF \sum_1^n ET_{r,24} \quad (19)$$

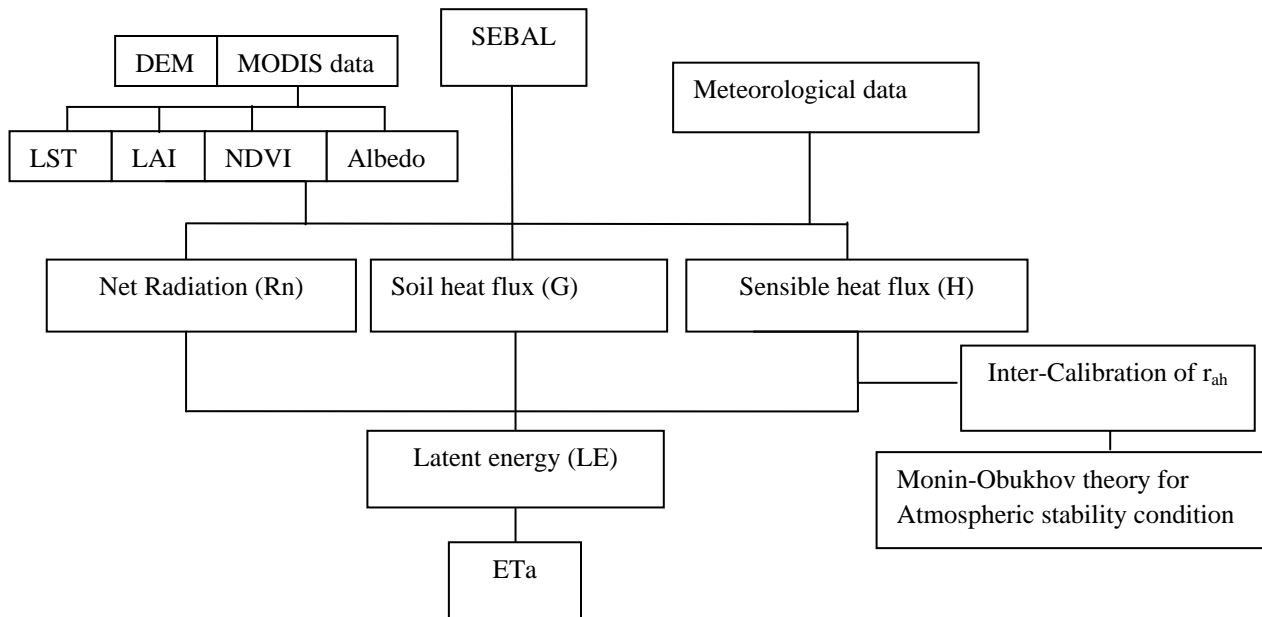


Figure 6-2. Flowchart of process of surface energy balance technique to estimating actual evapotranspiration (ETa)

6-2-5. A hydrological model for water balance assessment

Soil and Water Assessment Tools (SWAT) is one of the physical, distributed and continuous time models that was used in this study. In the SWAT, the watershed subdivides into sub basins based on digital elevation model (DEM). Hydrological response units (HRUs), which are the basis of the water balance calculations, were further created by integration of soil, land use and slope within the sub basins. Therefore, a total of 83 sub basins and 831 HRUs were created in the RGB. The soil-water-balance equation is the basis of the SWAT. The water balance model was analyzed based on the HRUs by adding meteorological data such as daily precipitation, daily temperature, and solar radiation.

The general water balance model inside the SWAT can be indicated as such:

$$SW_t = SW_0 + \sum_i^t (P_{day} - Q_{sur} - ET_P - W_{seep} - Q_{gw}) \quad (19)$$

Where: SW_t is the final soil water content (mm), SW_0 is the initial soil water content (mm), precipitation, P_{day} is the precipitation (mm), Q_{sur} is the surface runoff (mm), ET_P is the amount of evapotranspiration (mm), W_{seep} refers to the amount of percolation and bypass flow exiting the soil profile bottom, and Q_{gw} indicates the amount of return flow (mm).

Potential evapotranspiration (ETP) in SWAT is simulated by the Hargreaves method (Hargreaves & Samani, 1985). Daily data of three different meteorological stations were used. The daily amounts of LAI are used to partition ETP into potential soil evaporation and plant transpiration (Akhavan et al., 2010). Actual evapotranspiration (ETa) is further estimated using the Ritchie (1972) method. The soil water content applies actual soil evaporation. It is reduced exponentially when soil water content decreases less than field capacity. Actual plant transpiration is equal to the actual plant water uptake. It is calculated based on depth of root development, actual daily crop height and LAI (Immerzeel & Droogers, 2008).

The SWAT model was calibrated and validated by means of considering monthly river discharge and yearly crop yield by SUFI-2 algorithm within the SWAT-CUP package developed by Abbaspour (2011). In SUFI-2 all source of uncertainties (e.g. input data, conceptual model, and parameters) are depicted into parameter range. The model tries to capture most of the measured data within 95 percent prediction uncertainty (95PPU). The output is mapped as 95PPU band, which is calculated at 2.5% and 97.5% levels of the cumulative distribution of an output variable. In the calibrated model, all water components (e.g. evapotranspiration) can be computed in the temporal and spatial patterns. More details about calibration, validation and uncertainty analysis of SWAT model is presented by Rafiei Emam et al. (2015a).

6-3. Results

Based on the results of the hydrological model, the actual evapotranspiration was estimated precisely due to the calibration of model both by river discharge and crop yield. A good calibration by crop yield would result in a good calibration of evapotranspiration (Rafiei Emam et al., 2015a; Faramarzi et al., 2009).

The statistical results showed the Nash-Sutcliffe (NS) coefficients are close to or more than 0.5 for all hydrometric stations for both the calibration and validation periods. According to Moriasi et al.(2007), NS more than 0.5 shows a good performance of the model. Furthermore, the calibration of the model by crop yield shows that the root mean error (RMS) is less than 0.07 ton/ha for rain-fed lands, whereas the RMS in irrigated areas are 0.69 and 0.19 ton/ha for calibration and validation periods, respectively. Vaghefi et al. (2014) calibrated the hydrological model in southwestern Iran by winter wheat yield using harvest index and heat units. They found that observed yields are within or close to the predicted yield band. Akhavan et al. (2010) calibrated

the hydrological model based on wheat and potato as representative crops in the Hamedan-Bahar area in Iran. The RMSE were 0,08 and 1.69 ton ha⁻¹ for rain-fed wheat and potato in calibration period. They mentioned that the lack of accounting of management practices (e.g. tillage operation, fertilizer application, planting date) is the result of large RMSE for potato. Figure 6-3 shows the anomaly graph of calibration and validation of model by crop yield in the RGB. The results of calibration and validation of SWAT model show the good performance of the model. The results are comparable with Akhavan et al., (2010) and Vaghefi et al., (2014).

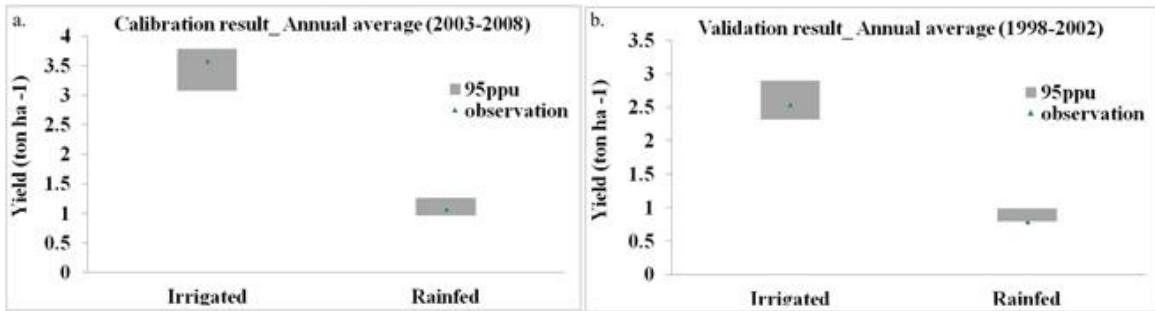


Figure 6-3. The calibration and validation of the crop yield in the RGB

6-3-1. Reference Evapotranspiration, ETr

The reference evapotranspiration is the ET rate of full- cover alfalfa. ETr is used in SEBAL to compute the evapotranspiration fraction in order to extrapolate the ET_inst to ET_24 or longer. Table 6-3 shows ETr at day of satellite overpass calculated at the Hamedan synoptic station by Ref-ET program based on Hargreaves method (Hargreaves & semani,1985). Maeda et al., (2011) compare three reference evapotranspiration methods. They mentioned the Hargreaves model as the most appropriate method among others. The result shows that the ETr is the lowest in January and is the highest in May due to climate conditions and crop growth stages.

Table 6-3. ETr calculated at the time of satellite image based on Hargreaves method

Nr.	Overpass time	ETr (mm/day)
1	14.01.2008	0.02
2	05.02.2008	0.03
3	08.03.2008	0.59
4	20.03.2008	0.76
5	13.04.2008	0.82
6	24.04.2008	1.32
7	15.05.2008	1.28
8	25.05.2005	1.67

6-3-2. SEBAL energy fluxes

To solve the surface energy balance equation (equation 1) and compute H, as a most difficult parameter, one should use cold and hot pixel information in order to calculate dT and r_{ah} . For instance, table 6-4 shows the information of cold and hot pixels (e.g. R_n , G, albedo and H) on April 13, 2008. The table reveals that at the cold pixel the net radiation (R_n) is higher than the hot pixel, whereas the amount of heat flux transfer into the soil (G) in hot pixel is more than cold pixel. The cold pixel reveals the high vegetation cover. Therefore, LST in this area is lowest. Feizizadeh et al., (2013) mentioned that LST is sensitive to LULC and vegetation cover. LULC classes with more vegetation have the lower LST.

Table 6-4. Surface energy fluxes at Hot and Cold pixels on 13th April 2008

	Cold Pixel	Hot pixel
X	320989	323833
Y	3884495	3871528
Ts	296.7	305.9
Rn	517	448
G	73	96.5
LE	214	0
H	230	351.5

After solving the surface energy balance, ET_{inst} was calculated based on the equation Nr. 13. However, daily evapotranspiration (ET_{24}) is useful than the instantaneous ET. To estimate ET_{24} we assumed that instantaneous ET_{TrF} is constant over 24 hours. The assumption has already been demonstrated by various researchers, including Romero 2004; Colaizzi et al. 2006; Allen et al. 2007a; Allen et al. 2011.

6-3-3. Mapping monthly actual evapotranspiration

The spatial distribution of ET_a in monthly scale was calculated. To estimate the monthly evapotranspiration, equation 18 was used. Figure 6-4a shows the monthly actual evapotranspiration in April. The result shows the ET_a estimated from 17 mm in the south to 73mm in the north and western part of the basin. The highest evapotranspiration is estimated in areas with high vegetation cover (white color in the image). However, areas with low vegetation cover or bare land have less actual evapotranspiration (dark color in the image). The map is comparable with NDVI map. As expected, high values of ET_a were observed for farmlands in the central of plain, and for high vegetation cover of rangelands in the north of the area. Du et al. (2013) mapped ET_a based on SEBAL algorithm in Sanjiang Plain, Northeast China. They revealed the high values of ET_a for the lakes, forests and farmlands, respectively.

The average monthly value of 95PPU of actual evapotranspiration estimated by SWAT from January to May was calculated to compare the temporal evapotranspiration for both models (Figure 6-5). The results show that the dynamic of both models are similar together but peak values are different in some months. However, the figure shows that the estimated ET_a by SEBAL is within or close to the 95PPU band, which indicates the high accuracy of estimation by the SEBAL model.

In May the highest ET of 95PPU ($>37\text{mm}$) was found at the eastern part of basin with elevation higher than 1888 m, whereas the smallest value of ET (L95PPU) was found at the area in the south of watershed. However, the average of the whole basin was between 5.2 mm and 7.6 mm for the lower (L95PPU) and upper prediction uncertainty boundaries (U95PPU).

The statistical evaluation of monthly ET_a revealed a high correlation coefficient of 0.77 and Nash-Sutcliff of 0.80 between M95PPU of SWAT and SEBAL models, and showed a good dynamic and monthly variation of ET_a .

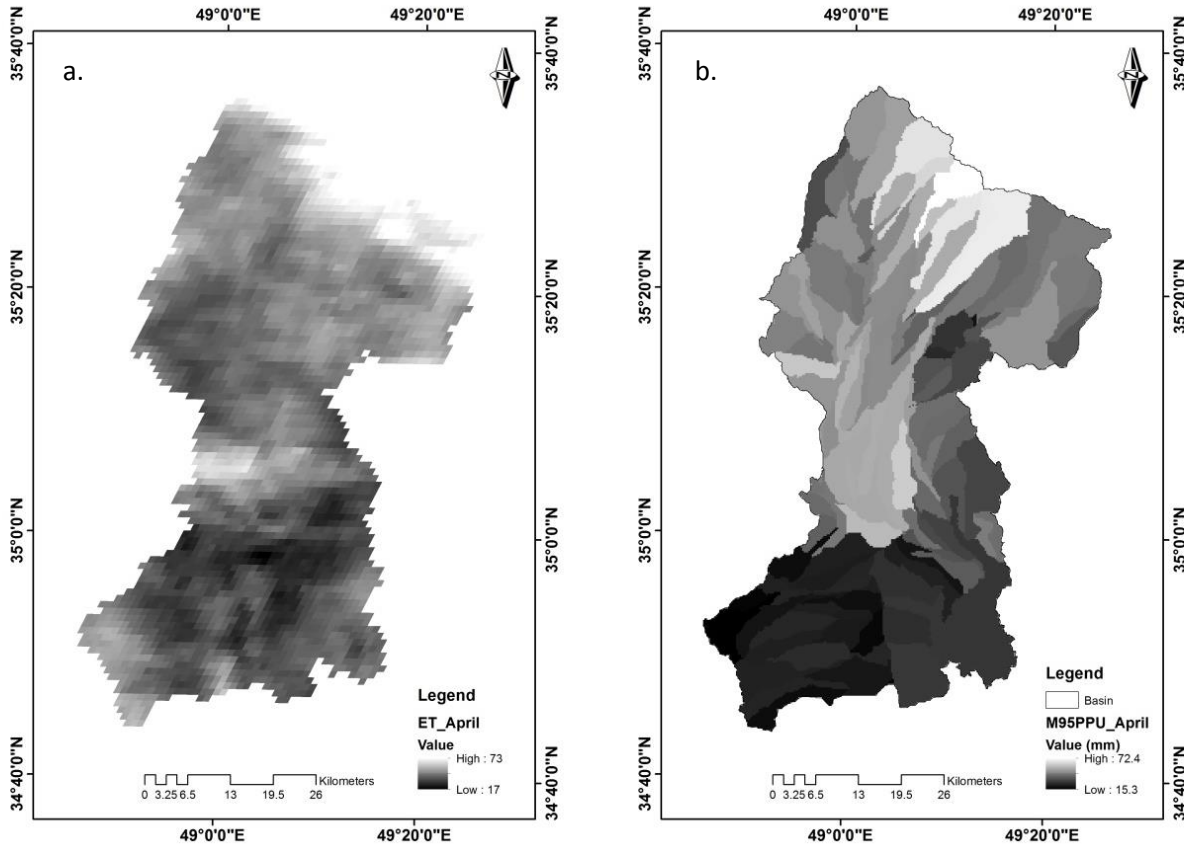


Figure 6-4. ETa in April, a: based on surface energy balance technique, b: surface water balance model

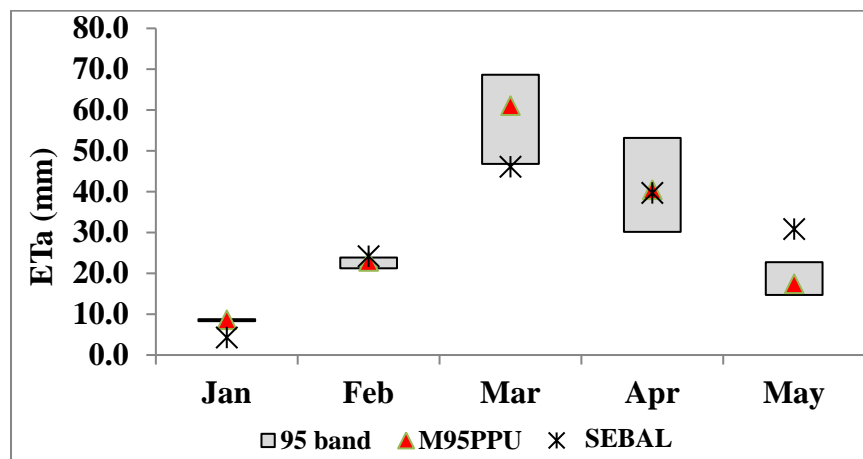


Figure 6-5. Anomaly graph of monthly average of ETa. The gray box shows the 95PPU band simulated by 500 iterations; M95PPU means the median of iterations. The star sign shows the ETa value simulated by SEBAL

6-4. Discussion and conclusions

Evapotranspiration maps were created for the RGB in the center of Iran using SEBAL/METRIC model. The model was further validated by SWAT hydrological model. In the SEBAL model, MODIS time Series data was used for the January-May periods of 2008. Some researchers used Landsat 7 and Landsat 5 to create evapotranspiration maps as it allows a high resolution of thermal band (Bastiaanssen et al., 1998b; Teixeira et al., 2009). However, Allen et al. (2007a) suggested MODIS data instead of Landsat due to the problems of Landsat 7 in 2003 and recent problems with the aging Landsat 5.

Several researchers mentioned limitations of the SEBAL model (Long et al. 2011; Long and Singh, 2012; Papadavid et al. 2013; Wang et al., 2014; Paul et al. 2014). Papadavid et al. (2013) improved the SEBAL model based on the crop parameters called CYSEBAL. The application of the SEBAL is suitable for flat areas. Therefore, Allen et al. (2007b) proposed the Mapping Evapotranspiration at High Resolution with Internalized Calibration (METRIC) model to mitigate this limitation. METRIC is a variant of SEBAL, which is able to consider the effects of topography.

Atmospheric correction of satellite data is not essential in the SEBAL/METRIC model. Tasumi et al (2005) stated that atmospheric correction of reflectance for albedo estimation and thermal bands is not necessary due to internal calibration of sensible heat flux. We used MODIS product of white sky albedo in shortwave resolution calculated by seven bands (Band 1-7). However, some researchers calculated albedo with two bands (band 1 and band 2) of MODIS. Tasumi et al (2007) mentioned that albedo should be calculated by bands 1-7 of MODIS, bands 1-5 and 7 of Landsat, and band 1-9 of ASTER.

The roughness length for heat transfer (Z_{oh}) is one of the most important parameters in the SEBAL model. Various researchers have stated different values for Z_{oh} . Paul et al. (2014) investigated the influence of Z_{oh} on the performance of SEBAL model and found that $Z_{oh}=0.1$ m resulted in the same estimate of ET_a as when $Z_{oh}=0.01$ m. In general, Z_{oh} is equivalent to the lower reference height for aerodynamic resistance (Z_1). We assumed $Z_1=0.1$ m in this study as suggested by Bastiaansen et al. (1998a).

In the earlier version of SEBAL (Bastiaansen et al 1998a), evaporative fraction was defined as the ratio of LE to (R_n-G) and assumed to be constant during 24-h period. However, Allen et al. (2005) mentioned that this assumption can sometime unpredicted daily ET in arid areas where

increases wind speeds in afternoon might raise LE in proportion to Rn (net radiation energy). However, in the newer version of SEBAL (Waters et al. 2002), and in the METRIC model, the evaporative fraction was modified by reference ET (ET_{rF}). Allen et al (2005) mentioned that “The assumption of constant ET_{rF} during a day may be better able to capture impacts of advection and changing wind and humidity conditions during the day, as expressed in the ET_r calculation (which is done hourly and summed daily)”.

The SEBAL model was validated successfully using ET_a estimated by SWAT model. In this study, the SWAT model was calibrated by crop production, which resulted in a good estimation of evapotranspiration. The results show that the ET_a estimated by SEBAL is very close to ET_a estimated by SWAT. The NS value of SEBAL model was greater than 0.80, which shows the reliability of the SEBAL model.

Besides the internal calibration of SEBAL/METRIC, it still has some uncertainty. A challenging part of energy balance approach is that the LE is only accurate if Rn, G and H are estimated precisely. However, the model attempts to overcome this error by inter-calibration of sensible heat flux (Allen et al., 2007a; Trezza, 2002). Additionally, estimation of dT is depend on the suitable selections of cold and hot pixels in the image. The accurate selection of cold and hot pixels is one of the limitations of the SEBAL model, which has been discussed by Wang et al. (2014); Long & Singh (2012). Any error in dT might have a negative effect on final residual results.

In spite of the limitations of the surface energy balance method, some researchers used evapotranspiration variable extracted by SEBAL model to calibrate hydrological models in instances of sparse data. Immerzeel & Droogers (2008) and Awan & Ismaeel (2014) used evapotranspiration extracted by SEBAL to calibrate a SWAT hydrological model in a catchment of the Krishna basin in southern India. The SEBAL model of evapotranspiration was validated by measured data. Hence, we can suggest that remote sensing data can be used to calibrate distributed hydrological models in case of low data availability.

6-5. References

- Abbaspour KC (2011) User Manual for SWAT-CUP: SWAT Calibration and Uncertainty Analysis Programs. Swiss Federal Institute of Aquatic Science and Technology, Eawag, Duebendorf, Switzerland. 103 pp.
- Akhavan S, Abedi-Koupai J, Mousavi SF, Afyuni M, Eslamian SS, Abbaspour KC (2010) Application of SWAT model to investigate nitrate leaching in Hamadan–Bahar Watershed, Iran. *Agriculture, Ecosystems & Environment* 139 (4): 675-88.
- Allen R, Tasumi M, Morse A, Trezza R (2005) Satellite-Based Evapotranspiration by Energy Balance for Western States Water Management. *Impacts of Global Climate Change*: 1-18. doi: 10.1061/40792(173)556
- Allen RG, Irmak A, Trezza R, Hendrickx JMH, Bastiaanssen W, Kjaersgaard J (2011) Satellite-based ET estimation in agriculture using SEBAL and METRIC. *Hydrological Processes* 25 (26):4011-27.
- Allen RG, Tasumi M, Trezza R (2007a) Satellite-Based Energy Balance for Mapping Evapotranspiration with Internalized Calibration (METRIC)—Model. *Journal of Irrigation and drainage engineering* 133 (4): 1-15.
- Allen RG, Tasumi M, Morse A, Trezza R, Wright JL, Bastiaansen W, Kramber W, Lorite I, Robison C (2007b) Satellite-Based Energy Balance for Mapping Evapotranspiration with Internalized Calibration (METRIC)-Applications. *Journal of Irrigation and drainage engineering* 133 (4): 395-406.
- Anderson FH (2008) Hydrological modeling in a semi-arid area using remote sensing data. Ph.D. Thesis. University of Copenhagen. Denmark
- Arnold JG, Srinivasan R, Muttiah RS, Williams JR (1998) Large area hydrologic modeling and assessment—Part 1: model development. *Journal of American Water Resources Association* 34:73–89

- Awan UK, Ismaeel A (2014) A new technique to map groundwater recharge in irrigated areas using a SWAT model under changing climate. *Journal of Hydrology* 519: 1368-1382.
- Bastiaanssen WGM (2000) SEBAL-based sensible and latent heat fluxes in the irrigated Gediz Basin, Turkey. *Journal of Hydrology* 229: 87–100.
- Bastiaanssen WGM, Menenti M, Feddes RA, Holtslag AAM (1998a) A remote sensing surface energy balance algorithm for land (SEBAL). 1. Formulation. *Journal of Hydrology* 212-213:198–212.
- Bastiaanssen WGM, Pelgrum H, Wang J, Ma Y, Moreno JF, Roerink GJ, Wal T (1998b) A remote sensing surface energy balance algorithm for land (SEBAL). 2. Validation. *Journal of Hydrology* 212–213:213–29
- Colaizzi PD, Evett SR, Howell TA, Tolk JA (2006) Comparison of five models to scale daily evapotranspiration from one-time-of-day measurements. *Transactions of the ASABE* 49(5): 1409–1417.
- Du J, Song K, Wang Z, Zhang B, Dianwei L (2013) Evapotranspiration estimation based on MODIS products and surface energy balance algorithms for land (SEBAL) model in Sanjiang Plain, Northeast China. *Chinese Geographical Science* 23(1):73-91.
- Engman ET, Gurney RJ (1991) *Remote sensing in hydrology*. Chapman and hall, ltd.
- Faramarzi M, Abbaspour KC, Schulin R, Yang H (2009) Modeling blue and green water resources availability in Iran. *Hydrological Processes* 23 (3):486-501. doi: 10.1002/hyp.7160.
- Feizizadeh B, Blaschke T, Nazmfar H, Akbari E, Kohbanani HR (2013) Monitoring land surface temperature relationship to land use/land cover from satellite imagery in Maraqeh County, Iran. *Journal of Environmental Planning and Management* 56 (9): 1290-315. doi: 10.1080/09640568.2012.717888. *Hydrological Earth System Sciences* 6: 85–100.
- Hargreaves G, Samani ZA (1985) Reference crop evapotranspiration from temperature, *Applied engineering in agriculture* 1: 96–99.

- Immerzeel W, Droogers P (2008) Calibration of a distributed hydrological model based on satellite evapotranspiration. *Journal of Hydrology* 349(3-4): 411-24. doi: 10.1016/j.jhydrol.2007.11.017.
- Kalma JD, McVicar TR, McCabe MF (2008) Estimating land surface evaporation: a review of methods using remotely sensed surface temperature data. *Survey Geophysics* 29: 421–469.
- Long D, Singh VP (2012) A modified surface energy balance algorithm for land (M-SEBAL) based on a trapezoidal framework. *Water Resources Researches* 48 .
- Long D, Singh VP, Li ZL (2011) How sensitive is SEBAL to changes in input variables, domain size and satellite sensor. *Journal of Geophysical Res. D: Atmos.* 116, D21107. <http://dx.doi.org/10.1029/2011JD016542>.
- Maeda EE, Wiberg DA, Pellikka PKE (2011) Estimating reference evapotranspiration using remote sensing and empirical models in a region with limited ground data availability in Kenya. *Applied Geography* 31 (1): 251-8.
- Moriasi DN, Arnold JG, Van Liew MW, Bingner RL, Harmel RD, Veith TL (2007) Model evaluation guidelines for systematic quantification of accuracy in watershed simulations. *Transactions of the ASABE* 50: 885–900.
- Norman JM, Anderson MC, Kustas WP (2006) Are single-source, remote-sensing surface-flux models too simple? In: D’Urso, G., Jochum M.A.O., Moreno, J. (Eds.), *Proceedings of the International Conference on Earth Observation for Vegetation Monitoring and Water Management*. American Institute of Physics 852: 170–177.
- Papadavid G, Hadjimitsis DG, Toullos L, Michaelides S (2013) A Modified SEBAL Modeling Approach for Estimating Crop Evapotranspiration in Semi-arid Conditions. *Water Resources Management* DOI 10.1007/s11269-013-0360-x
- Paul G, Gowda PH, Prasad PVV, Howell TA, Aiken RM, Neale ChMU (2014) Investigating the influence of roughness length for heat transport (zoh) on the performance of

SEBAL in semi-arid irrigated and dryland agricultural systems. *Journal of Hydrology* 509: 231-44. doi: 10.1016/j.jhydrol.2013.11.040.

- Rafiei Emam A, Kappas M, Akhavan S, Hosseini SZ, Abbaspour KC (2015a) Simulation of water balance components in a watershed located in central drainage basin of Iran. *Environmental Earth Sciences*
- Rafiei Emam A, Kappas M, Hosseini SZ (2015b) Assessing the impact of climate change on water resources, crop production and land degradation in a semi-arid river basin. *Hydrology research*
- Ritchie JT (1972) A model for predicting evaporation from a row crop with incomplete cover. *Water Resources Research* 8: 1204–1213.
- Romero MG (2004) Daily evapotranspiration estimation by means of evaporative fraction and reference ET fraction. PhD Diss., Utah State Univ., Logan, Utah.
- Ruhoff AL, Paz AR, Aragao LEOC, Mu Q, Malhi Y, Collischonn W, Rocha HR, Running SW (2013) Assessment of the MODIS global evapotranspiration algorithm using eddy covariance measurements and hydrological modelling in the Rio Grande basin." *Hydrological Sciences Journal* 58 (8):1658-76. doi: 10.1080/02626667.2013.837578.
- Schuol J, Abbaspour KC, Srinivasan R, Yang H (2008) Estimation of freshwater availability in the West African sub-continent using the SWAT hydrologic model. *Journal of Hydrology* 352 (1-2): 30-49. doi: 10.1016/j.jhydrol.2007.12.025.
- Spiliotopoulos M, Loukas A, Vasiliades L (2008) Actual evapotranspiration estimation from satellite-based surface energy balance model in Thessaly, Greece. EGU General Assembly, 13-18 April 2008, Vienna, Austria, Geophysical Research Abstracts: Vol 10.
- Su Z (2002) The Surface Energy Balance System (SEBS) for estimation of turbulent heat fluxes. *Journal of hydrology and earth system sciences* 6(1): 85–99.

- Tang R, Li ZhL, Chen KSh, Jia Y, Li Ch, Sun X (2013) Spatial-scale effect on the SEBAL model for evapotranspiration estimation using remote sensing data. *Agricultural and Forest Meteorology* 174-175:28-42. doi: 10.1016/j.agrformet.2013.01.008.
- Tasumi M, Allen RG, Trezza R (2007) Estimation of at-surface reflectance and albedo from satellite for routine, operational calculation of land surface energy balance. *Journal of Hydrological Engineering*.
- Tasumi M, Trezza T, Allen RG, Wright JL (2005) Operational aspects of satellite-based energy balance models for irrigated crops in the semi-arid U.S. *Journal of Irrigation and Drainage System* 19: 355-376.
- Teixeira ADC, Bastiaanssen W, Ahmad M, Bos M (2009) Reviewing SEBAL input parameters for assessing evapotranspiration and water productivity for the Low-Middle Sao Francisco River basin, Brazil: Part A: Calibration and validation. *Journal of agricultural and forest meteorology* 149: 462–476.
- Tobin KJ, Bennett ME (2013) Temporal analysis of Soil and Water Assessment Tool (SWAT) performance based on remotely sensed precipitation products. *Hydrological Processes* 27 (4): 505-14. doi: 10.1002/hyp.9252.
- Trezza R (2002) Evapotranspiration using a satellite-based surface energy balance with standardized ground control. PhD Diss., Utah State Univ., Logan, Utah.
- Vaghefi SA, Abbaspour K, Mousavi SJ, Srinivasan R, Yang H (2014) Analyses of the impact of climate change on water resources components, drought and wheat yield in semiarid regions: Karkheh River Basin in Iran. *Hydrological Processes* 28(4): 2018–2032.
- Wang XG, Wang W, Huang D, Yong B, Chen X (2014) Modifying SEBAL Model Based on the Trapezoidal Relationship between Land Surface Temperature and Vegetation Index for Actual Evapotranspiration Estimation. *Remote Sensing* 6 (7): 5909-5937. doi: 10.3390/rs6075909.

- Waters R, Allen RG, Tasumi M, Trezza R, Bastiaanssen W (2002) SEBAL: Surface Energy Balance Algorithms for Land(Idaho implementation), advanced training and user manual.

General Summary and Conclusion

The focus of this research is the investigation of climate change on water resources and crop production in a semi-arid river basin in Iran with the emphasis on remote sensing, GIS and a hydrological model. Additionally, the process of land degradation was also analyzed based on the results of hydrological and climate change models. Furthermore, a remote sensing process to estimate actual evapotranspiration was analyzed. The most important findings and some conclusions of the research is presented in this chapter:

- The current hydrological process of a semi-arid basin was addressed by soil and water assessment tools (SWAT). The model was calibrated by river discharge data in relevante sub-basins. The sensitive analysis showed that the curve number (CN) and snow melt parameters are the most sensitive parameters in the mountainous part of the basin and groundwater delay factor (GW_DELAY) is the most sensitive parameter in the lowland area. The performance of the model was satisfied by R^2 and NS assessment. The water cycle fluxes (e.g. surface runoff, evapotranspiration, percolation) were estimated at the monthly intervals. The flux distributions were mapped in the sub-basin level.

- The uncertainty analysis shows that the uncertainty of actual evapotranspiration (ETa) is higher in March, April and May, than in other months. There is a close relationship between precipitation and evapotranspiration. The highest precipitation the highest ETa, and the lowest precipitation (e.g. in September), the lowest evapotranspiration.

In April due to crop growth the highest precipitation, neither highest surface runoff (SURQ), nor highest uncertainty of SURQ is detected. However, the uncertainty of surface runoff and the rate of it is highest in February.

The soil water content (SW) is less in summer and more in winter. Therefore, the uncertainty of SW estimation in winter is higher than in summer.

- To precisely estimate groundwater recharge, the calibrated model was recalibrated by crop yield. The idea was that the calibration of model by crop yield would lead to a more precise

estimation of evapotranspiration resulting in the more precise prediction of the other water fluxes such as groundwater recharge.

- To calibrate the model by crop yield, all previous parameters which were calibrated by river discharge kept constantly, and parameters related to crop yield (e.g. heat unit, harvest index, bio target, water stress) were calibrated both in rain-fed and irrigated lands. The results of the calibration were very good with RMSE less than 70 kg ha⁻¹ for rain-fed yield, and 690 kg ha⁻¹ for irrigation yield. Lack of water use data in irrigated lands is one of the limitations of this research and probably the reason for the high uncertainty of yield in irrigated lands.

- Aquifer percolation coefficient (RCHRG-DP) is one of the important parameters in the groundwater recharge estimate. RCHRG-DP is ranged between 0 and 1. The lowest RCHRG-DP is the highest discharge and less groundwater recharge. The one-at-a-time sensitivite analysis of this parameter shows that the decreasing of this parameter by about 25 percent leads to a significant increase of baseflow (more than double).

- The annual average groundwater recharge was estimated at about 5 mm, and was verified by independently observed borehole data. The water table decreased sharply during temporal assessment, however it was constant in 2003 owing to the highest precipitation leading to the highest groundwater recharge.

- Borehole data independently show that the water level in the west of the basin decreased sharply, and the depth of water to the surface is more that 140 m, however, in some places, like in the northern part, the water table is very close to the surface (less than 1 m) even leading to water logging. The north eastern part of the area was recognized as having the highest capability of percolation and recharge.

- To assess the impact of climate change, the ensemble model leads to a decreasing of model uncertainty. Therefore a four GCMs model ensemble and three differencnt emission scenarios were assessed. The GCMs data were downscaled by LARS-WG model based on ten rain gages and temperature stations. The results showed that the mean annual precipitation is likely to decrease, while the mean annual maximum temperature increases. Therefore, the whole basin will tend to be drier in the future.

- Assessing the impact of climate change on water resources availability showed the reduction of groundwater recharge, evapotranspiration and soil water content, and the increase of surface runoff in the basin.
- According to the statistical center in Iran, the population growth rate in the basin is 2.63 %. Additionally, assessing the remotely sensed data by mapping LULC showed about a 100% increase of urbanization during the 20 year period from 1989 to 2009. This means that urban or built-up growth in the mid of 21st century will rise by about 190%. The effect of the increase of urban lands on surface runoff shows that an average annual runoff will increase by more than 60 % during this time.
- The impact of climate change on crop production shows the increase of production in irrigated lands. The reason is that irrigated lands are not dependent on precipitation as groundwater is the main source of irrigation in this area. Additionally, increasing CO₂ emission and rising temperature, especially minimum temperature, help to increase the yield.
- On the other hand, crop production in rain-fed areas will decrease in 2050. The reason is that rain-fed agriculture depends on rainfall and any changes in precipitation, which can reduce soil water content, have a pernicious effect on crop yield. Additionally, heat stress and water stress will increase in all scenarios and they significantly affect cereal yields in rain-fed lands.
- The remote sensing process to estimate evapotranspiration showed that the ET_a estimated by the surface energy balance method from MODIS data was close to that estimated by the hydrological model. Therefore, we can conclude that remote sensing data can be used to calibrate the hydrological models in the area with low data availability. However, the further consideration toward the calibration of the hydrological models by ET_a will be advisable in the area with low data availability.
- The prediction of water components in the future was used based on the soil map in the historical period. As soil parameter changes may have an influence on soil moisture, surface runoff and land degradation, considering these changes will be suggested for further research projects.

- To build constant stations in the rangelands area would be beneficial in order to measure the species yields and LAI. The SWAT can further be used to predict the rangeland's productions and the capacity of the animal units in the basin for the future. This measurement helps to improve management of the watershed by its stakeholders.

Curriculum Vitae

Ammar Rafiei Emam



1-Personal information:

Name:	Ammar Rafiei Emam
Date and Place of Birth:	1977 / Roodsar (Iran)
Gender:	Male
E-mail:	rafiei99@gmail.com

2-Employments:

Ph.D. Research Fellow	Full time	2010- 2015	Department of Cartography, GIS and Remote Sensing, University of Göttingen, Germany
Research Fellow	Full time	2008-2010	Department of studies and economical assessment, Agriculture Bank/ Iran.
Research Fellow	Full time	2003-2008	Department of desert research division, Research Institute of Forests and Rangelands, RIFR, Iran.
Lecturer	Part time	2005-2009	University of Shahroud, Tarbiat Modares, and University of Tabriz, Iran.

3-Educations:

Ph.D. in Remote Sensing/GIS	2010-2015	Department of Cartography, GIS and Remote Sensing, University of Göttingen, Germany
Ph.D. in Watershed Management (resigned)	2007-2008	Azad University / Tehran, Iran
M.Sc. in Natural Resources Engineering	2000-2003	University of Tehran/ Tehran, Iran
B.Sc. in Agricultural Engineering	1995-1999	Agricultural and Natural Resources University / Gorgan, Iran

4-Some selected Publications

Books/ chapters:

1. **Rafiei Emam A**, Kappas M, & Abbaspour KC. 2015. Simulation of water balance components in a watershed located in central drainage basin of Iran. In: Remote Sensing of the Terrestrial Water Cycle, Geophysical Monograph 206 (V. Lakshmi, ed.). American Geophysical Union. Wiley & Sons press. ISBN: 9781118872031.
2. **Rafiei Emam A**, 2009. Management and conservation of dry land forests. In: Dry land forest management (S.A Rezaei, ed.). Puneh Publication. Iran, 320 P. (Persian language).
3. Alavipanah SK, Matinfar HR, and **Rafiei Emam A**. 2008. Application of information technology in the earth sciences (on digital soil mapping). Tehran University press, Iran (Persian language).

International Peer-Review Journals:

1. **Rafiei Emam A**, Kappas M, Erasmi S, Akhavan S. 2015. Estimating actual evapotranspiration from MODIS time series, compared with using hydrological model in a semi-arid catchment in Iran. Journal of Spatial Science. Under review.
2. **Rafiei Emam A**, Kappas M, Hosseini SZ. 2015. Assessing impact of climate change on water resources, crop productions and land degradation in a semi-arid river basin in. Hydrology Research Journal. Accepted.
3. **Rafiei Emam A**, Kappas M, Akhavan S, Hosseini SZ, Abbaspour KC. 2015. Estimation of groundwater recharge and its relation with land degradation: Case study of a semi-arid river basin in Iran. Environmental Earth Sciences Journal. Under review.
4. Hosseini SZ, Kappas M, Zare Chahouki M A, Gerold G, Erasmi S, **Rafiei Emam A**. 2013. Modelling potential habitats for *Artemisia sieberi* and *Artemisia aucheri* in Poshtkouh area, central Iran using the maximum entropy model and geostatistics. Journal of Ecological Informatics. 18: 61–68.
5. Alavipanah SK, Matinfar HR, **Rafiei Emam A**, Khodaei K, Hadji Bagheri R, Yazdan Panah A. 2010. Criteria of selecting satellite data for studying land resources. DESERT Journal, 15:83-102
6. Alavipanah SK, Amiri R, Matinfar H, **Rafiei Emam A**, Shamsipor A. 2007. Cross-sensor analysis of TM and ETM spectral information content in arid and urban areas. World Applied Sciences Journal, 2(6): 665-673. IDOSI Publication.

Conference Papers:

1. **Rafiei Emam A**, Kappas M, Erasmi S. 2014. Estimation of actual evapotranspiration based on satellite images and a hydrological model. GIAN Conference. 8-9 October 2014. Karaj. Iran.
2. **Rafiei Emam A**, Kappas M, Hosseini S Z. 2014. Impact of climate change on water resources and crop production in a semi-arid region of Iran. GLP conference. 17-19 March 2014. Berlin. Germany.
3. **Rafiei Emam A**, Kappas M, Akhavan S, Abbaspour KC. 2013. Procedure of hydrological modeling in a semi-arid river basin with SWAT. SWAT conference, 16-19 July 2013. Toulouse, France.
4. **Rafiei Emam A**, Kappas M, Abbaspour KC, Hosseini SZ. 2013. Impact of climate change on water resources and land degradation in a semi-arid regions of Iran. Conference on desertification and land degradation. 17 & 18 June 2013, Ghent , Belgium.
5. Hosseini SZ, Kappas M, **Rafiei Emam A**, Propastin P. 2013. Application of ecological niche modelling and geostatistics for assessing distribution of *Seidlitzia rosmarinus* in a desert ecosystem, desert land conference, Gent, Belgium.

6. **Rafiei Emam A**, Kappas M, Abbaspour KC. 2012. Simulation of water balance components in a watershed located in central drainage basin of Iran. AGU Chapman Conference on Remote Sensing of the Terrestrial Water Cycle. 19 - 22 February 2012. Hawaii, USA.
7. Hosseini SZ, Kappas M, **Rafiei Emam A**, Propastin P, Erasmi S. 2012. Soil salinity mapping using satellite images and regression models in desert rangelands, 65th Annual Meeting of the Society for Range Management, Spokane, Washington, USA.
8. **Rafiei Emam A**, Kappas M, Hosseini SZ, Erasmi S. 2011. Estimation of the volume of groundwater recharge in part of central river basin in Iran. Göttinger Tropentag conference. 26-27 May 2011. University of Goettingen. Germany.

5-Training Courses:

- Short training courses in “ Semi-arid land management for crop production and restoration in man-made soils”. 18-25 September 2013. Bari, Italy. (Organized by COST action ES1104”arid lands restoration and combat of desertification).
- Short training courses on “SWAT-CUP”. October 2012. EAWAG, Dübendorf, Switzerland.
- Winter school on "Remote Sensing of Precipitation Using Microwave Links: Techniques and Applications". February and March 2012. Garmisch-Partenkirchen, Germany.
- Short training courses on “Introductory to SWAT”. Toledo, Spain. June 2011.
- Short training courses (three months) on “Environmental management of regional drainage basin ", May-July 2007. JICA, Obihiro, Japan.

